

AD-A044 535

IRT CORP SAN DIEGO CALIF

F/G 9/1

RADIATION EFFECTS IN INSULATOR MATERIALS.(U)

FEB 77 J WILKENFELD

DAAG39-76-C-0089

UNCLASSIFIED

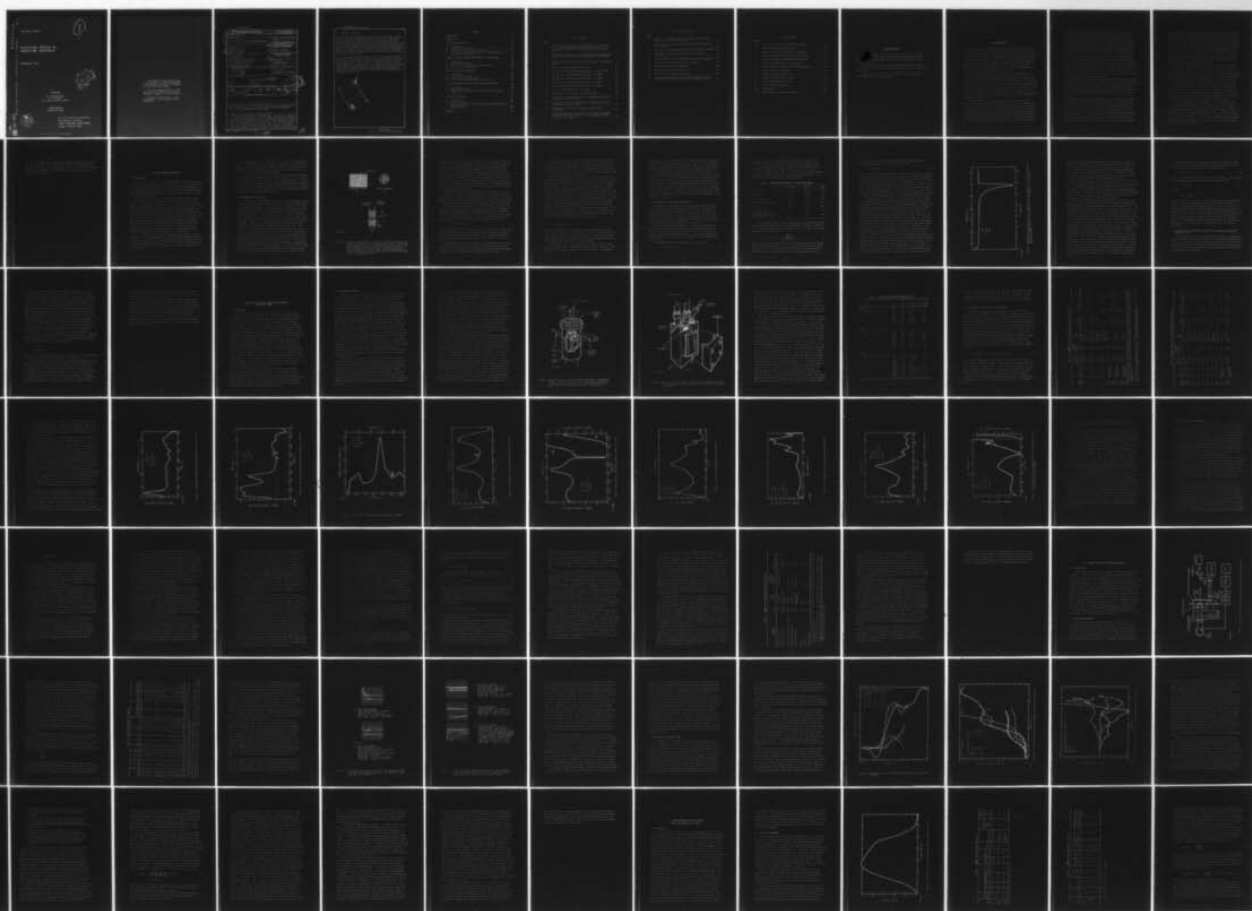
INTEL-RT-8148-011

HDL-CR-77-089-1

NL

1 OF 2

AD
A044535



AD A 044 535

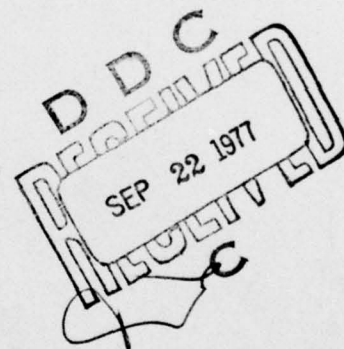
HDL-CR-77-089-1 - Radiation Effects in Insulator Materials, by J. Wilkenfeld

HDL-CR-77-089-1

1
BS

RADIATION EFFECTS IN INSULATOR MATERIALS

FEBRUARY 11, 1977



Prepared by

IRT CORPORATION
P.O. Box 80817
San Diego, California 92138

Under Contract

DAAG39-76-C-0089



U.S. Army Materiel Development
and Readiness Command
HARRY DIAMOND LABORATORIES
Adelphi, Maryland 20783

J. WU.
DDC FILE COPY

The findings in this report are not to be construed as an official Department of the Army position unless so designated by other authorized documents.

Citation of manufacturers' or trade name does not constitute an official endorsement or approval of the use thereof.

Destroy this report when it is no longer needed. Do not return it to the originator.

UNCLASSIFIED

SECURITY CLASSIFICATION OF THIS PAGE (When Data Entered)

19 REPORT DOCUMENTATION PAGE		READ INSTRUCTIONS BEFORE COMPLETING FORM
1. REPORT NUMBER HDL-CR-77-089-1	2. GOVT ACCESSION NO.	3. RECIPIENT'S CATALOG NUMBER
4. TITLE (and Subtitle) RADIATION EFFECTS IN INSULATOR MATERIALS	5. TYPE OF REPORT & PERIOD COVERED Final 4/28/76 through 3/31/77	
6. AUTHOR(s) J. Wilkenfeld	7. PERFORMING ORG. REPORT NUMBER INTEL-RT-8148-011	
8. PERFORMING ORGANIZATION NAME AND ADDRESS IRT Corporation P.O. Box 80817 San Diego, California 92138	9. CONTRACT OR GRANT NUMBER(s) DAAG39-76-C-0089	
10. CONTROLLING OFFICE NAME AND ADDRESS Harry Diamond Laboratories 2800 Powder Mill Road Adelphi, Maryland 20783	11. PROGRAM ELEMENT, PROJECT, TASK AREA & WORK UNIT NUMBERS 11 Feb 77	
12. MONITORING AGENCY NAME & ADDRESS (if different from Controlling Office) 12-133 p.	13. REPORT DATE February 11, 1977	
	14. NUMBER OF PAGES 140	
	15. SECURITY CLASS. (of this report) Unclassified	
	16. DECLASSIFICATION/DOWNGRADING SCHEDULE	
17. DISTRIBUTION STATEMENT (of this Report) DISTRIBUTION STATEMENT A Approved for public release; Distribution Unlimited		
18. DISTRIBUTION STATEMENT (of the abstract entered in Block 20, if different from Report) Final Rept. 28 Apr 76 - 31 Mar 77		
19. SUPPLEMENTARY NOTES		
20. KEY WORDS (Continue on reverse side if necessary and identify by block number) polymer; dielectric; cable; capacitor; polyethylene; polytetrafluoroethylene; radiation response; thermally stimulated current; morphology; trapped charge; polarization; crystallinity		
21. ABSTRACT (Continue on reverse side if necessary and identify by block number) The thermal- and radiation-induced charges released to an external circuit have been examined for a set of polyethylene capacitors made from materials of differing crystallinities and molecular structures. Persistent internal fields were created by burn-in. It was found that the net thermal or radiation response of samples subject to burn-in is significantly enhanced if compared to those that were annealed. There was no significant dependence of sample response on fractional crystallinity for		

409 1388

→ not part
JB

DDC
RECEIVED
SEP 22 1977
UNCLASSIFIED

UNCLASSIFIED

SECURITY CLASSIFICATION OF THIS PAGE (When Data Entered)

20. ABSTRACT (Continued)

capacitors polarized under burn-in. This is attributed to the fact that the magnitude of the persistent internal fields created in this manner depends on the concentration of dissociable impurities or orientable dipoles present and is thus sample- rather than morphology-dependent. The ability of this polymer to store persistent charge/polarization is related to the presence of trapping sites connected with specific morphological features. These include: (1) interfaces between crystalline and amorphous domains; (2) regions of large free volume between molecules in the amorphous domains; and (3) defects in the crystalline domains associated with chain folds and side branches.

→ The radiation and thermal response of a set of semirigid Teflon TFE dielectric cables has been evaluated. This has been done to (1) relate their behavior, especially the first pulse response, to the conditions of irradiation, and (2) to see if there is a correlation between the net charge released to an external circuit by radiation and by heating similar to that found for Teflon capacitors. The results of the thermally stimulated current measurements imply that the stored charge released from these cables is trapped near their surface rather than constituting a uniform volume polarization.

ACCESSING FOR	White Section <input type="checkbox"/>
	Burn Section <input type="checkbox"/>
NWS	
DATE	
J. S. F. 102-104	
DISTRIBUTION/AVAILABILITY CODES	SPECIAL
A	

UNCLASSIFIED

SECURITY CLASSIFICATION OF THIS PAGE (When Data Entered)

CONTENTS

ACKNOWLEDGMENTS	7
1. INTRODUCTION	8
2. POLYMER CHARACTERIZATION	14
2.1 Introduction	14
2.2 Morphology of Polyethylene	15
2.3 Determination of Fractional Crystallinity	19
2.4 Correlation of Morphological Features of Polyethylene with Persistent Internal Fields	24
3. THERMALLY STIMULATED CURRENT MEASUREMENTS IN POLYETHYLENES	29
3.1 Introduction	29
3.2 Experimental Technique	30
3.3 Description of the TSC Data on Polyethylenes	36
3.4 Discussion of TSC Measurements	52
4. RADIATION RELAXATION MEASUREMENTS	65
4.1 Introduction	65
4.2 Experimental Procedure	65
4.3 Post-Irradiation Thermal Anneal	75
4.4 Discussion of Radiation Relaxation Measurements	81
5. TETRAFLUOROETHYLENE DIELECTRIC CABLE AND CAPACITOR STUDIES	89
5.1 Introduction	89
5.2 Radiation Measurements	90
5.3 Thermal Measurements on Cables and Capacitors with Teflon Dielectrics	99
6. SUMMARY AND ASSESSMENT	114
6.1 Introduction	114
6.2 Principal Findings	115
6.3 Relationship Between Polymer Morphology, Charge Storage, and Radiation Response	122
6.4 Recommendations	124
REFERENCES	128

LIST OF FIGURES

Figure

1	Schematic diagram showing (a) the gross structure of a polymer, (b) the fibril arrangement in a single spherulite, and (c) the orientation of lamellae and amorphous domains along a single fibril	16
2	Differential scanning calorimetric (DSC) plot of heat absorbed as a function of temperature for an ARCO high-density polyethylene film	22
3	Temperature bath for carrying out TSC measurements in polyethylene samples	32
4	Detail of the sample chamber and heat sink	33
5	TSC spectrum of ARCO HD polyethylene burned in at 90 to 102°K . . .	42
6	TSC spectrum of ARCO HD polyethylene burned in at 180°K	43
7	TSC spectrum of ARCO HD polyethylene burned in at 300°K	44
8	TSC spectrum for a HD polyethylene burned in at 343°K	45
9	TSC spectrum of ARCO HD polyethylene burned in at 343°K	46
10	TSC for a GW LD E1016 burned in at 297°K	47
11	TSC spectrum of a low-density polyethylene sample	48
12	TSC spectrum for a Golden West Plastics type W703 medium-density polyethylene burned in at 290°K	49
13	TSC spectrum of a Golden West Plastics type W703 medium-density polyethylene burned in at 366°K	50
14	Experimental configuration for radiation depolarization measurements	66
15	Response of Golden West medium-density, polyethylene type W703, sample MDT4 which had been burned in at $T_B = 353^\circ\text{K}$, $t_B = 16\text{h}$, $V_B = 325, \text{V}$, $E_B = 100 \text{ kV/cm}$	72

LIST OF FIGURES (Continued)

Figure

16	Response of an ARCO high-density polyethylene capacitor HDE3 to a series of 40-MeV electron pulses	73
17	TSC spectra for a series of MD polyethylene samples which had been irradiated	77
18	TSC spectra for HD polyethylene samples which had been irradiated .	78
19	TSC spectra for low-density polyethylene which had been irradiated	79
20	SPI Pulse 6000 x-ray spectrum determined from deposition profile .	91
21	TSC spectra for a Teflon-TFE dielectric capacitor	102
22	TSC spectra for 0.100-inch AFWL cable	106
23	TSC spectra for 0.141-inch Cujack cable	107
24	TSC spectra for 0.085-inch Cujack cable	108
25	Normalized radiation and thermal depolarization response versus nonelectronic polarizability for samples charged by burn-in	125

LIST OF TABLES

Table

1	Fractional Crystallinity of Polyethylene Samples	20
2	Polyethylene Capacitor Characteristics	35
3	Summary of TSC Data for High-Density Polyethylene	37
4	Summary of TSC Data for Medium-Density Polyethylene	38
5	Summary of TSC Data for Low-Density Polyethylene	40
6	Summary of TSC Measurements on Polyethylene	62
7	Summary of Burn-In Conditions for Irradiated Samples	68
8	Radiation Response of Capacitors	70
9	Summary of Test Cable Structures	92
10	Summary of Cable Responses - IRT/SPI	93
11	Relative Cable Radiation Response	95
12	Teflon TFE Capacitor Response	100
13	Cable Response	105
14	Charge Released from Teflon Dielectrics	110

ACKNOWLEDGMENTS

We wish to thank Mr. William H. O'Bryan of Golden West Plastics and Mr. H. Peoples of the ARCO Polymer Division of ARCO, Incorporated for polymer samples, and Mr. Haskel Joseph of Alissa Manufacturing Co. for capacitor samples.

Gene Staley of the General Atomic Company performed the DSC measurements, while Peter Ganzel of General Atomic carried out the x-ray diffraction measurements.

The invaluable assistance of Vesa Junkkarinen in the early phases of this program is gratefully acknowledged.

1. INTRODUCTION

Polymers can store trapped charge or persistent polarization for periods as long as several years. Radiation-induced relaxation of such stored charge or polarization in components containing polymers can lead to an enhanced radiation response, which may cause system malfunction or failure. Without realistic bounds on such a response, it is difficult to make survivability/vulnerability assessments or specify a sufficient level of hardening for systems containing these dielectrics. Specific components that may show deleterious effects because of persistent charge include capacitors, cables, and spacecraft dielectrics such as thermal blankets and dielectric spares.

The goal of this program has been to provide an understanding of the effect of a stored charge on the radiation response of polymer dielectrics in order to make survivability/vulnerability assessments possible. This program has been directed toward (1) identification of those mechanisms by which polymer dielectrics store persistent charge or polarization and relation of them to the molecular structure and morphology of these materials, (2) determination of the bounds of the radiation response of such polarized dielectrics, and (3) provision of prescriptions for minimizing the effect of this charge on the radiation response of systems containing polymer dielectrics or at least to make their response predictable.

The initial impetus for this program was the observation that high-reliability polymer film dielectric capacitors, when exposed to ionizing radiation, released unexpectedly large amounts of charge into circuits of which they were a part. Our initial studies (Ref 1) demonstrated that the origin of this phenomenon was the radiation-induced relaxation of persistent internal polarization fields in the bulk polymer. These fields are created as a consequence of a quality assurance procedure known as burn-in, i.e., holding the capacitor at its maximum working temperature and voltage for periods of a day or so.

Last year's effort (Ref 2) demonstrated that the effect of the burn-in technique was to create persistent internal polarization by the alignment of molecular dipoles intrinsic to the polymer structure or impurity space charges in the polymer introduced as a consequence of the manufacturing processes. A systematic study was carried out to relate the measured thermal and radiation response of the polymers commonly used as capacitor dielectrics to their molecular structure. It was found that the charge released by a polymer dielectric capacitor to an external circuit on thermal annealing or irradiation after burn-in is proportional to the nonelectronic component of the polymer polarizability, i.e., that portion of its total polarizability due to the presence of dipoles or to space charge trapped at interfaces in these inhomogeneous materials. In other words, the more highly polar a polymer, the greater its thermal or radiation response after burn-in. One could therefore prescribe the employment of capacitors with nonpolar dielectrics such as polypropylene or polytetrafluoroethylene (Teflon) to minimize the charge released to an external circuit from capacitors that might have been exposed at some time in their prior history to a combination of elevated temperature and bias.

It was also found that there was a correlation between the amount of charge released to an external circuit by the thermally induced relaxation of persistent charge and that induced by radiation. This finding suggests that the presence of stored charge in metal-polymer dielectric systems that might affect the irradiation behavior could be screened by thermal testing so that only components that show an anomalously large thermal response would have to be radiation tested.

Understanding the factors that cause the inconsistent behavior of cables to radiation pulses has become an important problem. It has been argued that one source of this anomalous behavior is the radiation-induced relaxation of persistent internal fields that are created by stored charge introduced into the polymer dielectric as a consequence of manufacturing processes such as polymerization or extrusion or because of trapped charge introduced by exposure to ionizing radiation. In this report data is presented that shows that when irradiated the amount of charge released by polyethylene capacitors in which persistent internal fields have been created is significantly greater than that

released by samples which have been thermally annealed. The behavior of such capacitors mimics the incremental response of cables when exposed to a series of radiation pulses. Radiation-induced charging may occur in dielectrics that are a part of spacecraft components, such as cables, thermal blankets, insulating spaces, and optical components. Such dielectrics are exposed to a constant electron flux because of the exoatmospheric electron environment, both natural and artificial (Ref 3). Accumulation of such charge in a dielectric can lead to a catastrophic failure as a consequence of dielectric breakdown or may be released to external circuitry if the satellite is exposed to a threat pulse. In order to predict the behavior of cables or spacecraft dielectrics in this radiation environment, it is necessary to understand the mechanisms by which space charge can be stored in polymer dielectrics.

The work carried out this year is an extension of last year's program, and had as its main goal to determine the influence of polymer morphology, i.e., the structural organization of the polymer chains in the bulk material, on the ability of a polymer to store persistent internal charge under burn-in and how this charge is released consequent to irradiation. The intent was to identify any correlation between specific morphological features, such as degree of crystallinity, presence of chain branching, defects, and the ability of the polymer to store trapped charge. For this study polyethylene was chosen as a model polymer. This choice was made because the polymer is commonly used in cable dielectrics and is readily available in a variety of states encompassing a range of crystallinities and degrees of branching. It is also the basic polymer from which other types are derived through the substitution of atoms or functional groups for the hydrogen atoms on the main chain.

The second chapter of this report presents a brief description of the current state of knowledge about the morphology of polyethylene. While the basic chemical structure of the polymer is simple, because of the length of its constituent molecules its actual structure is quite complex. In this chapter, the procedures are described that were used to characterize the three types of polyethylenes studied. These samples were chosen to cover a reasonably wide range of morphologies. A summary is presented of current knowledge about possible charge trapping sites in this polymer in relation to specific features of polyethylene morphology.

The third chapter of this report describes the thermally stimulated current measurements (TSC) made on polyethylene capacitors consequent to burn-in in which the current evolved as a function of temperature was monitored. The purpose of these measurements were threefold. First, to bound the amount of charge released to an external circuit in thermal depolarization as a consequence of burn-in. Second, to see if a correlation could be found between features of the TSC spectra, such as peaks, and temperatures at which characteristic molecular motion occurs in order to ascertain which specific features of the polymer morphology are related to the charge trapping responsible for the creation of persistent polarization. Third, to provide data to see if a correlation exists between the thermal response of these capacitors consequent to burn-in and that induced by radiation.

In the fourth chapter of this report are described the experiments carried out to bound the radiation response of the polyethylenes in which persistent internal fields have been created. These irradiations were carried out on matched sample sets in which one sample had been polarized by burn-in while the other was thermally annealed before irradiation. This was done in an effort to separate that portion of the radiation response of this polymer that is due to the relaxation of internal fields and that portion that is due to the driven charge (i.e., the replacement currents which flow in an external circuit as a consequence of the radiation-generated charge motion in the polymer bulk). Our measurements clearly show that the presence of persistent internal space charge or polarization can significantly enhance the radiation response of this dielectric. It is well known that the exposure of polymer dielectrics to ionizing radiation can store trapped charge in them. An example of this is the charging of spacecraft dielectrics exposed to the exoatmospheric electron environment. The charge released by a cable or capacitor exposed to a series of radiation pulses eventually becomes constant. A metal-dielectric system which has been brought to such a state is said to be radiation annealed. However, the behavior of such a system when exposed to subsequent radiation pulses would undoubtedly be dissimilar to a similar system which had been thermally annealed, because the former contains significant amounts of trapped charge. To study this phenomenon, a series of post-irradiation thermal annealing

measurements were carried out on the polyethylene capacitor samples in order to make an estimate as to the time over which this trapped charge persists and also to bound the amount of such charge in a dielectric that has been radiation annealed. These measurements were also carried out in order to compare the efficiency of radiation charging with that of burn-in in creating a persistent internal field in our model polymer.

The original thrust of this program was to elucidate the mechanisms responsible for the anomalous response of capacitors. As it progressed, it became more important to focus on those features of charge trapping in polymers which might be relevant to understanding the inconsistent response of cables. Therefore, at the request of the contracting agency, we shifted our attention to gathering information by which the responsible mechanisms for the anomalous response of cables might be identified.

The fifth chapter presents a first-cut evaluation of the behavior of a group of semirigid coaxial cables with polytetrafluorethylene dielectrics (Teflon-TFE) that have been used in satellites and also to instrument simulator and UGT experiments exposed to irradiation. This work has been carried out to generate information to guide the forthcoming Defense Nuclear Agency (DNA) cable program. The cables were chosen for study because radiation experiments carried out earlier this year at the SPI Pulse 6000 x-ray facility indicated that they showed large first-pulse anomalies. We have tabulated the radiation response of these cables, for a variety of different experimental conditions in terms of what we feel to be relevant parameters of exposure in an effort to try to understand why they showed different specific responses under different conditions of irradiation. In addition, thermally stimulated current measurements have been carried out on samples of these cables to see if the charge release as a consequence of thermal annealing is comparable to that released in a radiation annealing in analogy to the observed behavior of capacitors. This has been done to determine whether thermal methods could be used as a screening test for identifying cables which may show anomalously large responses because of trapped charge or because of the presence of gaps between the dielectric and conductors. Finally, some TSC measurements have been performed on TFE capacitor dielectrics for comparison with the cables.

The concluding chapter of this report contains a general discussion of our work. It summarizes our findings concerning the relationship between the morphology of the model polymer and its ability to store persistent charge/polarization. Suggestions are made for the problems to be addressed in any forthcoming cable program.

2. POLYMER CHARACTERIZATION

2.1 INTRODUCTION

A major aim of this year's study was to search for correlations between the morphological properties of a polymer and its ability to store (and release) persistent space charge/polarization. As we have noted in the introduction, features thought to be relevant for charge storage include the degree of crystallinity, chain branching, the presence of particular functional groups, and the presence of unsaturated bonds.

Polyethylene was chosen as the model polymer for this study for several reasons. First, it is an important dielectric used in many coaxial cables. Second, it is commercially available in a variety of morphological forms which cover a range of densities, crystallinities, and degrees of branching (i.e., the presence of side groups). Third, a large number of other polymers are structurally derivable from polyethylene through the substitution of various functional groups in place of the hydrogens attached to the main carbon chain. The charge release behavior of some of the derivative polymers such as polypropylene, polystyrene, and polytetrafluoroethylene (Teflon-TFE), poly(ethylene terephthalate) (Mylar) were studied during last year's program (Refs 2 and 4). Finally, a great deal of information exists which correlates the physical properties of polyethylene with its morphology. The availability of such information facilitates the interpretation of our measurements.

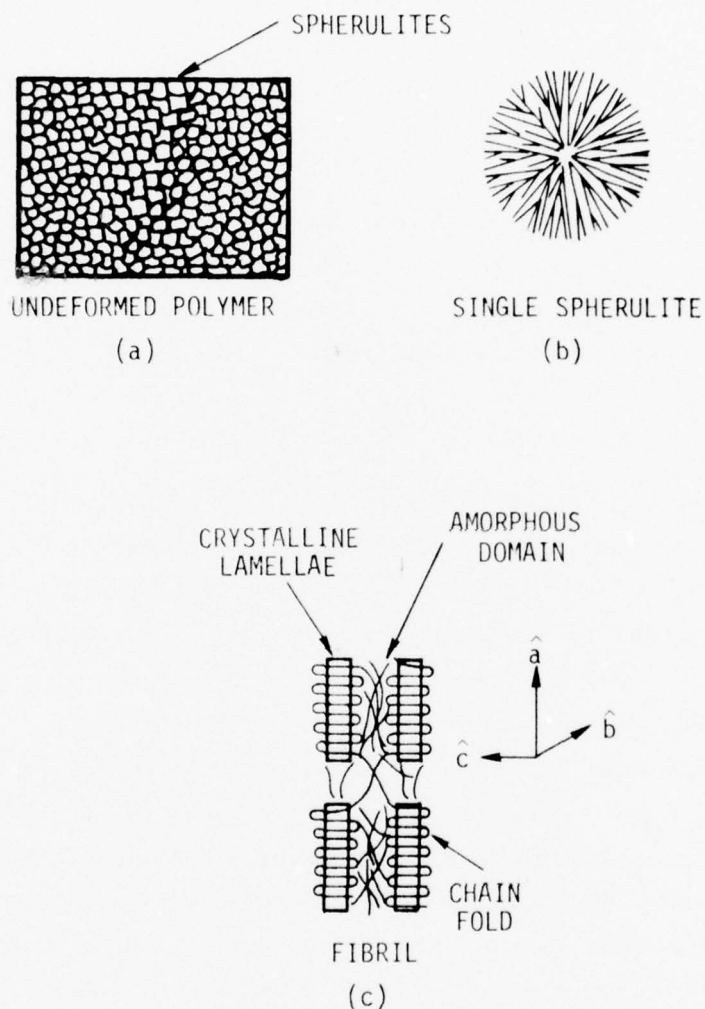
In this chapter, we first present a general description of the relevant features of the morphology of polyethylene to provide a background for discussion of the results of the radiation-induced and thermally stimulated relaxation of samples of different species of this polymer. Basically, this material consists of the intermingling of domains of two phases, one is crystalline, the second amorphous.

The properties of a given kind of polyethylene are, to a good approximation, a weighted average of the properties of the crystalline and amorphous phases. The most important single parameter characterizing the state of the polymer is the determination of its relative degree of crystallinity, i.e., the weight fraction of the crystalline domains.

The third section of this chapter presents our data on the determination of the fractional crystallinity for the samples examined. Part of the relaxation of persistent internal fields is ascribed to molecular motion. Therefore, to correlate charge trapping or dipole alignment with morphology, a knowledge of those transitions at which significant molecular motion occurs is important. The fourth section of this chapter describes the relevant phase transitions in polyethylene which mark this molecular motion.

2.2 MORPHOLOGY OF POLYETHYLENE

The currently accepted model for the structure of polyethylene is that of a material comprising two phases (Refs 5 and 6). A schematic diagram showing the structure of the polymer is given in Figure 1. One phase is crystalline, in which the polymer chains are aligned in lamellae. The thickness of these lamellae are typically of the order of 100 to 300 Å. Each polymer molecule, whose extended length is an order of magnitude or more than this dimension, is typically folded back upon itself many times to form parallel chains in the same lamella (Figure 1c). The chain axes are perpendicular to the surface of the lamella. The polymer typically crystallizes about nucleation centers into spherical volumes which are denoted spherulites (Figure 1a). The lamellae are arrayed radially out from the nucleation center such that the normal to a lamella and to the axes of the polymer chains are perpendicular to the spherulite radii (Figure 1b). These radial chains are called fibrils. Between the lamellae are noncrystalline regions comprised of polymer chains that cannot enter into the crystalline lattice (Figure 1c). The molecular chains in the amorphous domains are arranged in random fashion characteristic of a glass below the glass transition temperature, T_g , and of a viscous liquid above T_g . The inability of a particular polymer chain to form part of the crystalline lattice may be due to the departure of all or portions of the



RT-15199

Figure 1. Schematic diagram showing (a) the gross structure of a polymer, (b) the fibril arrangement in a single spherulite, and (c) the orientation of lamellae and amorphous domains along a single fibril. The crystallographic axes are also shown. The radial direction of a fibril is parallel to the unit vector \hat{a} , while the surface of a lamella is perpendicular to the molecular chains which are parallel to the crystallographic axis \hat{c} .

polymer molecule from the structural regularity required for crystallization because of variation in molecular size, the presence of bulky side groups such as the ethyl (C_2H_5) or butyl (C_4H_9), or the presence of unsaturated bonds. It is evident that, the more highly branched the constituent polyethylene molecules are, the less efficient the molecular packing, and the less crystalline is the bulk polymer likely to be. As the dimensions of a molecule are much larger than the dimensions of a lamella or amorphous domain, one molecule may be part of several lamellae or amorphous regions. Molecules that pass through several domains serve to tie different parts of the spherulite together. The bulk polymer is comprised of contiguous spherulites, all of which have the same general structure (Figure 1a).

The polyethylene unit cell is orthorhombic, with dimensions $a = 7.40 \text{ \AA}$, $b = 4.93 \text{ \AA}$, and $c = 2.54 \text{ \AA}$. The \hat{a} axis is parallel to the spherulite fibril, while the \hat{c} axis is parallel to the polymer chains. Of course, the crystalline domains also contain lattice imperfections such as strains, vacancies, and dislocations, which may serve as trapping sites for space charges in the polymer.

Underlying the two-phase model is the assumption that each phase of the polymer has distinctive properties of its own which are largely independent of the presence of the other phase. The macroscopic properties of a randomly oriented polycrystalline polymer will thus be the result of the mixing of these phases. A given physical property, P , will be a weighted mean value for the property of the crystalline and amorphous states, P_c and P_a , such that

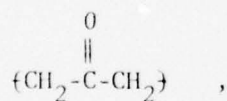
$$P = w_c P_c + (1 - w_c) P_a, \quad (1)$$

if w_c is the weight fraction of the polymer that is crystalline. The fact that many polymer measurements can be interpreted in terms of Equation 1 provides strong experimental support for the two-phase model. Properties that reflect this averaging include the specific volume, V , and the heat of fusion Δh_f , where $\Delta h_{fa} = 0$.

Another parameter by which crystallinity can be determined is the relative intensity of the sharp lines in a wide angle x-ray diffraction pattern with respect to the total intensity of the coherently scattered radiation, provided the crystallites are randomly oriented relative to the x-ray beam.

The first means of characterizing an inhomogeneous polymer such as polyethylene is therefore its fractional crystallinity w_c . As one objective of this program was to study the relationship between the ability of the model polymer polyethylene to store charge and its morphology, the determination of w_c for each sample was required. Thus, the samples chosen for examination show a reasonably wide variation in this parameter.

Based on a two-phase model, one can envision an entire spectrum of polyethylenes ranging from one that is totally crystalline to one that is completely amorphous. In practice, the range of crystallinities available in commercial polyethylenes is limited. Polyethylenes are commonly identified by density, which is a readily measurable property related to fractional crystallinity by Equation 1. The density of the material is a measure of the packing efficiency of its constituent molecules. It is evident that polymers in which there are few branches per unit chain will be most dense and most crystalline. The range of molecular structures found in a polymer reflect the conditions of polymerization. An ideal polyethylene molecule would have the structure $\{CH_2CH_2\}_n$ where n is a very large number of the order of 10^3 to 10^4 . In fact, real polyethylenes are characterized by a distribution of molecular weights (n variable), the presence of branching, i.e., ethyl (C_2H_5) or butyl groups (C_4H_9) pendant to the main chain, which make crystallization more difficult. Also present are impurities such as the polar carbonyl group



introduced by oxidation, and unsaturated bonds. These bonds include the vinylenes $\{CH=CH\}$ found in a main chain, vinyl ($CH_2=C$), located at the ends of chains, and vinylidene $\{CH=C\}$, found in side chains. The presence of such unsaturated bonds are significant, as they have been identified by Charlesby and co-workers (Ref 7) as sites for electron trapping.

Three general classes of polyethylenes are recognized (Ref 8): high-, medium-, and low-density. High-density polyethylenes ($d = 0.94 \text{ g/cm}^3 - 0.97 \text{ g/cm}^3$) are linear, highly crystalline (75 to 90%) polymers. The amount of

chain branching is low, typically less than seven ethyl or butyl branches per 1000 C atoms. Medium-density polyethylene ($d = 0.926 \text{ g/cm}^3 - 0.940 \text{ g/cm}^3$) and low-density polyethylene ($d = 0.910 \text{ g/cm}^3 - 0.925 \text{ g/cm}^3$) are more highly branched, having between 20 to 30 ethyl and butyl branches per 1000 C atoms.

The concentration of unsaturated bonds in one of these polymers is typically determined from its IR spectrum and reflects the particular polymerization process. Clearly, the concentration of pendant vinylidene groups in a linear high-density polymer will typically be much lower than that in more branched polymers. On the other hand, high-density polyethylenes often have relatively high concentrations of terminal vinyl groups. Typical concentrations of these groups for representative series of polyethylenes can be found in References 8 and 9. On the average, the number of double bonds per 1,000 carbon atoms that appear in both high- and low-density polyethylenes is of the order of 0.3 per 1000 C.

2.3 DETERMINATION OF FRACTIONAL CRYSTALLINITY

In order to study the dependence of stored charge effects on polymer morphology, three polyethylene samples were chosen. The first was a low-density film manufactured by Golden West Plastics (their type E1016). The second was a medium-density film from the same supplier (their type W703). The third polyethylene was a high-density film manufactured by the Atlantic Richfield Corporation (ARCO). Some data for the Golden West polymers with $T > 293^\circ\text{K}$ was reported in last year's Final Report (Ref 1).

The weight-fractional crystallinity, w_c , has been determined for the three types of polyethylene from their x-ray diffraction patterns, from their densities, and by measuring their heats of fusion. The results of these determinations are presented in Table 1. To check the consistency of these measurements, results are normalized to that of the low-density (LD) sample, E1016.

The mean weight-fractional crystallinity, w_c , is given by

$$w_c = (V - V_a)/(V_c - V_a) \quad (2)$$

for a sample of specific volume, V , equal to the reciprocal density, d^{-1} , comprising amorphous domains with $V_a = d_a^{-1}$ and crystalline domains, where $V_c = d_c^{-1}$. The values of V_a and V_c as a function of temperature have been determined for polyethylene. At 20°C, these are $V_a = 1.171 \text{ cm}^3/\text{g}$ and $V_c = 1.003 \text{ cm}^3/\text{g}$ (Ref 9). The values of w_c determined for the three polyethylene samples studied, based on their densities, are given in Table 1. The film densities have been supplied by the manufacturers.

TABLE 1. FRACTIONAL CRYSTALLINITY OF POLYETHYLENE SAMPLES

	GW E1016	GW 703	ARCO
Density (g/cm^3)	0.922	0.935	0.950
w_c (Eq. 2)	0.51	0.60	0.71
$(1-w_c)/[(1-w_c)_{LD}]$	1	0.82	0.69
Heat of fusion, Δh_f^* (cal/g)	28.6	34.6	48.0
w_c (Eq. 4)	0.41	0.50	0.69
$(1-w_c)/[(1-w_c)_{LD}]$	1	0.85	0.53
Normalized coherent x-ray amplitude for $2\theta = 18^\circ$	1	0.87	0.61

The second method by which sample crystallinity was determined was through the measurement of the heat of fusion of each sample. According to Wunderlich (Ref 10), the specific heat at constant pressure, c_p , of a sample with a weight-fractional crystallinity, w_c , is

$$c_p = w_c c_{pc} + (1-w_c) c_{pa} + \left[\frac{dw_c}{dT} \right] \Delta h_f, \quad (3)$$

where c_{pa} and c_{pc} are the specific heats at constant pressure for the amorphous and crystalline materials and $\Delta h_f = 69.4 \text{ cal/g}$ is the heat of fusion of polyethylene (Ref 11). The contribution of the third term is significant only in the temperature region where melting occurs. By an appropriate choice of

baseline, one tries to eliminate the contributions of the amorphous and crystalline heat capacities to c_p near melting. Then

$$w_c = \Delta h_f^* / \Delta h_f \quad , \quad (4)$$

where Δh_f^* is the measured heat of fusion. The most common choice of a baseline for eliminating the contribution of specific heat (i.e., the first two terms in Equation 3) is typically chosen to be the extrapolation of the DSC curve above the melt to the temperature region below, as shown in Figure 2. Since $c_{pc} < c_{pa}$, such a procedure tends to underestimate the value of the heat of fusion. The error is more significant in samples of lower crystallinity where melting occurs over a wide range of temperatures. In fact, a glance at Table 1 reveals that crystallinity values determined by DSC are lower than those determined by density. As expected, the discrepancy diminishes as the sample crystallinity increases.

For determination of crystallinity by x-ray diffraction, both a film and a diffractometer recording was made of the Debye-Scherrer diffraction pattern for each of the films studied. The most accurate determination of crystallinity is based on measuring the relative intensity of the narrow lines in the wide-angle scattering curves due to Bragg scattering from lattice planes in the crystalline domains to the total coherent scattering intensity (Ref 12). The balance of the coherent scattering intensity other than from peaks comes from the diffuse diffraction from amorphous domains and from defects. In a careful analysis, the observed intensities must be corrected for effects connected with the measurement process, which include x-ray absorption in the sample, normalization to equal numbers of scattering centers, which is proportional to the surface density of the samples, change in intensity due to polarization of the beam on reflection, and a background due to incoherent Compton scattering (Ref 12). Moreover, the real departure of polymer morphology from an idealized two-phase model is also reflected in the observed broadening of the diffraction patterns and serves to diminish the magnitude of the crystalline peaks. These imperfections are of two kinds: those in which the size of the disorder is small relative to the dimensions of long-range order (i.e., crystallite size), which includes the thermal vibrations of the lattice and imperfections such as defects or dislocations, and those which disturb the long-range order of the

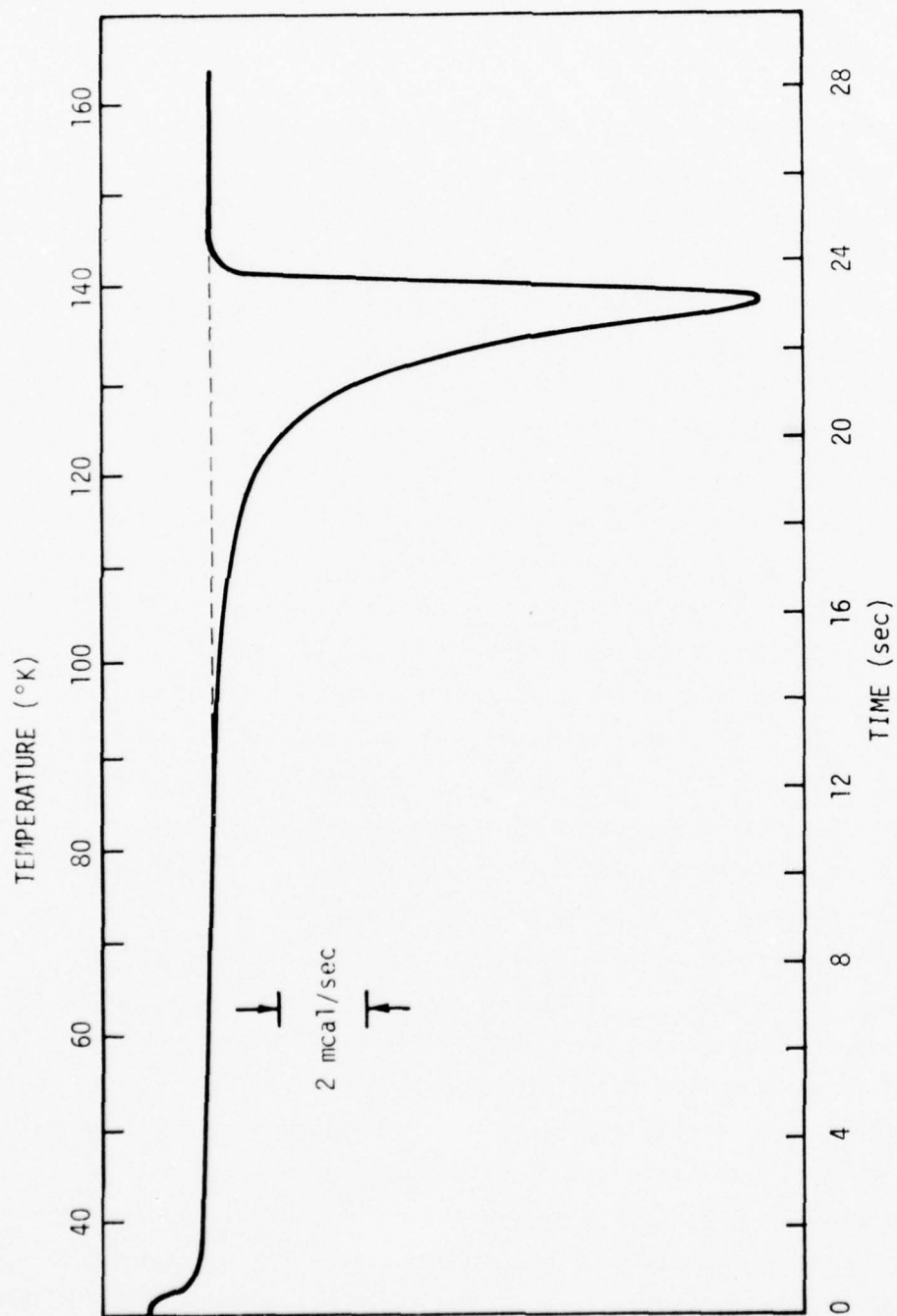


Figure 2. Differential scanning calorimetric (DSC) plot of heat absorbed as a function of temperature for an ARCO high-density polyethylene film. The dashed line is the baseline described in text.

polymer as manifest in paracrystalline domains in which lattice planes are misaligned. An equally serious practical problem arises from the fact that partial alignment of the crystallites through processes such as uniaxial or biaxial orientation during manufacture changes the Debye-Scherrer pattern. In consequence, the observed dependence of the scattered intensity displays an azimuthal variation which must be accounted for in an analysis of relative intensities of the crystalline peaks and amorphous halo (Ref 13).

Debye-Scherrer diffraction patterns were obtained for each of the three kinds of polyethylene. The x-ray source was obtained from a Cu target filtered by Ni. The principal component of the x-radiation is thus the K_{α} line of Cu at 1.5418 Å. Both a film record and a diffractometer tracing were obtained for each sample. Unfortunately, they covered only a limited range of azimuthal angles. Subsequent examination of the film showed evidence of crystallite orientation, probably due to stretching during manufacture.

Because the complete Debye-Scherrer pattern was not available for each sample, the relative crystallinity of the three polyethylenes was determined by an adaptation of a procedure developed by Krimm and Tobolsky (Ref 14). The relative intensity of each diffractometer trace was determined at $\theta = 9^{\circ}$. This corresponds to the major peak in the coherent amorphous scattering intensity and contains a negligible contribution from scattering by crystallites. The intensities were normalized to correct for the differences in the sample thickness. The correction for self absorption of the x-ray beam in these samples was insignificant. Since all the data were read at the same angle, no correction was needed for polarization of the beam by the samples. No correction was made for the contribution to the total scattered intensity for incoherent scattering, which was presumed small (see Figure 3 of Ref 14). Based on the diffractometer data, the relative amounts of amorphous material in the three samples were 1:0.87:0.61 for the low-medium-, and high-density polyethylenes, respectively. These ratios are 1:0.82:0.69 from the density data and 1:0.85:0.53 from the heat of fusion measurements and thus are in reasonable accord with each other, given the degree of sophistication of the analysis. In fact, it is well known that the degree of crystallinity determined for a material is a function of the measurement process. It is probably more meaningful to speak of the relative crystallinity of a series of samples as we have done (Ref 15).

From the width of the x-ray diffraction peaks, one can obtain a lower limit on the size of the crystallites from the Scherrer relationship (Ref 16). The mean dimension of crystallites normal to the plane (hkl) is

$$L_{hkl} = A/(\delta S)_s \quad , \quad (5)$$

where A is a geometry-dependent constant of order 1 and $(\delta S)_s$ is the full width at half maximum of a peak in units of the reciprocal space vector

$$S = 2 \sin \theta / \lambda \quad (6)$$

such that

$$L_{hkl} = \frac{A\lambda}{2 \sin \theta \delta \theta} \quad (7)$$

in terms of the diffraction angle θ . The observed peaks are broadened both by the effect of finite instrumental resolution and by the distortion of the lattice (i.e., uneven spacing between planes). No analysis was made on the magnitude of these effects, which tend to make the apparent crystallite size smaller than their actual size. The observed full width at half maximum of the (110) line at $\theta = 10.7$ degrees is 0.25 degree for the low-density sample, 0.22 degree for the medium-density sample, and 0.20 degree for the high-density sample. These lead to lower bounds of the crystallite size in the direction perpendicular to the (110) plane of polyethylene of 180, 204, and 224 Å, respectively.

2.4 CORRELATION OF MORPHOLOGICAL FEATURES OF POLYETHYLENE WITH PERSISTENT INTERNAL FIELDS

An important objective of this study was the correlation of morphological features of the model polymer with its ability to store space charge/polarization. To do this, the technique of measuring the TSC spectra as a function of temperature was adopted. This technique has been shown to be especially sensitive in detecting the molecular motions that accompany the release of charge from trapping sites in polymers.

We now present a brief description of the possible trapping sites for stored charge/polarization in polyethylene and how they may be affected by molecular motion.

The origin of persistent polarization in polymers lies in the alignment of polar functional groups attached to the polymer chains. At sufficiently low temperatures, this alignment is stable, because no molecular motion can occur to cause disorientation. If the sample temperature is subsequently raised, the ensuing molecular motion at characteristic temperatures marking phase transitions relaxes the polarization with the release of image charge from the capacitor electrodes. As we demonstrated last year (Ref 2), one may observe a correlation between peaks in the TSC spectrum and transition temperatures which are quite pronounced in polar polymers. In such polymers, dipole orientation is the major contributor to the persistent internal fields. The second component for creating internal fields in polymers is the trapping of space charge. The most comprehensive classification of potential trapping sites for persistent charge in polymers has been given by Perlman (Ref 17), which is largely based on the work of Boustead and Charlesby (Ref 7), who measured the thermoluminescent spectra of gamma-irradiated polyethylenes as a function of temperature. While concrete evidence for specific trapping sites is not well established, the classification is heuristic. Primary trapping sites are associated with individual atoms and bonds. These sites include unsaturated bonds such as the vinyl ($\text{CH}=\text{CH}_2$), vinylenes ($\text{CH}=\text{CH}$), and vinylidene ($\text{CH}_2=\text{C}$) groups. In polyethylene, these occur at the ends, in the middle, and on branches of the main chain, respectively. There are comparable groups in Teflon in which the hydrogen atoms are replaced by those of fluorine. Secondary trapping sites include the volume between neighboring chains that are themselves bound together by van der Waals forces. One might also include here defects or voids caused by misalignment of chains, regions of large free volume in the amorphous domains, and add at chain folds in the crystalline lamellae. Tertiary trapping sites include the boundaries between crystallites or at the interfaces between crystalline and amorphous domains.

Aside from the familiar detrapping that takes place because of thermal activation, detrapping is also believed to occur because molecular motion

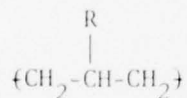
destroys the trapping sites. It has been argued that detrapping of charges located at primary sites occurs at the lowest temperatures, below the glass transition temperature (T_g), as destruction of such sites involves the motion of relatively small groups of atoms. Sites of the second type will tend to be disrupted at temperatures comparable to T_g , at which motion of large chain segments relative to each other occur. Destruction of tertiary sites only occurs at temperatures above T_g , as the onset of melting is approached. At these temperatures large-scale motion of entire polymer chains relative to one another occurs. This regime is also marked by a rapid rise in the polymer conductivity.

Polyethylene, because of its apparent structural simplicity, has often been used as a model polymer to study molecular motions in these materials. However, even this polymer has a highly complex structure, as was discussed in the second section of this chapter entitled "Morphology of Polyethylene". Because this polymer typically contains two distinct phases, the variety of structural motion observed is quite complex. Two general classes of phase transitions occur. One observes normal first-order transitions that represent change of state. An example of such a transition is the melting of the crystalline domains of the polymer, which for single-crystal, linear polyethylene occurs at about 410°K. Polytetrafluoroethylene (Teflon TFE) shows, in addition to crystalline melting, a change in its crystalline order between 391 and 403°K. Polymers that contain an amorphous phase, such as polyethylene, also undergo a set of quasi-second-order transitions in their amorphous phase which involves the molecular motion of increasingly large sections of the polymer chains. In these transitions, state variables such as volume or entropy are constant, but the derivatives with respect to such variables of the state functions change discontinuously; i.e., the specific heat or the coefficient of expansion are discontinuous. It is difficult to specify precisely where these transitions occur, as they are very dependent on the method used to detect them and especially the frequency of the molecular motion that the technique probes.

Three transitions are identified in polyethylene (Ref 18). The gamma transition, which typically appears at 143 to 153°K, is ascribed to the crankshaft rotation of portions of the polymer chain $(CH_2)_n$, where n is ≈ 4 . There

is evidence that this transition can be observed at temperatures as low as 128°K with low-frequency mechanical measurements (<0.1 Hz). It is to be noted that TSC measurements carried out at rates $\sim 1^\circ\text{K}/\text{minute}$ have a resolution comparable to mechanical or electrical (dielectric loss) measurements at frequencies ($<10^{-2}$ Hz) (Ref 19). There is some disagreement as to whether the gamma transition is the principal amorphous transition--the glass transition. The latter marks the onset of large-scale coordinated chain motion in the amorphous phase about the chain axis. It is usually so described. Evidence presented in Reference 18 by Boyer points to $T_g \sim 188^\circ\text{K}$, which is not resolved in typical measurements. It is significant that the TSC spectra of oxidized low-density polyethylenes do not show such a peak. However, Fischer and Röhl (Ref 20) claim that the spectra for $T < 300^\circ\text{K}$ can be represented by the sum of three Gaussian curves. Two of these are centered at 138°K and 245°K, respectively, near the gamma and beta transition for this polymer. The third is located at $\sim 200^\circ\text{K}$ close to the theoretical glass transition temperature.

The precise molecular motions marking the beta transition that is observed at 243 to 253°K are also in dispute. The most careful assessment of available data implies that this transition is due to the crankshaft motion of regions of the polymer chain containing branches of the type



where R is a side group or branch such as an ethyl (CH_3CH_2) or butyl ($\text{CH}_3\text{CH}_2\text{CH}_2$) group present in large numbers in low-density polyethylenes.

The third commonly identified transition in polyethylene (denoted α), which appears at 333 to 353°K, is ascribed to the motion of entire polymer chains in the amorphous domains and hence will be most strongly present in the less crystalline species of this polymer. The presence of an α transition in the polyethylenes studied in this work was marked, as expected, by discontinuities in the slope of the DSC spectrum that become more pronounced as the sample crystallinity diminished. The small size of the slope change in the polymers studied prevented a highly accurate determination of the location of the α

transition. We estimate that this transition occurs between 322 to 343°K in the low-density polymer, between 322 to 349°K in the medium-density sample, and between 326 to 339°K in the high-density sample.

Because one polymer chain may connect several amorphous and crystalline domains (cf. Figure 2), during the α transition, cooperative motion of chain segments in the crystalline domains must also occur, which leads to disruption of the crystalline order. In addition, the phenomenon of premelting, which involves motion of chains in the crystalline domains is known to occur. As is evident from the specific heat curve for the high-density polyethylene (Figure 2), the melting of this polymer is not sharp, but occurs over a wide temperature range of 378 to 407°K. The DSC spectra for the low- and medium-density samples show that significant melting in them occurs from 377 to 397°K and 373 to 405°K, respectively.

3. THERMALLY STIMULATED CURRENT MEASUREMENTS IN POLYETHYLENES

3.1 INTRODUCTION

In this chapter are presented the results of the thermally stimulated current (TSC) measurements carried out on a series of polyethylenes configured as capacitors of size ~ 100 nF, in which persistent space charge/polarization was introduced consequent to burn-in. These measurements were carried out for three reasons. First, they were intended to bound the amount of charge release to an external circuit as a consequence of the thermally induced relaxation of the internal polarization fields. Second, they were designed to determine whether the mechanisms responsible for persistent charge/polarization could be related to particular features of the polymer structure. Here the intent was to look for correlations between significant features in the shape of the TSC spectrum and those temperatures at which a significant molecular motion or structural reorientation takes place. Third, they were conducted to provide data to assess whether the current released by a thermally stimulated relaxation of a sample was comparable to that released in the radiation depolarization of the same sample charged in an identical manner. Last year evidence for such a correlation was found (Ref 2), indicating that the thermal response of a metal-polymer dielectric system containing a stored charge could be related to its radiation response. Such a correlation, if substantiated, would permit assessment of the response of capacitors or cables containing persistent charge/polarization with minimal radiation testing.

The means by which the TSC measurements were carried out is discussed briefly. Next, the characteristics of the samples are described. Finally, representative TSC data for the three types of polyethylene studied are presented. In order to assess the final charge state in a dielectric after irradiation, TSC spectra were obtained for many of the samples exposed to electron irradiation. These data are described in the fourth chapter of this report, which describes the radiation depolarization measurements.

3.2 EXPERIMENTAL TECHNIQUE

A detailed discussion of the principle and practice of TSC measurements has been given in Reference 2. Therefore, the procedures used and changes made to the experimental setup for this year's work are only outlined.

Persistent polarization/space-charge fields are established in a sample by the simultaneous application of temperature and bias. The applied field will align those molecular dipoles that were mobile at the burn-in temperature. It also causes the motion and polarization of internal charges due to impurities that are mobile at the burn-in temperature. These charges will drift toward the electrodes, and many are stopped at phase boundaries (Ref 21). Because the polymers are inhomogeneous, Maxwell-Wagner or interfacial polarization also occurs. When a field is applied to such an inhomogeneous system, unequal conduction currents flow in the different phases (which have slightly different dielectric constants and conductivities) until equilibrium is reached. At equilibrium, the true current flowing across the phase boundaries becomes constant, and the displacement currents which cause charge buildup decay to zero.

Charging by burn-in is an example of heterocharging. The excess charge distributions are, for the most part, intrinsic and bipolar. Except at high fields or with imperfectly contacting electrodes, the amount of injected charge or homocharge, is probably quite small. Burn-in temperatures for these polymers were chosen to cover the regions around the important phase transitions in polyethylene that occur at approximately 148°K, 243 to 253°K, and 333 to 353°K. These second-order transitions are associated with significant coordinated motion of polymer chains.

After a burn-in time judged sufficient to reach an equilibrium state, which is characteristically of the order of one hour or more, the samples are cooled to a much lower temperature than that for burn-in, with the external bias still applied such that the molecular and charge motions responsible for creation of the internal polarization at the forming temperature cease. The space-charge distribution and dipole orientations are frozen in. The sample is then short circuited, which places an image charge on the electrodes in order to cancel the internal field. Nearly all of our measurements were taken with burn-in voltages, V_B , which yielded burn-in fields $-B$ across a sample of 100 kV/cm.

After the sample is shorted, the prompt component of the polarization field decays. These are processes which have activation energies corresponding to temperatures at or below the shorting temperature. This relaxation is typically complete after about an hour or so. The temperature of the sample is then raised at a constant rate (ramped). The external current evolved as a function of temperature is monitored in order to search for correlations between charge motion and molecular motion. This charge flow results from the net internal current (total solenoidal current) which flows inside the capacitor. This current flow is the result of the relaxation of molecular dipoles, the drift of excess space charge, and the motion of intrinsic carriers responsible for the normal conductivity of the dielectric. In those cases where persistent charge/polarization was not completely relaxed at the highest temperatures reached in the thermal ramp, which might be limited because of a desire to prevent irreversible damage to a sample, a further isothermal anneal was carried out at the highest temperature reached until the sample was completely relaxed or reached a state of constant current emission.

The electrometers and data measurement system used for these measurements were essentially the same as those employed in last year's work and described in Reference 2. In order to study the TSC behavior of the polyethylene samples over a wide range of temperatures that covered all of the significant phase transitions, the lowest of which is at $\sim 148^\circ\text{K}$, a new temperature bath was constructed which allowed samples to be cooled to temperatures below 100°K . The bath is shown schematically in Figures 3 and 4. In addition, a new thermal control unit for generating the temperature ramp was constructed. This unit employed a copper resistance thermometer as the reference sensor. Such an element was chosen because its rate of change of resistivity as a function of temperature is relatively constant over the range 100 to 400°K . This constancy simplified the linearization of its output as a function of temperature. In order to minimize temperature gradients across a sample, which was typically $1/8$ to $1/4$ inch thick, the bath itself was evacuated and filled with dry helium gas. Placing the polyethylene samples in such an inert atmosphere prevented oxidation of the polymer at elevated temperatures. Sample temperatures were monitored with a pair of Cu-Constantan thermocouples whose junctions were

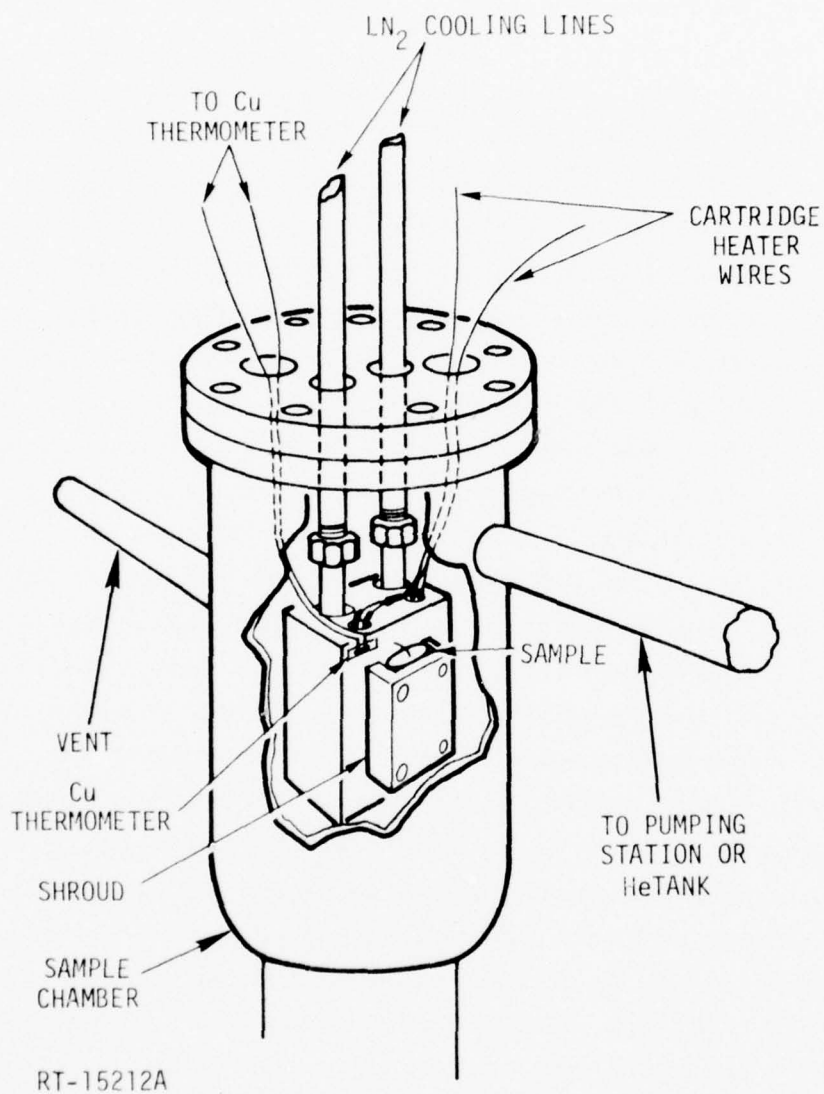


Figure 3. Temperature bath for carrying out TSC measurements in polyethylene samples. All wires were brought out through vacuum-tight feed-throughs. Both the inlet and the vent had high-vacuum valves on them. Leads from the sample are not shown in the drawing.

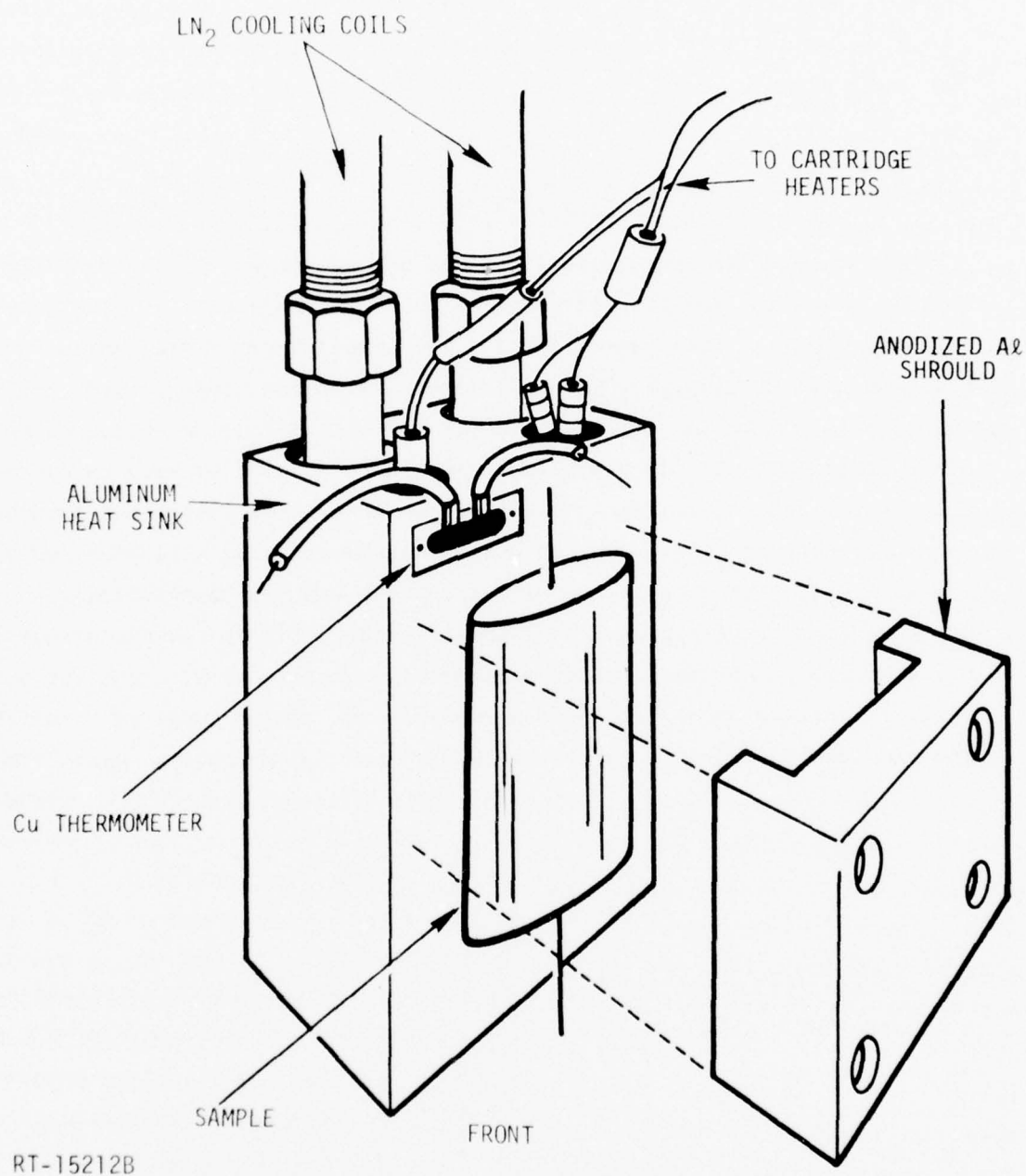


Figure 4. Detail of the sample chamber and heat sink. In operation, the heat sink and shroud were tightly wrapped in annealed Cu foil to minimize heat gradients.

wrapped in Teflon tape to match their response to that of the sample. One junction was placed on each side of the sample. The thermocouples were calibrated at fixed temperature points from 77.35 to 373°K and were accurate to better than 0.5°K over the entire measurement range. For most of a temperature cycle which typically ranged from 100 to 380°K for polyethylene, the temperature gradient across a sample was about 1 to 2 degrees, except at the lowest temperatures reached, where the gradient was sometimes as large as 10°K for a thick sample. Such a gradient was not as serious as might be imagined, for little TSC is emitted below 110°K.

The characteristics of the polyethylene capacitors examined are given in Table 2. They were configured as capacitors of ~100 nF. Metalized electrodes of aluminum were evaporated onto one side of 10-foot pieces of film, about 1-1/4 inches wide. The electrodes were about 10^3 Å thick, comparable to those placed on commercial metalized capacitors. Care was taken to avoid the heating of a film during the deposition by heat-sinking that portion of the film being metalized. Capacitors were constructed by winding together two strips of film, one on top of the other, on a thin, flat Teflon-TFE form. The metalization of each strip was on the same relative side (e.g., face up), so that the ensuing structure had alternate layers of metalization and film. Electrodes were brought out two ways. In one, aluminum foil tabs of 1-mil thickness were interleaved with the film. The ends of these tabs were spot-welded together. This yielded a capacitor with a low dissipation factor. Samples with foil tab contacts have the letter T in their identifying code in Table 2. These capacitors were somewhat fat because of the inserted metal tabs which also left small gaps between alternate layers of film. Therefore, a second method for making samples that is similar to that used in the manufacture of commercial metalized capacitors were also tried. In it, the metalization was brought out to one edge of a film strip. The films were then wound with metalized edges of alternate layers on opposite sides of the capacitor. Leads were attached to the samples with high-temperature conducting epoxy (Emerson & Cummings, Type 56C) placed on the end of each sample. This arrangement made capacitors with reasonably low dissipation factors that were appreciably thinner than those with inserted tabs. However, after repeated thermal

TABLE 2. POLYETHYLENE CAPACITOR CHARACTERISTICS

Film Properties	Sample	Surface Area (cm ²)	C (nF) (at 1 kHz)	D x 10 ⁴ (at 1 kHz)
Arco HD d = 0.950 w _C = 0.70 t = 9.3 μm κ = 2.34	HDT1A	947	207-215	8
	HDE1	890	198.2	8
	HDE2	891	198.6	23
	HDE3	1091	242.9	11
	HDT1B	991	221-239	5-50
	HDT2	778	173-176	10-0
GW E1016 d = 0.922 w _C = 0.46 t = 20.7 μm κ = 2.28	LDT1	791	77.2	5
	LDT4	898	91-84	6-5
	LDE6	909	88.7	131
	LDE11	731	71.3	47
	LDE10	1137	111	495
	LDT4	946	92.3	11
	LDT6	1027	100.2	18
GW W703 d = 0.935 w _C = 0.55 t = 32.5 μm κ = 2.30	MDT1	901	56.3-53.6	0.7
	MDT2	1063	65.7-68.5	0
	MDT2	767	48	7
	MDT3A	960	60.5	5
	MDT5	887	55.6	8
	MDT4B	1647	102.9-104.9	7-0
	MDT3B	1300	81.5-80.9	21-2
	MDT4A	995	62.5	5

cycling, the epoxy tended to separate from the film. This covered a marked increase in the dissipation factor of the capacitor. The state of a sample was monitored by measuring its capacitance and dissipation factor on an HP 4270A Automatic Capacitance Bridge before and after each run at a frequency of 1 kHz.

3.3 DESCRIPTION OF THE TSC DATA ON POLYETHYLENES

A quantitative summary of the TSC measurements on the three types of polyethylenes is presented in Tables 3 through 5. These tables contain information on the burn-in conditions, e.g., the burn-in temperature T_B and forming time t_B . Except where noted, the burn-in voltage, V_B , across each sample was chosen to yield an applied field of 100 kV/cm. Also included is the range of temperatures over which each sample was cycled and the temperature at which a consequent isothermal anneal was carried out. Significant features of each TSC spectrum, such as a peak, a shoulder, or a minimum ($i < 0$), are also listed. Thermally stimulated currents are defined as positive if they flowed from the electrode which was at the higher potential during burn-in to that at ground, and conversely. To facilitate a comparison between samples of different capacitance or samples that were burned in under different applied fields, the net charge released, Q_T , has been expressed as a nondimensional parameter, κ_T , where

$$\kappa_T \equiv \frac{Q_T \kappa}{C V_B} = \frac{1}{\epsilon_0} \cdot \frac{Q}{A} \cdot \frac{t}{V_B} = \frac{1}{\epsilon_0} \cdot q \cdot \frac{1}{E_B} \quad (8)$$

for a sample of capacitance C , surface area A , and a dielectric thickness t , with a relative dielectric constant κ , burned in under an applied voltage V_B corresponding to a field $E_B = V_B/t$. To convert to total charge release, or, more significantly, charge per unit area (q), one can use Equation 8 and the sample parameters given in Table 2. We have shown separately for each run (1) the net charge released during the temperature ramp at constant rate $\kappa_T(\text{Ramp})$, (2) the net charge released during the consequent isothermal anneal $\kappa_T(\text{Isothermal})$, and (3) the total charge released $\kappa_T(\text{Total})$ by the thermal anneal.

TABLE 3. SUMMARY OF TSC DATA FOR HIGH-DENSITY POLYETHYLENE

Sample	T_B (°K)	t_B	Isothermal		TSC Peaks (°K)	κ_T (Ramp)	κ_T (Isothermal)	κ_T (Total)
			Anneal Temperature (°K)	Anneal Temperature (°K)				
HDT1A	90-102	15 h	106-388	392	125,347	2.2×10^{-5}		
	180	16 h	104-392	392	120?, 147, 196, 332	6.4×10^{-5}		
	300	16 h	105-392	392	150, 241, 328	2.0×10^{-2}	-2.1×10^{-3}	1.8×10^{-2}
	343	68 m	107-390	383	144, 243, 294?, 358	2.3×10^{-2}		
	343*	85 m	108-308	388	148.5, 242, ~295, 364	2.0×10^{-2}		
	343	16 h	107-393	383	148, 241, 295(n)	0.27	0.11	0.38
	392	77 m	101-400	400	~121, 146, 242, 298(n), 385	0.26	0.13	0.39
HDE1	One day after irradiation		297-388	389	350	0.815	0.57	1.38
HDE2	"	"	297-388	389		5.07×10^{-3}	4.2×10^{-3}	9.2×10^{-3}
HDT2	28 days after irradiation		299-389	387	359, 378	1.2×10^{-2}	-1.9×10^{-4}	1.2×10^{-2}
HDT1B	"	"	299-389	387		1.1×10^{-2}	1.56	1.57
HDE3	56 days after irradiation		296-424	410	360, 410	1.31	0	1.31

1. The symbol "?" denotes the probable presence of a peak at the temperature indicated. The symbol "~" denotes a broad peak centered at the temperature indicated. The symbol "n" denotes a current minimum where $i < 0$.

2. For all samples except that marked "**", $V_B = 93$ volts corresponding to 100 kV/cm. The exception had $V_B = 31.4$ volts corresponding to 33.0 kV/cm. Ramp rates were $1.9 \pm 0.05^\circ\text{K}/\text{minute}$.

TABLE 4. SUMMARY OF TSC DATA FOR MEDIUM-DENSITY POLYETHYLENE

Sample	T _B (°K)	t _B	Anneal Temperature (°K)	Isothermal Anneal Temperature (°K)	TSC Peaks (°K)	κ _T (Ramp)	κ _T (Isothermal)	κ _T (Total)
MDT4	105	65 m	105-380		122?	1 x 10 ⁻³		0.001
MDT4	180	60 m	105-376	581	125, 270, 340	7.5 x 10 ⁻³	5.9 x 10 ⁻³	1.1 x 10 ⁻²
MDT1	264	70 m	100-380		~129, 232, 295, 366	9.2 x 10 ⁻³	~0	9.2 x 10 ⁻³
MDT2	292	75 m	100-378		~127, 235, 292, 355, 368?	4.9 x 10 ⁻³	~0	4.9 x 10 ⁻³
MDT2	342	60 m	100-377	379	129, 235, 272, 364	9.2 x 10 ⁻³	1.9 x 10 ⁻³	1.1 x 10 ⁻²
MDT1*	340	81 m	100-375	380	125, 225, ~295, 340	7.8 x 10 ⁻³	5.1 x 10 ⁻³	1.1 x 10 ⁻²
MDT1	343	16 h	110-380		120, 235, 295, 350	2.4 x 10 ⁻²	0	2.4 x 10 ⁻²
MDT2	366	66 m	101-378	389	126, 241, 295(n), 340	2 x 10 ⁻²	5.5 x 10 ⁻²	3.5 x 10 ⁻²
MDT1	368	70 m	100-375	380	~122, 235, 305, 365	9.8 x 10 ⁻³	6.9 x 10 ⁻⁴	1.1 x 10 ⁻²
MDE2	One day after irradiation		297-388	389	327(n), 361	1.5 x 10 ⁻²	1.5 x 10 ⁻²	3.0 x 10 ⁻²
MDE5	"	"	297-388	389	362-373(sh)	3.2 x 10 ⁻³	7 x 10 ⁻⁴	3.9 x 10 ⁻³
MDT4	28 days after irradiation		299-389	387	366?	1.3 x 10 ⁻²	1.5 x 10 ⁻²	2.8 x 10 ⁻²

TABLE 4 (Continued)

Sample	T_B (°K)	t_B	Anneal Temperature (°K)	Isothermal Anneal Temperature (°K)	TSC Peaks (°K)	κ_T (Ramp)	κ_T (Isothermal)	κ_T (Total)
MDT3	28 days after irradiation		299-389	387	353	1.92×10^{-1}	5×10^{-2}	2.22×10^{-1}
MDE3	56 days after irradiation		296-424	410	368,414	2.5×10^{-3}	3×10^{-2}	3.2×10^{-2}

1. The symbol "?" denotes the probable presence of a peak. The symbol "sh" denotes a shoulder, while the symbol "n" denotes a minimum with $i < 0$. The symbol "o" denotes a broad maximum whose center is approximately at the temperature given.

2. All samples were burned in at $V_B = 525$ volts corresponding to $E_B = 100$ kV/cm, except for the run marked "**", where $E_B = 65.4$ kV/cm. The ramp rate was $1.9 \pm 0.05^\circ\text{K/minute}$.

TABLE 5. SUMMARY OF TSC DATA FOR LOW-DENSITY POLYETHYLENE

Sample	T_B (°K)	t_B	Anneal Temperature (°K)	Isothermal Anneal (°K)	TSC Peaks (°K)	κ_T (Ramp)	κ_T (Isothermal)	κ_T (Total)
LDT4	180	67 m	102-375	385	122, 180(s)	5.3×10^{-3}	4.1×10^{-3}	9.4×10^{-3}
LDT4	297	69 m	104-381	381	122, 234, 305(s)	1.57×10^{-2}	1×10^{-3}	1.67×10^{-2}
LDT1	343	76 m	100-382	378	122, 238, ~305, 358	2.6×10^{-2}		
LDT4	343.4	12.2 h	105-381	381	~125, 235, 315?, 355?, 355	1.5×10^{-2}	8.9×10^{-3}	2.4×10^{-2}
LDT4	343.4	16 h	106-396		121, 235, ~307, 339, 351	4.6×10^{-2}		
LDT4	343.4	16.8 h	104-380	380	128, 234, 339	3.8×10^{-2}	2.9×10^{-2}	6.7×10^{-2}
LDT4	358	60 m	110-381	381	124, 232, 305(s)	1.8×10^{-2}	1.9×10^{-3}	2.0×10^{-2}
LDT4	368	75 m	100-385	373-383	120, 235, 295?, 340	1.7×10^{-2}	6.5×10^{-4}	1.8×10^{-2}
LDE11	65 days post irradiation		299-404		375(n), 394	-4.1×10^{-3}		-4.1×10^{-3}
LDE10			299-404		360, 393?	3.8×10^{-3}		3.8×10^{-3}
LDT4	"	"	299-404		344(n)?, 373?, 392(n)	-5.1×10^{-3}		-5.1×10^{-3}
LDT6	"	"	299-404		~337(n)?, 364, 385(n)	-1.1×10^{-3}		-1.1×10^{-3}

1. The symbol "s" denotes a shoulder in the TSC spectrum. The symbol "?" denotes the probable presence of a peak at this temperature. The symbol "n" denotes a broad maximum whose center is approximately at the temperature indicated. The symbol "n" denotes a minimum ($i < 0$).

2. For all samples $V_B = 207$ volts corresponding to $E_B = 100$ kV/cm. The ramp rate was $1.9 \pm 0.05^\circ\text{K}/\text{minute}$.

In Figures 5 through 9 the TSC spectra for the ARCO high-density film for different burn-in temperatures is shown to demonstrate the change in the general shape of these spectra as a function of this important parameter. The TSC for the other polymer shows similar trends with temperature; we have therefore shown only four representative spectra for the low- and medium-density films in Figures 10 through 13.

Some general remarks may be made about the shape of the TSC spectra. As long as the burn-in temperature is sufficiently high ($T_B \geq 250^\circ\text{K}$ or so), all samples show two peaks at ~ 122 to 138°K and ~ 232 to 238°K . The polarity of this current flow was always positive. For a given sample, the magnitude, shape, and location of these peaks remain relatively constant for higher burn-in temperatures if the applied field is kept constant. The amount of charge released in that portion of the spectrum with $T < 275^\circ\text{K}$ is proportional to the applied burn-in field. If T_B is diminished below 250°K , the magnitude of the higher of the two peaks diminishes and its centroid shifts toward lower temperatures (Figure 6). At sufficiently low temperatures, this peak essentially vanishes (Figure 5). A similar diminishing in the size of the lower of these two peaks is also observed at the lowest burn-in temperature (Figure 5). If T_B were sufficiently low, this peak would also vanish. Fischer and Röhl (Ref 20) have observed the same behavior as a function of burn-in temperature in a series of low-density polyethylenes. We have shown that these peaks are present not only in low-density polyethylene but also in the medium- and high-density varieties. Although we have only examined a limited range of samples, there appears to be no correlation between the size of these peaks and sample crystallinity.

The appearance of the high-temperature portions of the TSC spectra for our samples show much less regularity. Generally, two patterns were apparent. In one, which we call Type I, there was evidence of a relatively small but sharp peak at $\sim 300^\circ\text{K}$, which often was accompanied by reversal; i.e., the flow of negative current if the burn-in temperature was less than that of this peak (Figures 5 and 6). Also evident was a peak at ~ 340 to 360°K . The location of both of these peaks was relatively insensitive to the burn-in temperature. However, their amplitude increases as T_B is increased (cf. Figures 7 and 8).

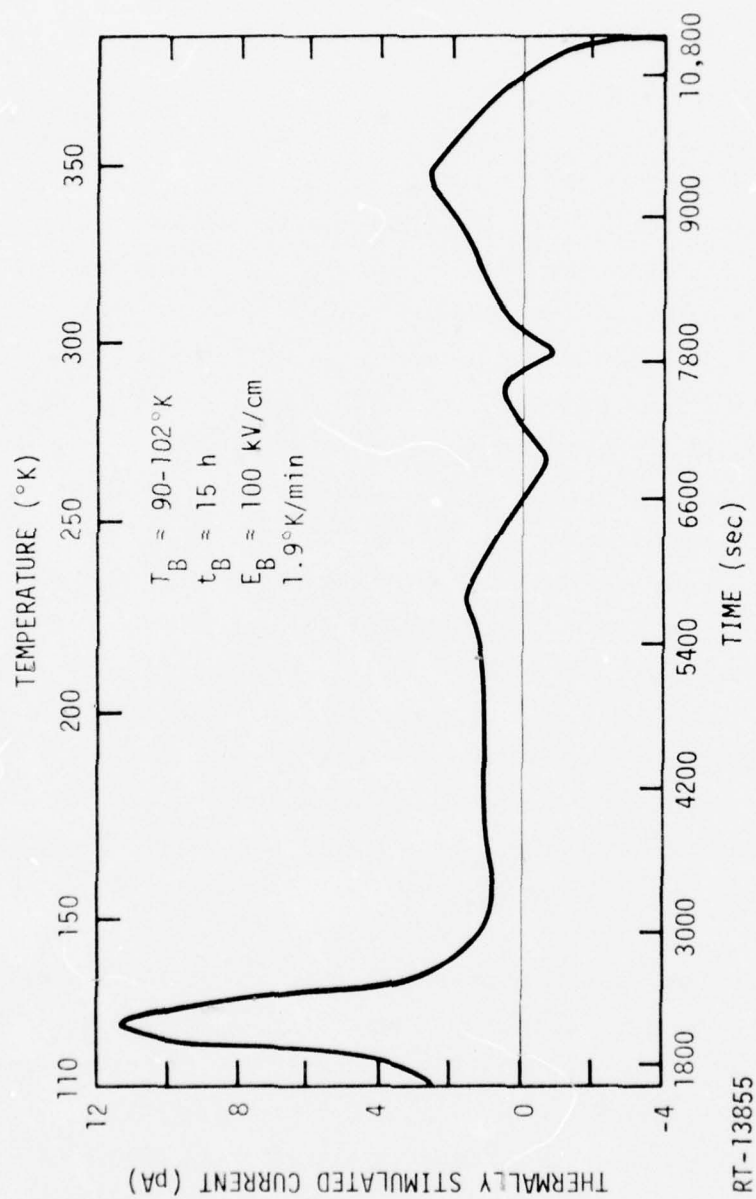


Figure 5. TSC spectrum of ARCO HD polyethylene burned in at 90 to 102°C

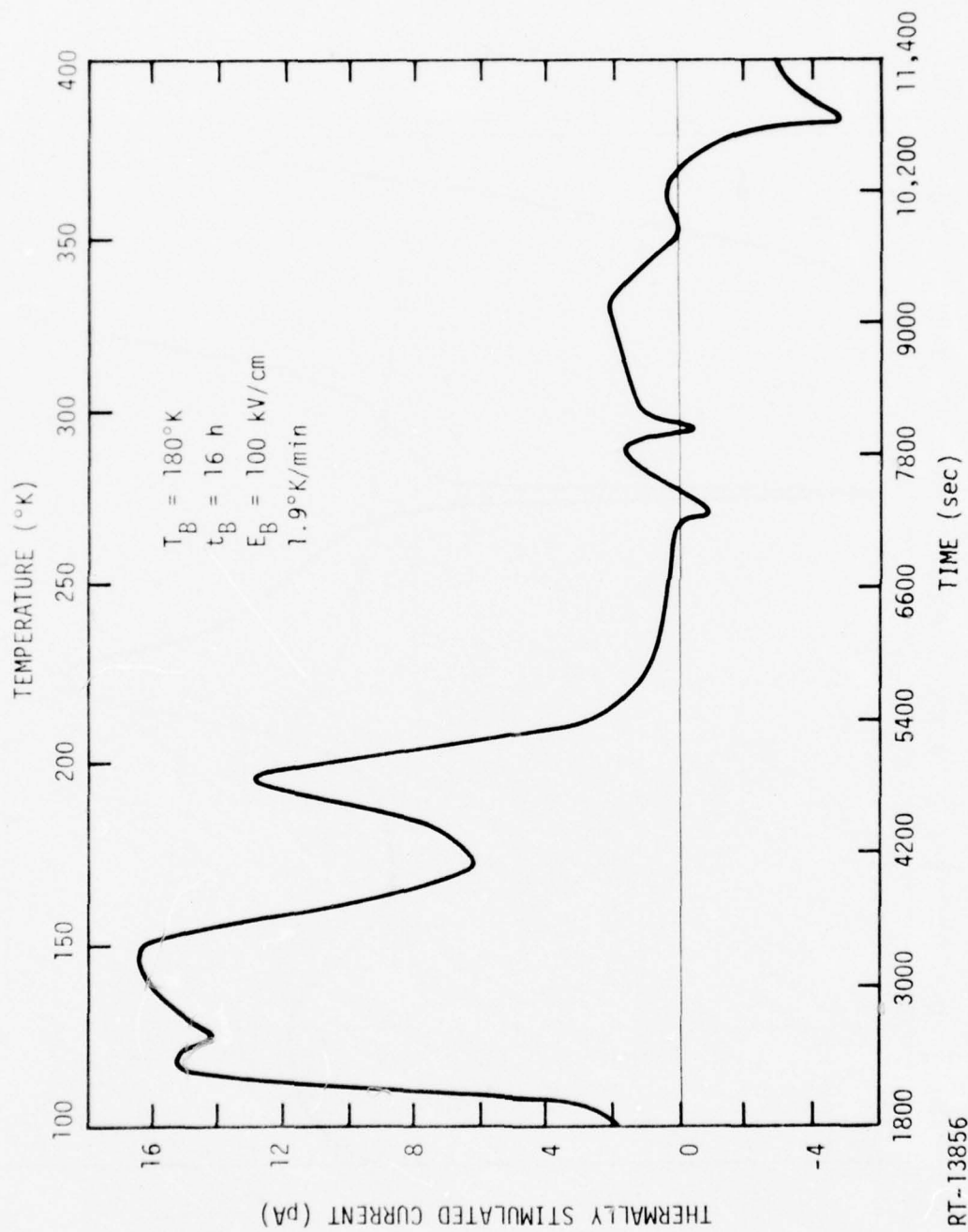


Figure 6. TSC spectrum of ARCO HD polyethylene burned in at 180°K

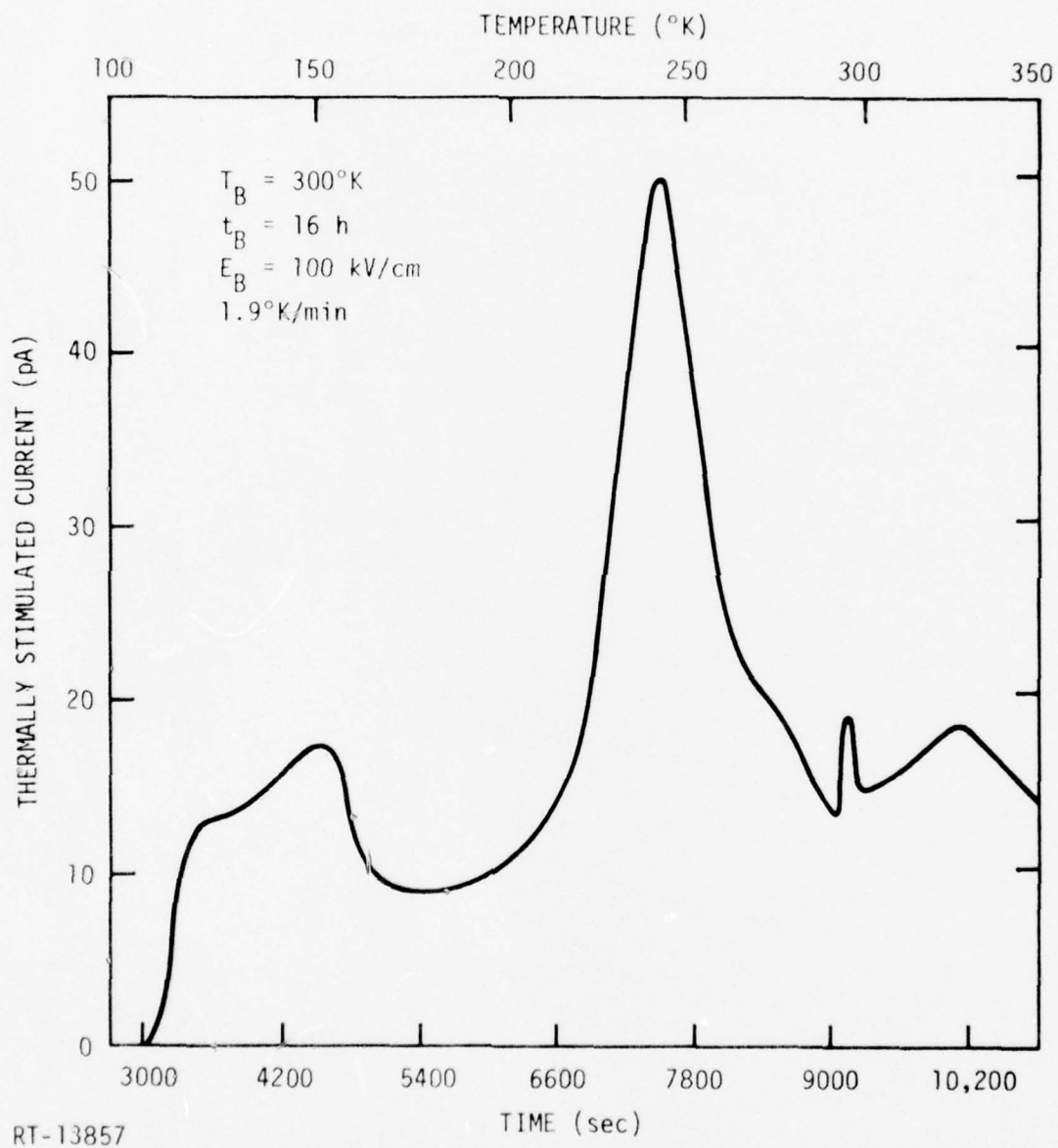


Figure 7. TSC spectrum of ARCO HD polyethylene burned in at 300°K

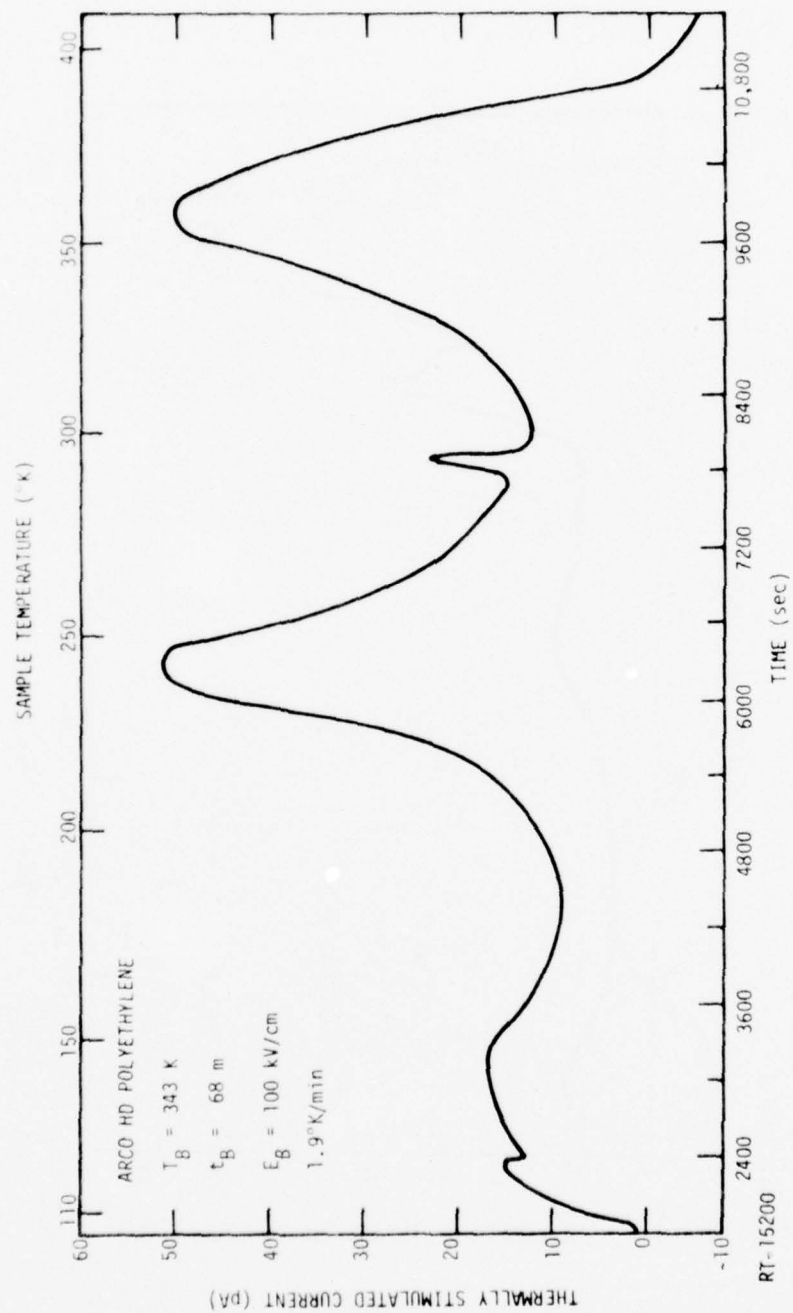


Figure 8. TSC spectrum for a HD polyethylene burned in at 343°K

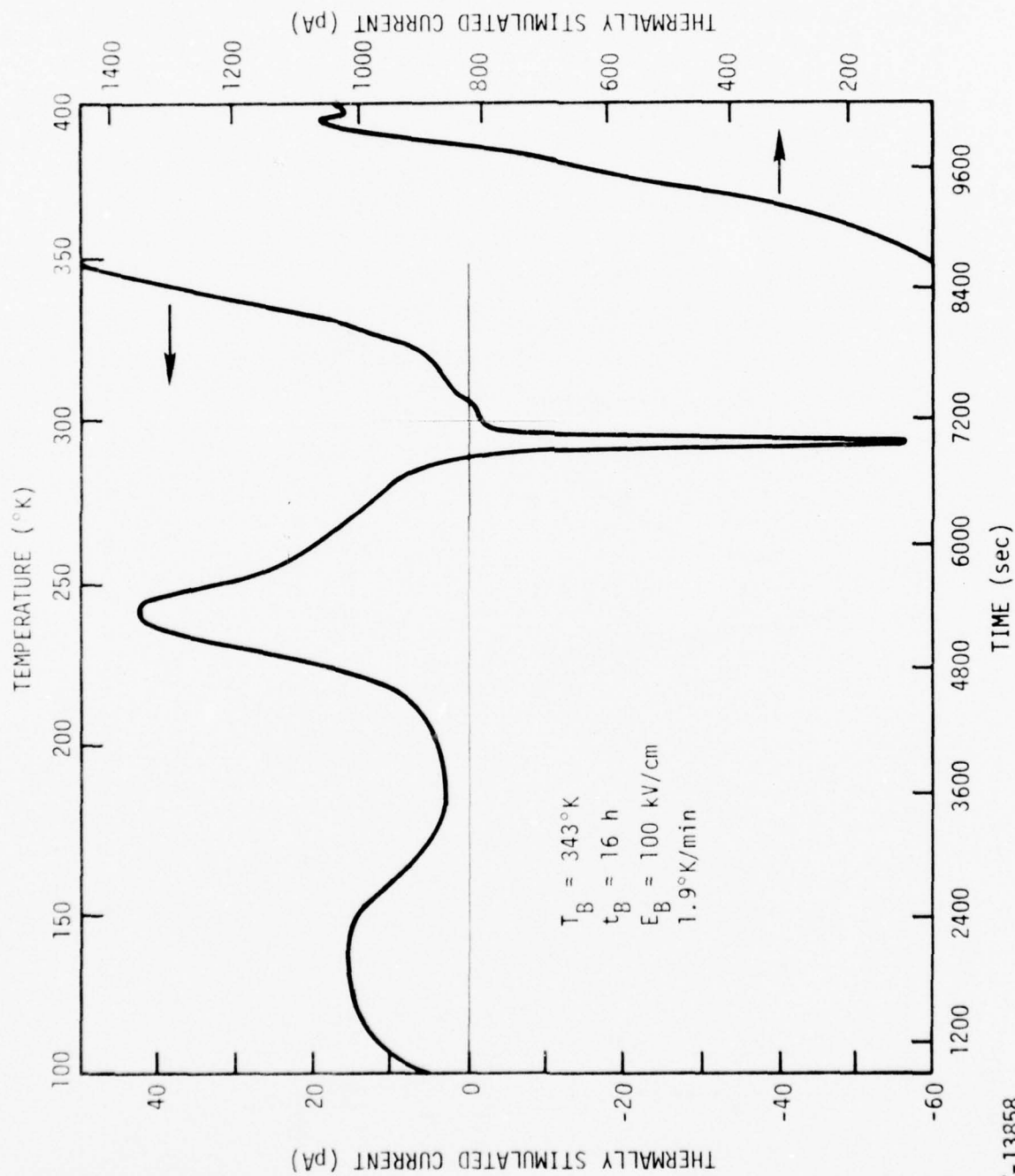


Figure 9. TSC spectrum of ARCO HD polyethylene burned in at 343°K

RT-13858

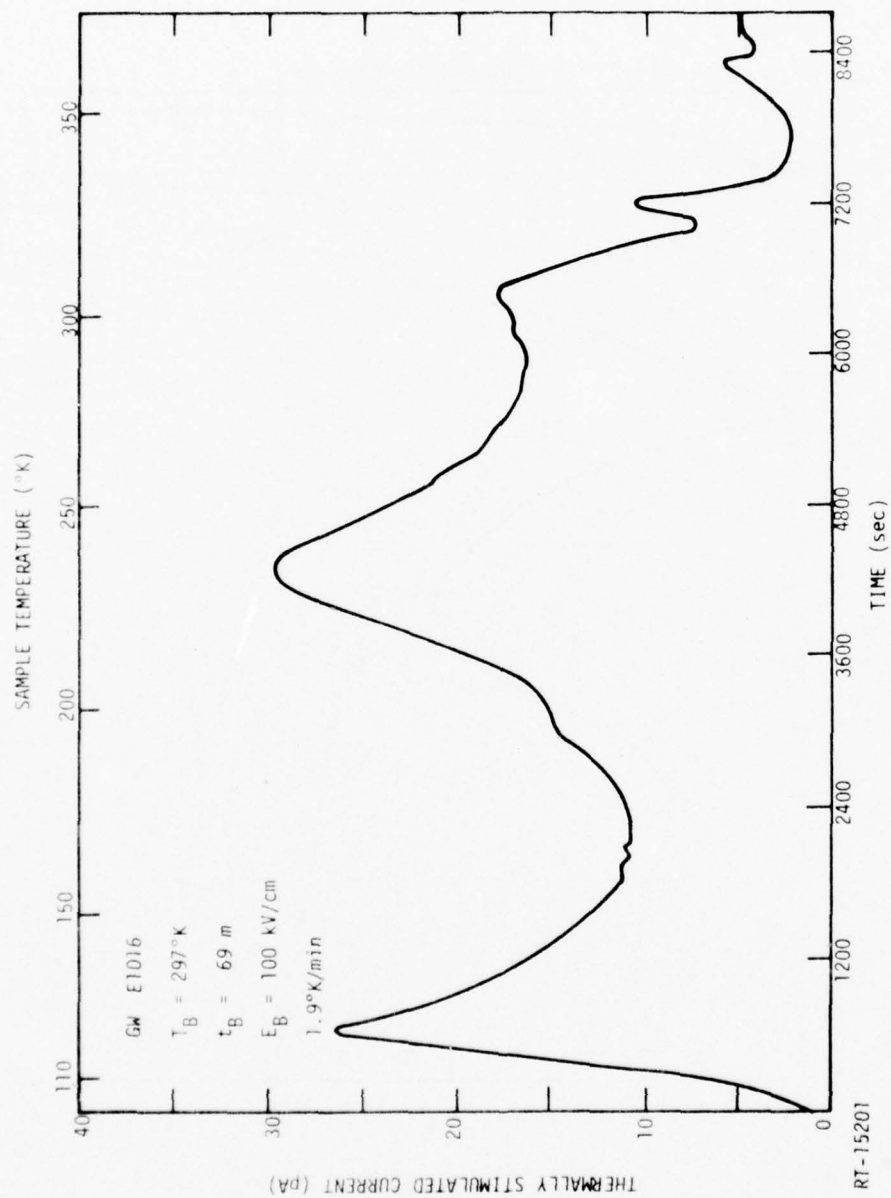


Figure 10. TSC for a GW LD E1016 burned in at 297°K

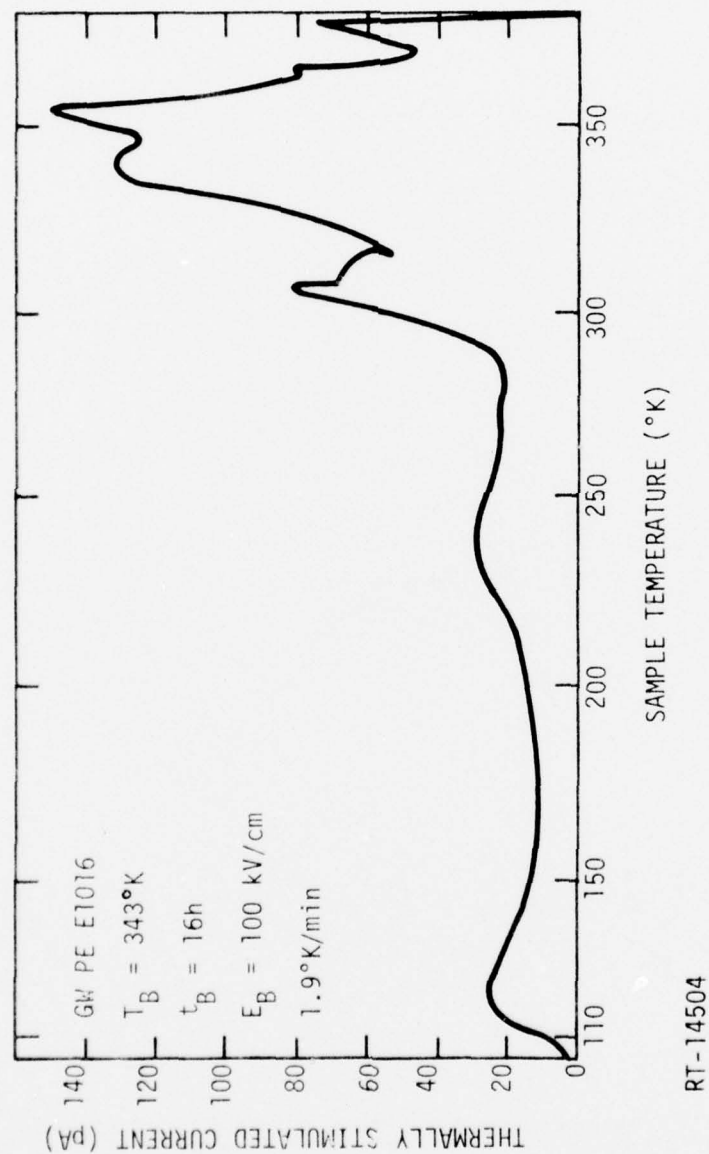


Figure 11. TSC spectrum of a low-density polyethylene sample

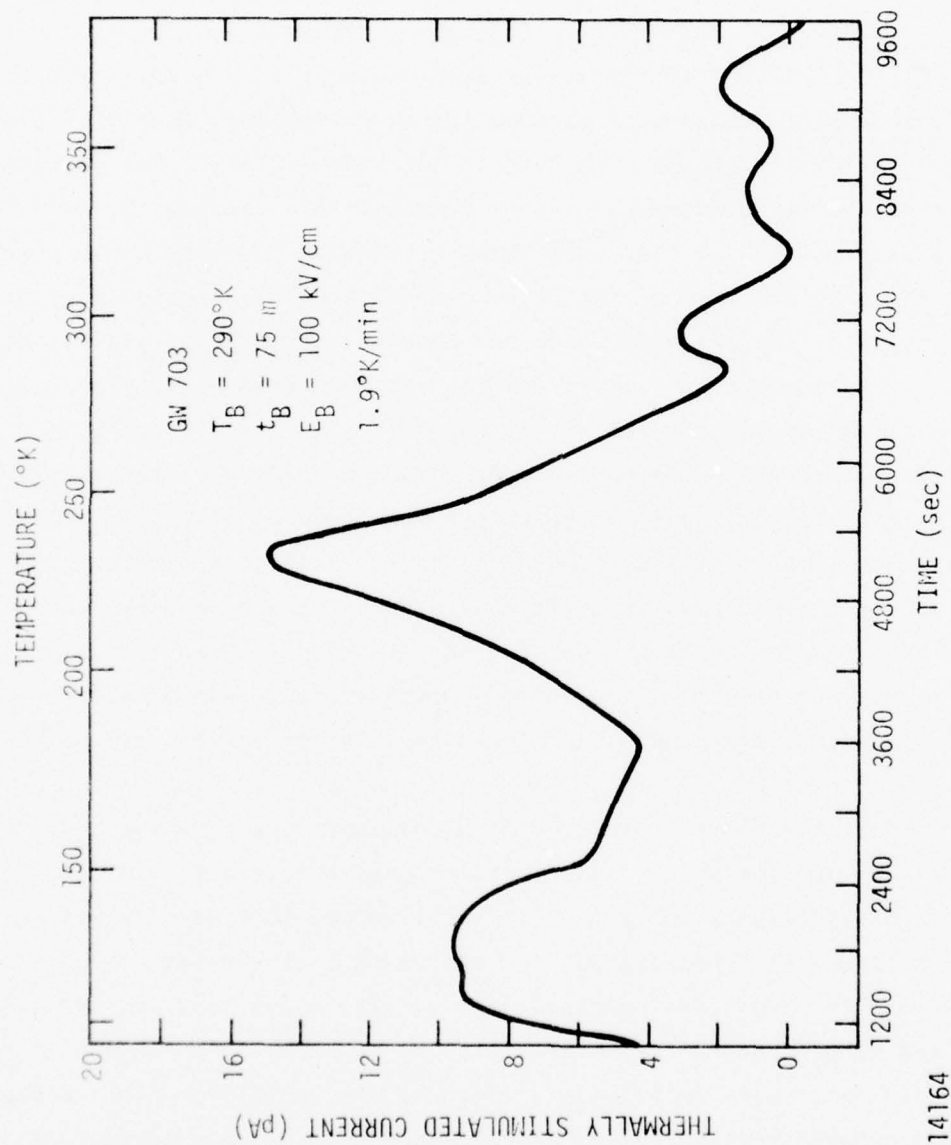


Figure 12. TSC spectrum for a Golden West Plastics type W703 medium-density polyethylene burned in at 290°K

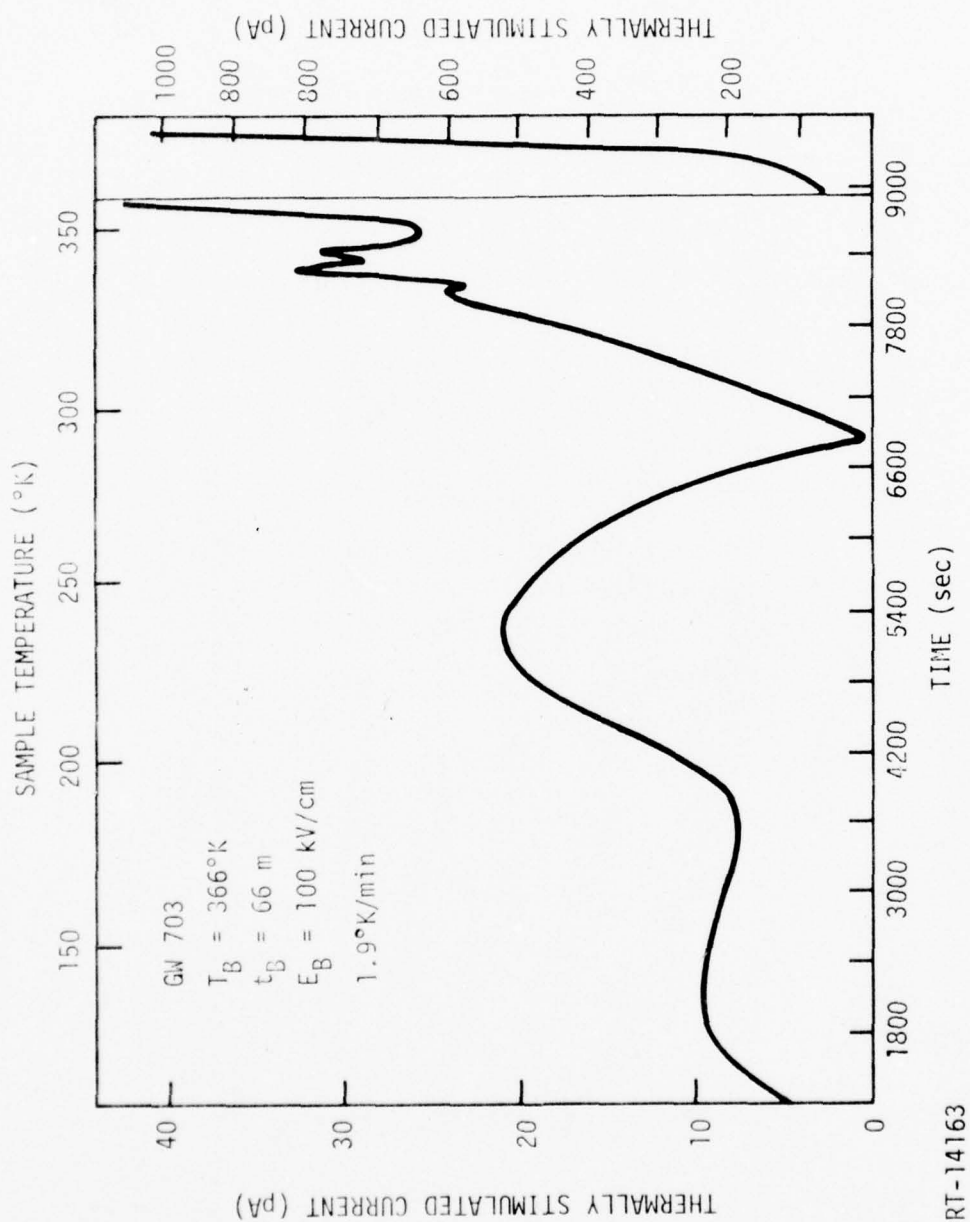


Figure 13. TSC spectrum of a Golden West Plastics type W703 medium-density polyethylene burned in at 366°K

At the highest temperature reached in a temperature ramp, the TSC current diminished markedly and went to zero or even negative. The observed range of $\kappa_T(\text{Ramp})$ was <0.05 .

For a relatively few samples of each type, designated Type II, the shape of the high-temperature portion of the TSC spectrum was significantly different. This type of spectrum appeared when a sample was burned in at relatively high temperature, i.e., $T_B \gtrsim 343^\circ\text{K}$. The TSC showed a large rise above this temperature that in some cases masked the peak that typically appeared at ~ 340 to 360°K . The net amount of charge emitted to an external circuit was often quite large where $\kappa_T(\text{Ramp}) > 0.1$. Concomitant with the release of a large amount of charge at the high ramp temperatures was the presence of a sharp current reversal (negative) at $\sim 295^\circ\text{K}$ (Figure 9). When the temperature ramp was started above this temperature, no evolution of negative current was evident (q.v., Figures 28 and 30 of Reference 2). This large current emitted at high temperatures must be in part due to the relaxation of stored charge distributions rather than an artifact as it does not appear in samples which have been annealed and then heated. This behavior has been observed in Mylar capacitors (Ref 22) and in copper jacketed (Cujack) Teflon dielectric cables (q.v., Section 5.3).

In most cases, considerable TSC was being emitted at the highest temperature reached (380 to 390°K) during the temperature ramp. A subsequent isothermal anneal was effected until the TSC went to zero. For some samples this current reached an asymptotic limit and remained constant or even started to increase after several hours. The polarity of this persistent current varied from sample to sample. Such currents, which appear to be independent of the charging conditions, have been attributed to a weak electrochemical potential that arises because of differences in the state of the electrodes (Ref 23). The presence of this current appears to be connected with a deterioration of the aluminum electrodes as a consequence of thermal cycling and is manifest in a rise in the measured sample dissipation factor. The onset of this current is probably accompanied by changes in the state of the polymer. The values for $\kappa_T(\text{Isothermal})$ presented in Tables 3 through 5 were corrected for the presence of this current.

3.4 DISCUSSION OF TSC MEASUREMENTS

The TSC spectra for the three types of polyethylene studied are entirely similar to each other. The observed spectral shapes of samples burned in under the same conditions tended to be similar. The values of κ_T found for given burn-in conditions are comparable. If one had to rank them as a function of crystallinity it would probably be $\kappa_T(\text{HD}) > \kappa_T(\text{LD}) > \kappa_T(\text{MD})$, although there is enough fluctuation in the data to make even this ranking tentative. Moreover, all three polymers under the proper conditions showed both Type I and Type II spectra. The observed variations between spectra seem to be more sample dependent than morphology dependent, that is the construction of the sample has greater influence. However, one can make some specific observations on the relationship between the observed κ_T 's, the location of peaks in the polymer spectra, and the morphology of polyethylenes.

We first present a description of the behavior of an idealized electret under burn in. In this we follow the comprehensive discussion of van Turnhout (Ref 24). It will be seen that some aspects of the depolarization behavior do not follow the predictions of the idealized model. An explanation of why our measurements show departures from the idealization is presented. The relaxation of excess charge in the polymer depends on many of the same factors that determine the ordinary ohmic conductivity, such as the presence of trapping sites that control charge motions. These similarities will be discussed.

Consider a planar capacitor with metalized electrodes subject to an applied field at elevated temperature. With such electrodes there are no gaps between electrode and dielectric. Under the applied field, those molecular dipoles that are free to rotate will be aligned. In addition, mobile space charges that are intrinsic (in the sense that they are not injected) and due to the disassociation of impurities present in the polymer drift under the applied field until they are trapped, typically at interfaces either between the dielectric and the electrodes, or at the boundaries between the crystalline and amorphous domains in these heterogeneous polymers. Such interfacial charging is known as Maxwell-Wagner polarization. At a given burn-in temperature the particular molecular or space-charge motions which take place depend

on their relative energies for activation. Typically, the orientation of molecular dipoles associated with segmental chain motion occurs at a lower temperature, i.e., possesses a lower activation energy than those conduction processes which depend on the motion of the free carriers, which may be not only electrons and holes but also ions in a polymer. When the internal polarization equilibrium state is reached in the polymer, the sources of this field are frozen in by cooling the sample under bias. Such a charging process is called heterocharging, in that the internal polarization field opposes the forming field.

In the thermally stimulated current measurement, the sample is then short circuited. This places image charges on the electrodes to make the average electric field in the polymer zero. On heating, molecular motion occurs, which produces a solenoidal current in the dielectric that is equal to the external replacement current. In this model it has two components: first, there is the displacement current due to the relaxation of the aligned dipoles. As we have shown last year, these relaxations typically occur at second-order transition temperatures making coordinated molecular motion of segments of the polymer chain. The most important of these is the glass transition temperature. Second, the polarized charge distribution, which is inhomogeneously distributed in the polymer, begins to relax under the inhomogeneous internal field. The relaxation process has a double temperature dependence. First, there is the usual exponential dependence on temperature of the mobility of the space charges, which is determined by the activation energy for detrapping. Second, there is an additional temperature dependence, in that molecular motion itself may destroy the trapping sites and enhance the release of charge. As the capacitor is kept in a short circuit, the average conductivity current is zero. While the net conduction current in the dielectric is zero, it can help to more rapidly neutralize the initial space-charge distribution. If the ordinary conductivity is large compared to the product of the space-charge mobility and space-charge density, the observed contribution to the external replacement current because of the net motion of space charge will be small. Thus, a thermally stimulated current spectrum will show features that can be related to both molecular and charge motion in the dielectrics.

For the idealized case of heterocharging, the net external replacement current that flows will be positive, i.e., from the electrode at the higher potential during burn-in to that at lower potential. If the persistent internal fields are due to hindered dipole motion or reversible charge displacement over microscopic distances, then it can be represented by a persistent polarization $\vec{P}(x,t,T)$ (Ref 25), which is not only a function, in general, of position, but also of time and temperature. For example, this approximation is valid if the displacement of space charge occurs by accumulation of charge at the interstices between crystalline or amorphous domains after motion across one of these domains. Their size is typically a few hundred angstroms, (cf. Chapter 2), which is small in comparison to the film thickness, 10^{-3} cm. The net charge released is, in general, a function of the specific temperature ramp used during thermal cycling. However, if the only contribution to the persistent internal field is due to polarization, then the charge released, $Q[t_0, T_0, (t_0)]$, depends only on the internal polarization and is independent of the rate at which the sample is cycled. This charge given by Equation 9.

$$Q[t_0, T(t_0)] = \frac{A}{t} \int_0^t P[x, t_0, T(T_0)] dx \quad , \quad (9)$$

i.e., equal to the average value of the polarization times the area of the sample for a film of area a and thickness t . In the case of a uniform volume polarization, this is equivalent to

$$Q = AP \quad . \quad (10)$$

The persistent component of the polarization P can be written

$$P = (\kappa_0 - \kappa_\infty) \epsilon_0 E \quad (11)$$

where κ_0 and κ_∞ are the static and optical values of the relative dielectric constant, and E is the applied field at the burn-in temperature, $T_B = T_0$. Then

$$Q[t_0, T(t_0)] = A(\kappa_0 - \kappa_\infty) \epsilon_0 \frac{V}{t} = (\kappa_0 - \kappa_\infty) \frac{CV}{\kappa_0} \quad . \quad (12)$$

or

$$\kappa_0 - \kappa_\infty = \frac{\kappa_0 Q[t_0, T(t_0)]}{CV} \quad (13)$$

The term $(\kappa_0 - \kappa_\infty)$ is equivalent to our κ_T . Thus, for an idealized dielectric that is heterocharged, i.e., that has no macroscopic space charging, the amount of charge released is proportional to the nonelectronic component of the polarizability. The principal finding of our last year's work was the demonstration that there is indeed a correlation between κ_T and κ_R (the charge released by radiation consequent to the burn-in) and $\kappa_0 - \kappa_\infty$. The contribution to the net charge released due to the motion of internal space charge that is transported over macroscopic distances, comparable to the size of the dielectric film, will increase κ_T as defined in Equation 8 if compared to $\kappa_0 - \kappa_\infty$.

In fact, polyethylene is a nonpolar polymer. Nonpolar polymers such as this one have relatively low concentrations of ionizable impurities that may form space-charge polarization. Therefore, one expects that the value of κ_T to be observed in a thermal anneal consequent burn-in under ideal conditions will be small, comparable to $\kappa_0 - n^2$, where n is the optical index of refraction. This difference is ~ 0.01 to ~ 0.03 , based on published values of dielectric constant and indices of refraction (cf. Table 17 of Ref 2). In fact, most of the measured values for κ_T given in Tables 3 through 5 are of this magnitude. Any significant increase in κ_T above the value is evidence that significant amounts of charge have been injected into the polymer (homocharge) as observed for the Type II spectra.

The impurity charges are introduced as a consequence of manufacturing processes; for example, additives are put into a commercial polymer to prevent oxidation or to cause termination of the polymerization (Ref 26). Under these circumstances, the observed range of κ_T should show no strong dependence on crystallinity. The detailed shape of the thermally stimulated current spectra will, insofar as they arise from the relaxation of intrinsic space charge, reflect not only the impurity concentrations, but also the particular distributions of trapping sites, which depend on the specific morphology.

There is a relatively straightforward interpretation for the shape of the low-temperature portion of the TSC spectra for polyethylene. It has been shown (Ref 20) that the origin of these peaks, which appear at $\sim 130^\circ\text{K}$ and $\sim 235^\circ\text{K}$ in all of our spectra, is due to the relaxation of molecular dipoles, which are primarily carbonyl groups (C=O) attached to the polymer chains as a consequence of oxidation. As the temperature of a sample is increased during a thermal ramp, the molecular motion concomitant with the γ and β transitions that take place at these temperatures cause the disorientation of these dipoles. As we have shown, the magnitude of these peaks is proportional to the applied field. This is to be expected for the charge release to an external circuit caused by the depolarization of a uniform-volume polarization. Since such oxidation faults are a function of the polymer history and independent of its crystallinity, the size of these peaks showed no correlation with crystallinity.

No quantitative conclusions can be drawn between the crystallinity of polyethylene and its ability to store trapped charge on the basis of heterocharging. In the case where only heterocharging occurs, i.e., no external charge injection, the concentrations of dissociable impurities and dipoles are purely sample dependent. As we have remarked, there is little difference in the values of κ_T observed for samples of the three crystallinities, burned in under identical conditions. The principal features of the TSC spectra for the three types of polyethylenes are similar. Moreover, all three types of polyethylene show Type II behavior. All three polyethylenes, being relatively inhomogeneous, possess sufficiently similar morphology, in that the relaxation processes that occur after heterocharging are similar.

We are not certain why some of our samples yielded relatively large $\kappa_T > 0.1$ (i.e., Type II spectra). This corresponds to a charge release of $\sim 1 \text{ nC/cm}^2$ dielectric surface. Type II spectra were observed only for some samples, and not restricted to a particular type of polyethylene. Such spectra were observed only after burn-in at a relatively high temperature ($\geq 343^\circ\text{K}$) as the melting point of the polymer was approached. The TSC spectra of these same samples burned in at lower temperatures after observing such an anomalous response were not in themselves anomalous, i.e., they were Type I. Equally puzzling is the presence of a strong negative component in the Type II TSC

spectra at 295°K. There are no reported phase transitions in polyethylene at this temperature. Such negative currents can only be due to the motion of space charge away from its injecting electrode. We consider it likely that Type II spectra are characteristic of those in which significant amounts of space charge are injected into the sample (homocharging). Their shape is similar to that observed by Sawa et al. (Ref 27) for samples charged by high field injection. Clearly, for a nonpolar polymer such as polyethylene, whose low conductivity is due to a relatively low concentration of charge carriers and dipoles and the presence of numerous traps, homocharging is a much more efficient method for storing persistent charge in nonpolar polymers than is burn-in. The charge that is released to an external circuit as the consequence of homocharging can easily be several tens of nC/cm^2 . That released under heterocharging in nonpolar polymers is usually less than one hundredth of this. Whether homocharging can occur under burn-in is dependent on several factors. It is clearly enhanced by very high fields and temperatures. It also depends on electrode conditions.

Our samples were assembled with polymer films metalized on one side in a manner similar to that in which high-reliability Mil-spec metalized-electrode capacitors are constructed. On heating these samples to high temperatures, it is possible the differential thermal expansion might introduce gaps between the metalized electrode and the unmetalized side of the adjacent polymer film. It is well known that Townsend breakdown can occur under such circumstances, with the concomitant injection of charge into the sample. Moreover, the electrode would be partially blocking because of the presence of such gaps. In this case (Ref 24) it is possible that a diffusion-induced drift of charge away from the blocking electrode can occur at some temperatures which would produce the observed current reversal in the thermally stimulated currents. Such an explanation without further measurement on samples which are purposely homocharged and in which gaps are purposely introduced must remain speculation. The creation of an internal charge state which results in a Type II spectrum, cannot be solely attributed to heterocharging, as burn-in under identical conditions of different samples of the same polymer type did not always produce identical spectra, Type I typically being more prevalent. It is evident that it would be better to study the ability of these films to store trapped charge by controlled charge injection, i.e., using electron beams.

We may make some additional remarks about morphological factors which determine the storage of space charge in these polyethylene samples, in particular their relationship to the factors that determine the normal conductivity of this polymer at the same temperature. The high-temperature portions of the polyethylene spectra can be explained in terms of the motion of space charge in the polymer. Above 300°K, the polymer conductivity begins to rise rapidly. A part of this rise is due to promotion of charge carriers into the conduction band from the valence band, and from traps. An additional contribution is due to large-scale molecular motion that occurs as the melting point of the polymer is approached, which also results in detrapping. During the α transition, which typically occurs between 333 and 353°K, many of the trapping sites for charge carriers in polymers are destroyed. As we discussed in Chapter 2, these include regions of relatively large free volume between the molecules in the amorphous domains of the polymer, in defects in the crystalline lamellae, at the boundary between the crystalline spherulites, and at the interfaces between crystalline and amorphous domains inside the spherulites. The rate at which these sites disappear is enhanced as melting begins to take place in the crystalline region, and as large-scale molecular motion occurs in the amorphous domains (α transition).

The presence of such trapping sites are not only important in controlling the motion of the impurity space charge, but they have also been postulated to play an important role in the mechanisms for conductivity in polyethylene and other polymers. According to Wintle (Ref 28), the mobility of long-chain polymers is determined by a combination of intramolecular and intermolecular motion, and trapping effects. The inverse macroscopic mobility, μ_{mac}^{-1} , can be approximately written as the sum of terms

$$\mu_{\text{mac}}^{-1} = \mu_{\text{mic}}^{-1} + \mu_{\text{tr}}^{-1} \quad (14)$$

The microscopic mobility, μ_{mic} , itself has two components. One is the mobility of charge transported along the polymer chain, μ_0 . The magnitude of this intramolecular mobility is thought to be $\sim 1 \text{ cm}^2/\text{V-sec}$. In order to travel longer distances, charge carriers must travel from chain to chain. As the

transition involves either tunneling through or jumping over the intermolecular barrier, the microscopic mobility, μ_{mic} , is limited by this term. In this crude picture, it can be shown that the net microscopic mobility is of the order of

$$\mu_{mic} \simeq \frac{d + \ell}{d/\mu_0 + t_{esc}} E \quad (15)$$

for a polymer of characteristic chain fold length ℓ , separated by spacing d , under an applied field E . The intermolecular transition time, t_{esc} , is

$$t_{esc} \simeq \nu_{esc}^{-1} \exp(\Delta E/kT) \quad (16)$$

where $\nu_{esc} \sim 10^{14} \text{ sec}^{-1}$ is the barrier collision frequency and ΔE is the height of the barrier across which the charge carriers must pass. The size of the intermolecular mobility is several orders of magnitude smaller than μ_0 .

Finally, the charge carriers that drift along between chains may be captured by a deep trap, associated with one of the morphological features listed in Chapter 2. In this case the inverse trap mobility is given by an expression of the type

$$\mu_{tr}^{-1} \simeq \mu_m^{-1} = \frac{E}{\nu_m \lambda_m} \exp(E_m/kT) \quad (17)$$

for a trap of the m^{th} type, with a mean free path between them of λ_m , of depth E_m , and a collision frequency ν_m .

If the traps are sufficiently deep, the effective macroscopic mobility is dominated by the trap-modulated mobility. As the trapping sites are related to morphological features of the polymers, one can hope to find that there is a correlation between morphology and conductivity. In fact, a dependence of the mobility for conductivity in polyethylene on crystallinity has been observed by Davies (Ref 29). He found that the mobility of polyethylene decreases as the crystallinity of the polymer is increased. Values of the order of $10^{-10} \text{ cm}^2/\text{V-sec}$ to $10^{-7} \text{ cm}^2/\text{V-sec}$ were observed at about 350°K corresponding to activation energies of 1.2 to 0.7 eV for high- and low-crystallinity polyethylenes,

respectively. At room temperature, the measured mobilities are of the order of 10^{-11} to 10^{-10} $\text{cm}^2/\text{V-sec}$ (Refs 30, 31) for low-density polyethylenes, values that are consistent with the trends of the data of Davies. The scatter in Davies' data for a particular sample are too great to see anything more than the trends with temperature. Moreover, his measurements begin at $\sim 345^\circ\text{K}$ so that it is not possible to search for a change of mobility as the α transition occurs.

The processes which occur during the polarization of intrinsic space charge (heterocharging) will be sensitive to the forming temperature. Hence, the corresponding charge motion connected with the relaxation of this hetero-charge will be substantially complete at temperatures comparable to the burn-in temperature T_B . This is observed for Type I spectra. On the other hand, charge injection, homocharging, depends more on the conditions of injection, i.e., the energy of the injected particles and less on the formation temperature. However, the depolarization processes depend on the temperature-dependent mobility of the relaxing space charge. Insofar as this mobility is similar to that which determines normal ohmic conduction, i.e., controlled by trapping, one expects to see an increase in the TSC current with temperature similar to the observed rise in conductivity. Whether a peak is seen in the TSC spectrum will depend on the highest temperature reached, and on the distribution of space charge in traps which is a function of the forming temperature.

The concentration of unsaturated bonds which have been postulated to be possible trapping sites in these polymers (cf. Chapter 2) is evidently less important in determining the motion of charge carriers above 300°K . Infrared spectroscopic analysis of Davies' samples yielded the concentrations of unsaturated bonds. This analysis shows that low-density polymer samples which have the highest mobilities at a given temperature also have a higher concentration of unsaturated bonds. Without invoking this spectroscopic evidence, Davies has attributed the observed dependence of mobility on crystallinity to the presence of barriers against conduction which serve as trapping sites. These sites are identified with the boundaries of crystallites at the interfaces between crystalline and amorphous domains.

In order to assess the factors which determine the shape of the TSC spectra for $T > 300^\circ\text{K}$, it is useful to compare our data to those obtained after charging by a variety of methods. These are presented in Table 6. Included is the method for charging, the location of peaks in the TSC spectra, and, where calculated, the activation energy corresponding to detrapping for each of these peaks. The majority of the data is for the depolarization of persistent internal fields created by homocharging, i.e., the injection of extrinsic charge into the bulk polymer. The magnitude of the charge released reflects the efficiency of the injection process. Many of the spectra show peaks in similar positions, which is indicative of the fact that the relaxation processes depend on specific morphological features of the polymer, rather than the manner of injection. The observed peaks in the TSC spectra fall into three groups, located at about 325°K , 350°K , and 380°K . The particular peaks observed are related to the conditions under which charge is injected across the electrodes, and the sample temperature and external bias which affect their diffusion in the sample.

The observed activation energies for detrapping fall into two groups, one at ~ 1.25 eV and another at ~ 1.45 eV. It is significant that the peak observed at $\sim 323^\circ\text{K}$ by Sawa et al. (Ref 27) is much stronger in high-density polyethylene than in low-density samples. The activation energy calculated for this peak is 1.23 eV. The authors attribute this peak to a trap located at the interface between crystalline and amorphous domains. It is significant that the activation energy for mobility in high-density polyethylene as found by Davies is also ~ 1.2 eV. The latter postulates a similar origin for this trap. It is relevant to note that 323°K is close to the temperature at which the onset of the α transition occurs. The transition is marked by large-scale motion of polymer chains in the amorphous domains, which must also influence the chain segments lying in the crystalline domains.

There is no direct evidence for the origin of the peaks appearing at high temperatures, i.e., at $\sim 350^\circ\text{K}$ and 370°K . As the temperature is raised above 350°K , melting of the crystallites begins to occur. This would release further charge if a significant fraction of traps were located in defects associated with the crystalline domains. In addition, the effect of thermal activation in releasing charge carriers cannot be discounted.

TABLE 6. SUMMARY OF TSC MEASUREMENTS ON POLYETHYLENE

Charging Method	Type	TSC Peaks ($^{\circ}$ K)	Trap Activation Energies (eV)	References	Notes
Burn-In $T_B < 300^{\circ}$ K	LD	138, 203, 245	0.419, 0.605, 0.734	20	(1)
Burn-In $T_B \leq 343^{\circ}$ K	LD, MD, HD	130, 235, 295, 355 385, 410		This Work	(2)
High-Field Injection $E = 1$ MV/cm	LD, HD	323, 358	1.23, 1.47	27	
Negative Corona Charge	HD	329, 343, 371	1.7, 1.5, 1.2	32	
Electron Charging	HD	Many between 149 and 258	0.35, 0.6, 1.1	33, 34	(3)
Burn-In	HD	384		35	
Friction	HD	384	1.52	35	
Positive Corona	HD	382	1.43	35	

1. TSC spectrum showed two peaks. Was represented by the sum of 3 gaussians with mean temperatures and energies as shown.

2. Not all peaks seen in each spectrum. The actual values might vary $\pm 10^{\circ}$ K in different spectra.

3. Authors claim that while many peaks were observed, only three activation energies were found. In Reference 34, they state that the TSC spectrum for electron-charged polyethylene was similar to that for corona-charged samples (Ref 32).

In an interesting series of measurements, Creswell et al. (Ref 32) compared the relative ability of a series of polyethylenes to store charge by measuring the decay of surface charge as a function of temperature. They found that, as the molecular regularity increased, i.e., as one went from a highly branched, highly amorphous polyethylene to a highly linear, highly crystalline species, the temperature at which the space-charge distribution relaxed increased. Such observations are consistent with the observations of Davies, in which he shows that the conductivity of polyethylene decreases with increasing crystallinity as marked by an increase in the mean activation energy of the mobility from 0.8 eV to 1.2 eV.

In an inhomogeneous material such as polyethylene, there are undoubtedly a series of traps that control the motion of charge carriers in the polymer. Except for the possible association of one with an energy of about 1.2 eV, with the interface between crystalline and amorphous domains, no precise identification of any of the others has been made. The qualitative difference in the shape of the Type I and Type II spectra may reflect the fact that different charge carriers are injected by homocharging as opposed to heterocharging. It is significant that most of the Type I spectra have peaks at $\sim 350^\circ\text{K}$, which is at the upper end of the α transition for this polymer. Such a consequence is suggestive of our assertion that impurity space charges accumulate primarily at the interface between crystalline and amorphous domains that are disrupted by the molecular motion that occurs during this transition and continues at higher temperatures as the crystallites begin to melt. It is possible, but speculative, that the large amount of charge released at $T > 353^\circ\text{K}$ in Type II spectra is the result of release and consequent motion of space charge trapped in the crystallites, which are stable until the onset of melting in these polymers.

Clearly, further experimentation is needed to resolve this point. Such experiments should be carried out on a set of polymers which show a wide variation not only in the degree of branching but also in the degree of crystallinity. This is necessary so that one can try to separate those effects due to trapping at interfaces or in amorphous domains and those due to trapping in crystallites.

Since burn-in is a relatively inefficient manner of creating persistent internal fields, these experiments should be done with some manner of homocharging, such as electron injection. A determination should be made of the amount of trapped space charge and its spatial distribution, both by measurement and by adaptation and use of one of the available transport codes.

4. RADIATION RELAXATION MEASUREMENTS

4.1 INTRODUCTION

In this chapter we describe the measurements that determined the charge released to an external circuit as a consequence of the radiation-induced relaxation of persistent space charge/molecular polarization in a series of polyethylene capacitors. These measurements had three principal goals: first, to bound the charge released by polyethylene when irradiated after burn-in. Second, to compare the radiation-induced charge released by samples of a given polymer type that contained stored charge to that from samples that were thermally annealed before irradiation. This was done to try to separate that portion of the response of such components due to the relaxation of internal polarization fields and that portion due to the motion of radiation-driven charge in the dielectric. Third, to see if the charge released by radiation could be predicted from thermal anneal measurements. In addition, thermally stimulated current measurements were made on most of these samples after irradiation. This was done to determine the magnitude and persistence of space charge created in this polymer by fully penetrating radiation in samples which showed their asymptotic response to radiation.

4.2 EXPERIMENTAL PROCEDURE

The radiation depolarization experiments were carried out by exposing samples to successive pulses of 40-MeV electrons at a dose per pulse of ~ 800 rad(Si) and measuring the charge released per unit dose. Irradiation was terminated when the specific response of a sample to radiation became constant. The experimental method for carrying out these measurements is essentially that described in the 1976 final report for this program (Ref 2). For reference we have reproduced Figure 25 from that report (see Figure 14).

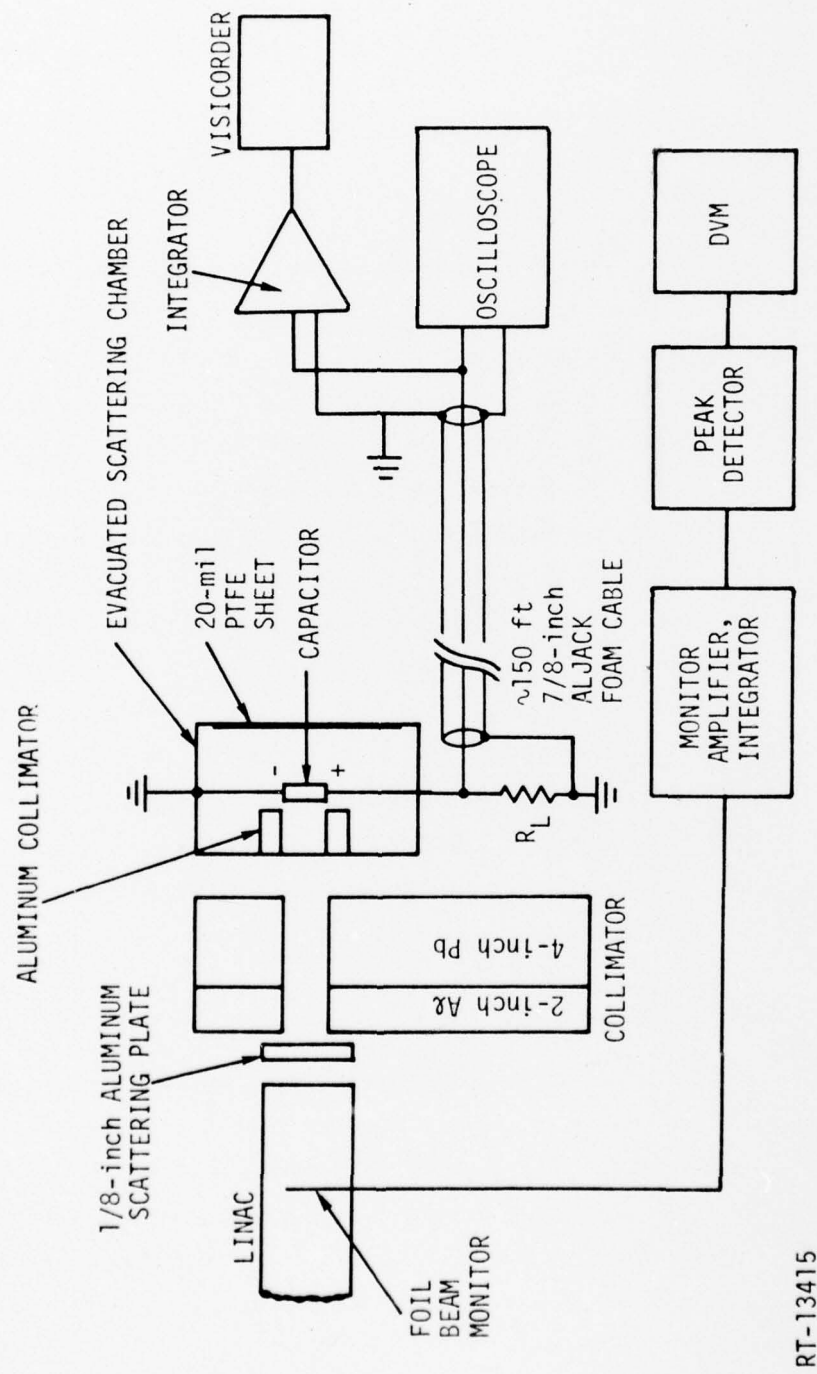


Figure 14. Experimental configuration for radiation depolarization measurements

RT-13415

The properties of the materials irradiated have been listed in Table 2. Sample conditioning prior to irradiation is given in Table 7. The three types of polyethylenes irradiated were identical to those studied by thermal annealing. For each type, five samples were irradiated. Three had leads attached to the metalized aluminum electrodes by conducting silver epoxy (designated type E) and two had 1-mil aluminum foils interleaved between layers of the film for connection between electrodes and external leads (type T). The samples were first annealed while shorted at 358°K for 17 hours to relax any persistent charge/polarization that might have been present. Three of the samples of each polymer type (two E and one T) were burned in at 353°K at a V_B , corresponding to an $E_B = 100$ kV/cm. Two samples of each type (one E and one T) were short circuited during the burn-in and maintained at the burn-in temperature. These burn-in conditions were similar to those used during the thermal annealing measurements. It was not possible to irradiate all samples simultaneously, so the burn-in times varied from 12 to 20.5 hours. This variation is not thought to be significant, for at $T_B = 353^\circ\text{K}$, these samples had reached their equilibrium charge state at the shortest burn-in time.

Samples were cooled under bias to room temperature over a period of about 20 to 30 minutes and were left in short circuit at room temperature for about the same length of time before irradiation to eliminate the promptly decaying components of stored charge and polarization. These conditions are similar to the procedure followed in the course of the thermal cycling measurements. Unfortunately, near the end of the burn-in period, a short circuit occurred in the power supply which provided the burn-in field for the low-density polymer samples while they were still at the elevated burn-in temperature. Therefore, the responses listed for the burned-in samples of this type (LDE6, LDE11, LDT4) are probably much reduced from what they would have been if they had not been inadvertently shorted at temperatures sufficiently high for significant relaxation of the persistent components of space charge and polarization to occur.

Each sample was irradiated with 5- μsec pulses of 40-MeV electrons from the IRT electron Linac. The dose per pulse was about 800 rad(Si). This was established by placing a silicon thermistor at the sample position between

TABLE 7. SUMMARY OF BURN-IN CONDITIONS FOR IRRADIATED SAMPLES^a

Sample	V_B (volts)	t_B
GW Low-Density Polyethylene		
LDE6	207 ^b	19 h 25 m
LDE11	207 ^b	19 h 50 m
LDE10	0	12 h
LDT4	207 ^b	20 h 15 m
LDT6	0	20 h 30 m
GW Medium-Density Polyethylene		
MDE2	325	12 h 35 m
MDE3	325	14 h 35 m
MDE5	0	15 h 40 m
MDT4	325	16 h
MDT3	0	16 h
ARCO High-Density Polyethylene		
HDE1	93	16 h 55 m
HDE3	93	17 h 25 m
HDE2	0	18 h 10 m
HDT1	93	17 h 40 m
HDT2	0	18 h 10 m

^a $T_B = 383^\circ\text{K}$ for all samples.

^bBecause of a power supply failure, these samples were short circuited while at T_B at sometime before the end of these times.

sample irradiations and measuring its response. The dose per pulse during a series of irradiations was monitored with a foil beam monitor calibrated against the thermistor. The charge released per unit dose was determined in two fashions. Photographs of the pulse shape that represented the current flowing through a 1-k Ω load resistor placed across the capacitor were taken throughout the series of pulses for each sample. The current flowing through the 1-k Ω load resistor was integrated and recorded. An active integrator had been constructed for these measurements. However, its noise level in the Linac RF environment was excessive. Therefore, the charge released per pulse was determined with a passive integrator consisting of a 59-k Ω resistor and a high-quality 0.1- μ F Teflon capacitor. The time constant of this circuit (5 msec) was much longer than the 1/e decay time, $\sim R_L C$ of any sample and load resistor. The output of the integrator was amplified by a Princeton Applied Research Model 113 amplifier. The amplifier lower frequency cutoff was set at 1 Hz to prevent long-term drift from affecting the output of the integrator. Its upper frequency cutoff was set at 10^3 Hz to remove extraneous high-frequency noise. The output of the amplifier was buffered by a line driver and recorded on a Visi-corder. With the passive integrator a charge release per pulse of <50 pC could be resolved.

Table 8 presents a qualitative summary of our results. For each sample we have listed the first pulse charge emission per unit dielectric surface area per unit dose (R_0), expressed in units of coulombs per rad(Si) per cm². The asymptotic response per unit dose per unit (R_∞) is also expressed in the same units. The net charge release per unit film area is given (q_∞). The net charge released has also been expressed in terms of the nondimensional parameter κ_R , which is defined as

$$\kappa_R = \frac{q_\infty A \kappa}{C V_B} \quad (18)$$

for comparison with the thermal relaxation data of Chapter 3 and the third subsection of this chapter entitled "Post-Irradiation Thermal Anneal". The listed values of q_∞ were calculated by subtracting from the total charge released by a sample the product of its asymptotic response (R_∞) and the total absorbed dose

TABLE 8. RADIATION RESPONSE OF CAPACITORS

Sample	R_0 (10^{-15} C/ rad \cdot cm 2)	R_∞ (10^{-15} C/ rad \cdot cm 2)	R_0/R_∞	D_∞ [krad(Si)]	q_∞ (pC/cm 2)	κ_R	κ_T	
							Pre-Irradiation (Ramp)	Post-Irradiation (Ramp)
LDE6(B) ^a	1.1	0.76	1.4	41	2.8	3.1×10^{-4}	0.55 ^c	-4.1 $\times 10^{-3}$ ^g
LDE11(B)	-10.3 ^b	0.43	-24.0	<15	-13.9	-1.6 $\times 10^{-5}$		3.8 $\times 10^{-3}$ ^g
LDE10(A)	1.4	0.46	3.0	16	3.3	3.6 $\times 10^{-4}$		-5.1 $\times 10^{-3}$ ^g
LDT4(B)	-5.1	0.59	8.6	14	-11.3	-1.3 $\times 10^{-5}$		-1.1 $\times 10^{-3}$ ^g
LTD6(A)	0	0.41	-1	4	1.0	1.1 $\times 10^{-4}$		3.0 $\times 10^{-2}$ ^d
MDE2(B)	19.7	1.17	16.8	48	11.6	1.3 $\times 10^{-2}$	3.4 $\times 10^{-2}$	2.5 $\times 10^{-3}$ ^f
MDE3(B)	-16.0	0.24	66.7	44	-8.0	-1.0 $\times 10^{-2}$		3.0 $\times 10^{-3}$
MDE5(A)	-0.79	0.59	-1.3	<5	0.4	5 $\times 10^{-5}$		3.2 $\times 10^{-3}$ ^d
MDT4(B)	16.7	1.9	8.8	32	36.6	4.1 $\times 10^{-3}$		1.3 $\times 10^{-2}$ ^e
MDT3(A)	0.90	0.42	2.1	40	4.1	4.6 $\times 10^{-4}$		0.19 ^e
HDE1(B)	-38	-0.81	46.9	44.5	-309	-3.5 $\times 10^{-2}$	0.27	0.81 ^d
HDE3(B)	22.9	-8.4	-2.7	140	971	4.4 $\times 10^{-1}$		1.31 ^f
HDE2(A)	-4.4	0.26	16.9	86.3	-62	-7.0 $\times 10^{-3}$		5.1 $\times 10^{-5}$ ^d
HDT1(B)	-2.0	0.47	4.3	40	-22	-2.5 $\times 10^{-3}$		1.1 $\times 10^{-2}$ ^e
HDT2(A)	2.4	0.35	6.9	64	22	2.5 $\times 10^{-3}$		1.2 $\times 10^{-2}$ ^e

^aThe symbol "B" means that sample was burned in. The symbol "A" means that a sample was annealed.

^bA negative sign indicates that the net charge flow through the load resistor was from the sample electrode at ground during burn-in to that at the higher potential.

^cThe preirradiation κ_T are the maximum for samples of the same type burned in under similar conditions.

^dThermal anneal carried out one day after irradiation. ^fThermal anneal carried out 56 days after irradiation.

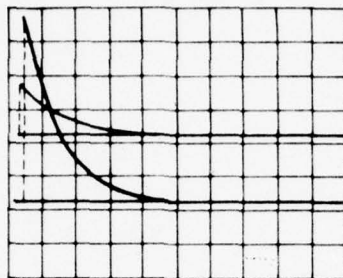
^eThermal anneal carried out 28 days after irradiation. ^gThermal anneal carried out 60 days after irradiation.

to reach equilibrium (D_∞). The κ_R for the shorted samples, where $V_B = 0$, was calculated by entering the value of V_B for the burned-in samples in Equation 18. To relate the data to cable responses, it is to be noted that a cable with a 0.1-inch o.d. dielectric, comparable to that of many high-quality coaxial cables used in systems such as missiles and spacecraft, has an outer dielectric surface area of 0.80 cm^2 per cm of cable length. For comparison, we have also included the maximum thermal response measured for each type of film, including data from last year when available. The charge released by an irradiated sample in a consequent thermal anneal is also given. These data have also been expressed in terms of the nondimensional parameter κ_T (Equation 8). A charge flow is positive if from the electrode at the higher potential during burn-in to that at ground, in analogy with the convention employed in the TSC measurements.

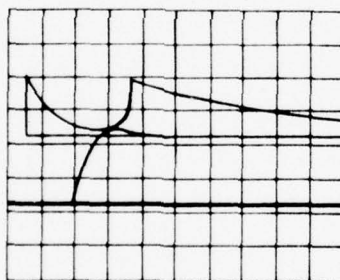
To convert the charge released per unit area to actual charge emitted, one can use the sample parameters given in Table 2.

Several qualitative comments can be made about the response of these capacitors. The shape of the radiation pulse for all samples except HDE3 was one whose amplitude rose more or less linearly during the Linac pulse and then decayed with a $1/e$ decay time, which was approximately $R_L C(\text{sample})$ as shown in Figure 15. For HDE3 the pulse shape changed considerably during irradiation (q.v. Figure 16a). Its initial response was positive and kept rising even after the Linac pulse ended; it then decayed slowly with a decay time $\gg R_L C$. As the irradiation progressed, the signal developed a large initially negative components, followed by the long positive decay as shown in Figure 16b. This negative component grew larger and larger, while the positive component became smaller. Similar behavior was seen in the radiation-induced relaxation of some of the polar polymer dielectric capacitors irradiated during last year's program. This sample was the only one of 15 examined that responded in this manner.

The initial response R_0 of a capacitor was almost always larger than its asymptotic response R_∞ . Typically, the charge release per unit dose diminished from pulse to pulse until the asymptotic response was reached after doses which ranged from 4 to 140 krad(Si). In some cases the net charge released per pulse changed sign, although the shape of the pulse remained constant. It can be



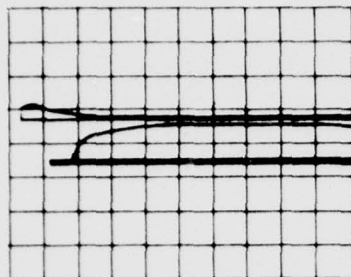
- (a) FIRST PULSE RESPONSE
 PRIOR ACCUMULATED DOSE = 0 rads(Si)
 DOSE THIS PULSE = 822 rads(Si)
 UPPER SCALE: 200 mV/div, 100 μ sec/div
 LOWER SCALE: 50 mV/div, 100 μ sec/div



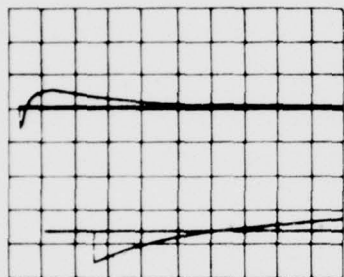
RT-15202

- (b) 31st PULSE RESPONSE
 NEAR ITS ASYMPTOTIC STATE
 PRIOR ACCUMULATED DOSE = 23.8 krad(Si)
 DOSE THIS PULSE = 844 rads(Si)
 THE STEP RISE ON PULSE IS DUE TO A SPIKE
 AT THE END OF LINAC PULSE.
 UPPER SCALE: 20 mV/div, 100 μ sec/div
 LOWER SCALE: 10 mV/div, 5 μ sec/div

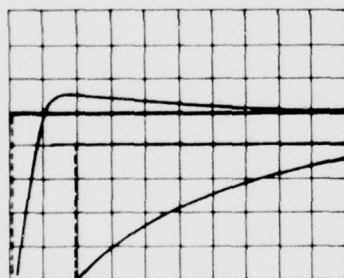
Figure 15. Response of Golden West medium-density, polyethylene type W703, sample MDT4 which had been burned in at $T_B = 353^\circ\text{K}$, $t_B = 16\text{h}$, $V_B = 325\text{ V}$, $E_B = 100\text{ kV/cm}$



- (a) SECOND PULSE RESPONSE
 ACCUMULATED DOSE = 582 rads(Si)
 DOSE THIS PULSE = 608 rads(Si)
 THE FIRST PULSE RESPONSE WAS
 ESSENTIALLY IDENTICAL.
 UPPER SCALE: 50 mV/div, 500 μ sec/div
 LOWER SCALE: 20 mV/div, 20 μ sec/div



- (b) 50th PULSE RESPONSE
 ACCUMULATED DOSE = 27.76 krad(Si)
 DOSE THIS PULSE = 634 rads(Si)
 UPPER SCALE: 5 mV/div, 500 μ sec/div
 LOWER SCALE: 5 mV/div, 20 μ sec/div



- (c) 110th PULSE RESPONSE
 ACCUMULATED DOSE = 64.6 krad(Si)
 DOSE THIS PULSE = 686 rads(Si)
 THE SHAPE OF THIS PULSE WAS ESSENTIALLY
 LIKE ITS ASYMPTOTIC APPEARANCE, EXCEPT
 THAT THE SIZE OF THE POSITIVE COMPONENT
 IS SOMEWHAT LARGER. THE AMPLITUDE OF
 THE NEGATIVE PEAK IS ABOUT -22 mV.
 UPPER SCALE: 2 mV/div, 1 msec/div
 LOWER SCALE: 5 mV/div, 50 μ sec/div

Figure 16. Response of an ARCO high-density polyethylene capacitor HDE3 to a series of 40-MeV electron pulses. This sample was burned in at $T_B = 350^\circ\text{K}$, $t_B = 17\text{h } 25\text{m}$, $T_B = 93\text{ V}$, $E_B = 100\text{ kV/cm}$.

seen from the table that the ratio of R_0/R_∞ was much larger for the samples in which internal space charge/polarization fields had been created by burn-in compared to those which had only been annealed. The asymptotic response of all the samples was fairly uniform. Independent of whether it had been burned in or not, the magnitude of this response was in the order of 10^{-15} C/rad-cm², with the exception of that for HDE3, whose behavior was generally unlike that of the other samples. Such a charge release per unit area per unit dose is comparable to that observed in high-quality coaxial cables with nonpolar dielectrics (q.v., Chapter 5). For the low- and medium-density annealed samples, $R_0/R_\infty < 3:1$, while for the high-density samples, the ratio was much larger. This suggests that 388°K was not a sufficiently high temperature to thoroughly anneal the high-density samples. To do this, one must approach the onset of melting to destroy the interface between crystalline and amorphous domains at which charge trapping can occur. For this polymer, one should go to ~405°K to reach such a state. The average ratio of the net charge release for the burned-in samples to that for the annealed samples was about 4:1 for low-density polyethylene, which had been partially depolarized before irradiation, 8.5:1 for the medium-density samples, and about 10.5:1 for the high-density samples.

Expressed in terms of the parameter κ , it can be seen that the charge released during irradiation is comparable to that released in a thermal annealing in which charge had been stored as a consequence of burn-in. This had been noted during last year's irradiations, when it was found that κ_R was proportional to, but typically less than, κ_T (q.v. Figure 25) of this report. As expected, κ_R and κ_T are all smaller than κ , the relative dielectric constant for the polyethylenes, which are 2.28 for the low-density polymer, 2.30 for the medium-density polymer, and 2.34 for the high-density material. The proportionality between κ_R and κ_T suggests that the presence of stored charge/persistent polarization in metal-dielectric systems such as capacitors or cables may be determined by thermally annealing samples without going through extensive radiative testing except of those samples which show an anomalously large thermal response.

The asymptotic response of each sample was judged to be attained when the charge per unit dose ceased to change from pulse to pulse. In practice, the

total dose at which this state was reached was difficult to determine. Some evidence of space charging of the polyethylene dielectric by high-energy electrons was observed. When the cable response per unit dose ceased to change very much from pulse to pulse, the asymptotic state was approached by firing a burst of approximately 10 to 25 single pulses at a rate of one pulse per second or so. The first one or two pulses of such a series of 10 to 25 showed a specific response, which was 25 to 50% larger than that of the remainder. A few minutes then elapsed, during which time the data was examined to determine whether the capacitor response had become constant before firing another set of pulses. After the equilibrium state for a given capacitor was reached, this phenomenon of a relatively large first-pulse response followed by smaller succeeding pulses was reproducible. Such behavior appears to be evidence of the fact that the radiation-driven charge induces a field inside a dielectric, which diminishes the net cable response because of the generation of currents that oppose the driven charge (Ref 37). From our data it is clear that some relaxation of these internal fields can occur in a matter of minutes. If such radiation-induced space charging could be made persistent, it might be possible to reduce the radiation response of a cable dielectric by the introduction of trapped space charge.

4.3 POST-IRRADIATION THERMAL ANNEAL

It is known that, if a polymer is exposed to ionizing radiation, significant space charging of the dielectric can occur because of trapping of the generated secondary electrons (Ref 38). These space-charge fields will persist for long periods of time--of the order of several months after irradiation has ceased. When the charging is by a nonpenetrating beam of electrons, very high fields may be built up, which can lead to dielectric breakdown. Such charging has been observed in satellite dielectric structures exposed to the exoatmospheric electron environment (Ref 3). While continued exposure to radiation of a given spectrum and at dose rate tends to build up return currents that limit space charging (an example of dielectric polarization-reducing radiation response), the presence of such persistent trapped charge may significantly alter the response of a dielectric exposed to a different kind of radiation,

e.g., if an electron-charged dielectric is subsequently exposed to a gamma or x-ray pulse. In fact, the data presented in the previous section indicate that polyethylene capacitors that contain persistent trapped charge/polarization induced by burn-in show a much enhanced radiation response if compared to annealed specimens.

In order to make an estimate of the amount of charge contained in our polyethylene capacitors which had been brought to a state of constant radiation response and to test for the persistence of this charge, most of the irradiated samples were thermally annealed after periods ranging from one day to two months after irradiation.

The results of these measurements are presented in Table 8, and Figures 17 through 19. The TSC spectra for the medium-density samples are shown in Figure 17, for the high-density samples in Figure 18, and for the low-density samples in Figure 19. The net charge released has been expressed in terms of the nondimensional parameter κ_T (post irradiation), defined in analogy to κ_R (Equation 18), for comparison with the preirradiation thermal anneal charge response [κ_T (preirradiation)] and the net charge release as a consequence of irradiation κ_R . To calculate the post-irradiation κ_T , V_B was set equal to 93 volts for the high-density sample, 325 volts for the medium-density samples, and 207 volts for the low-density samples, identical to the values used for burn-in. Of course, in the post-irradiation case, the samples were annealed without any prior burn-in. To convert these nondimensional parameters to actual charge release, one can use Equation 8 and the sample parameters given in Table 2.

Some general remarks may be made about the data. First, the net charge released by thermal annealing is positive for the medium- and high-density samples. Second, the range of values of κ_T (post-irradiation) observed for these samples did not significantly change over the 56 days that these measurements were carried out, but seemed to depend more on sample type. This finding is consistent with other data on the rate of relaxation of space charge in nonpolar polymers at room temperature (Ref 39). In fact, electrets made from Teflon FEP film have lives of several years (Ref 40). Sawa et al. (Ref 27) have shown that the relaxation of electrons, injected by the application of a

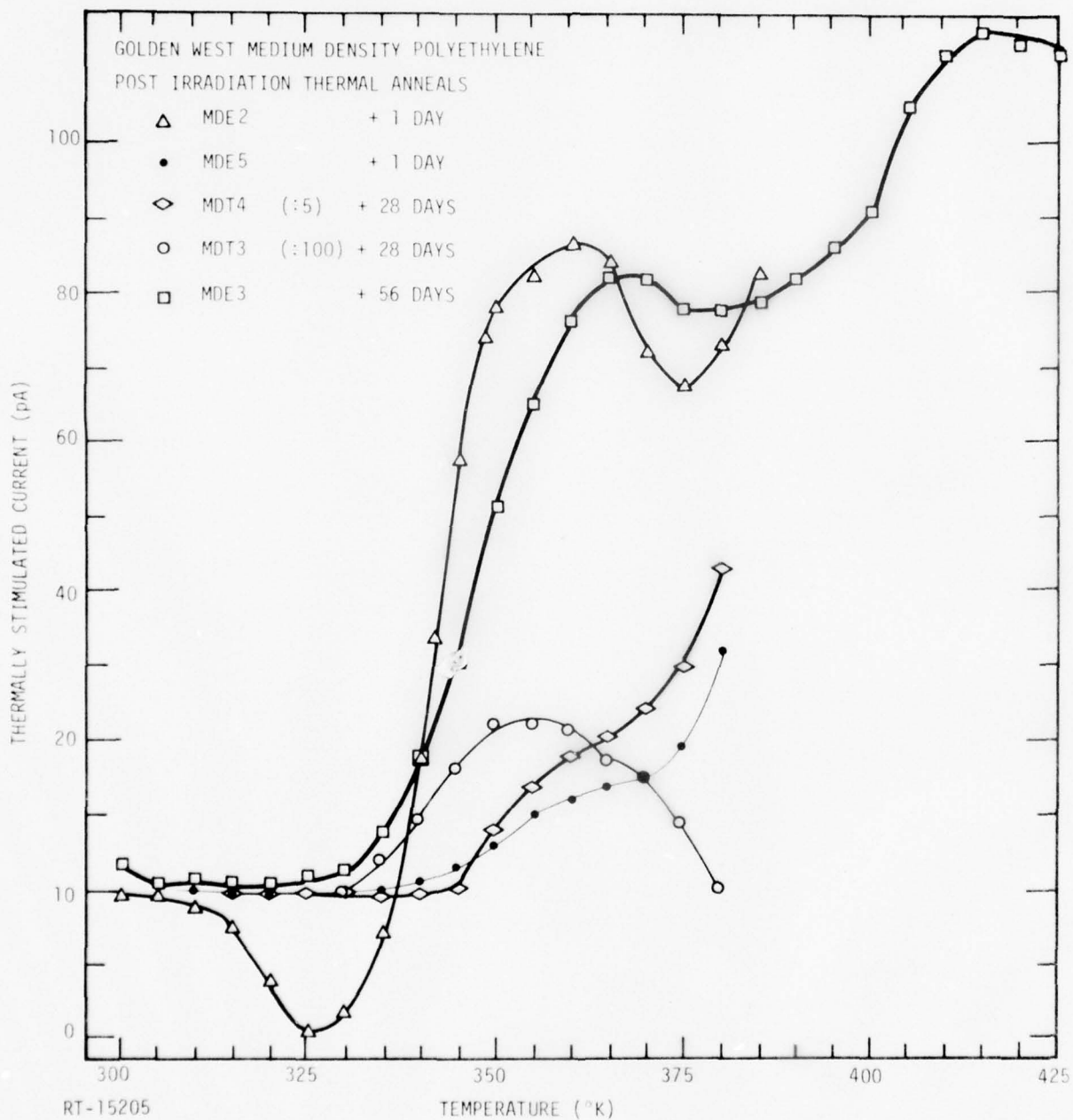


Figure 17. TSC spectra for a series of MD polyethylene samples which had been irradiated

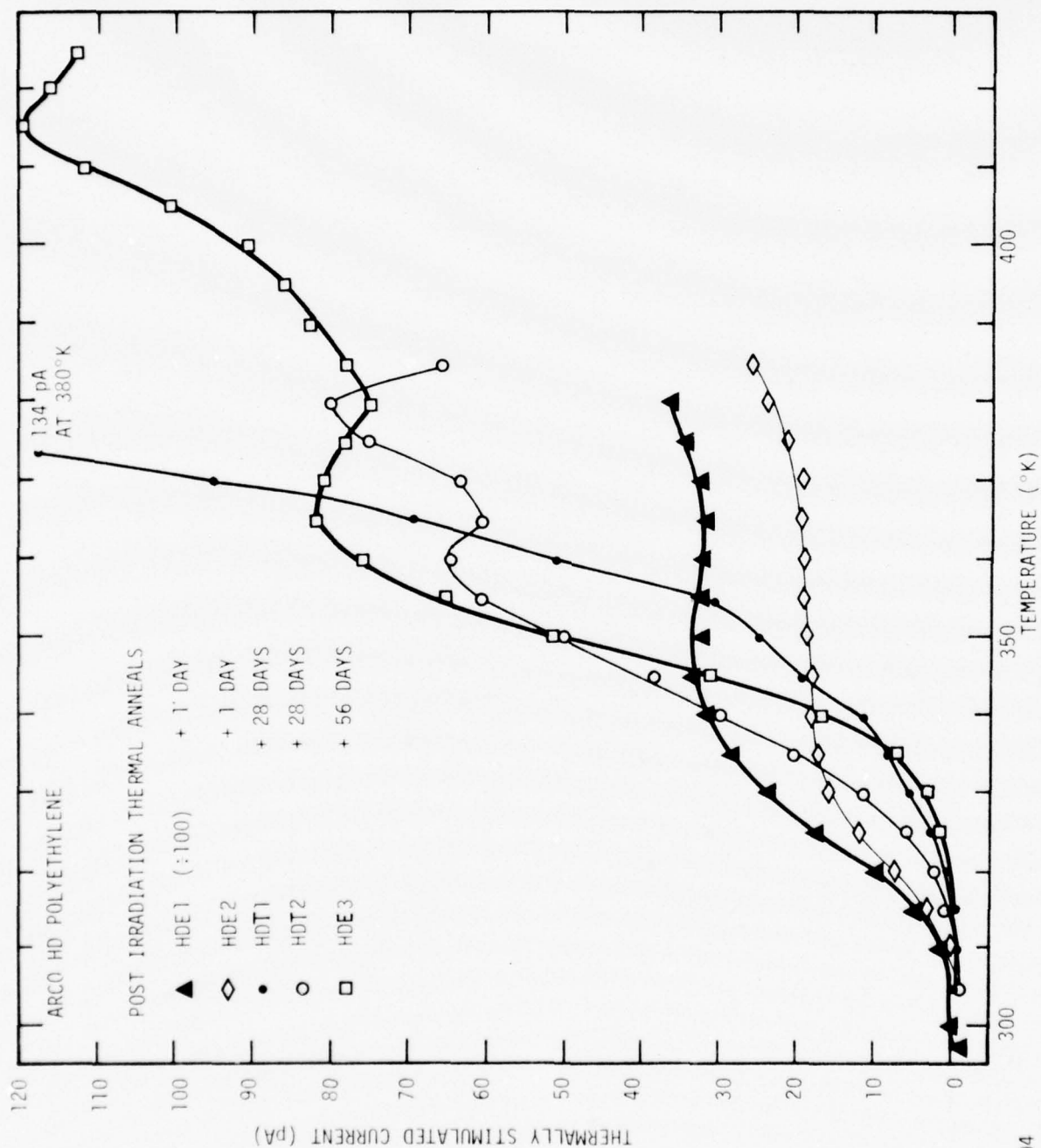


Figure 18. TSC spectra for HD polyethylene samples which had been irradiated

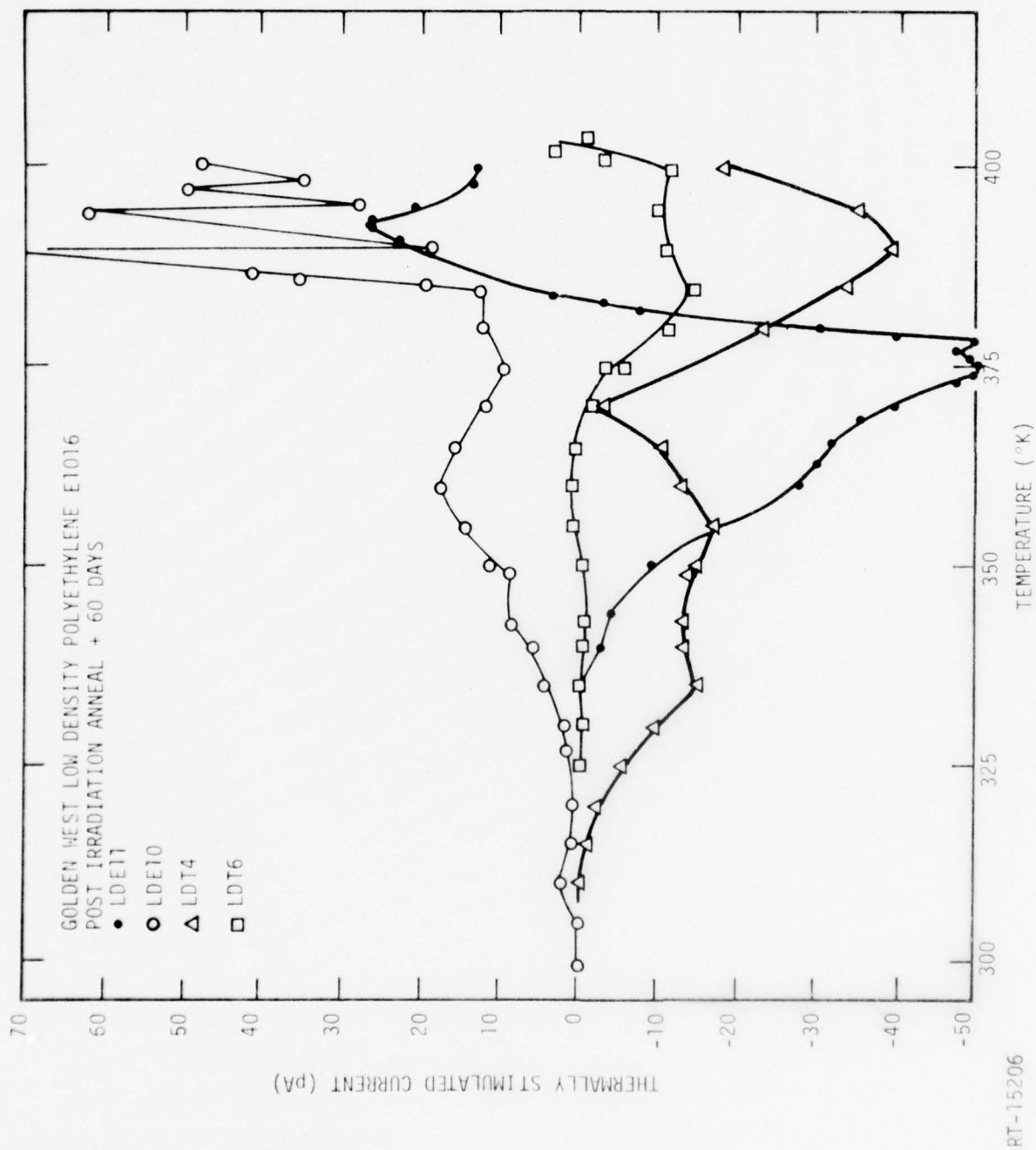


Figure 19. TSC spectra for low-density polyethylene which had been irradiated

high external field of ~ 1 MV/cm, trapped in polyethylene is very small over periods of several months. The response of the low-density polyethylene samples was relatively small. No estimate of the rate of relaxation of space charge could be made for these samples as all of the data was taken at one time. Only for some of these samples the net current evolved was negative.

It is difficult to make any additional statements about the trend of the data, because at least one sample of a given type did not behave quite like the remainder. For example, for a given film type, the net charge released by the burned-in samples (B) was on the average greater than that released by the annealed samples (A). However, the amount of charge released by MDT3 is the largest for the samples of this type of polymer. As a group, the net amount of charge released by the high-density samples were greater than that released by the medium-density samples, again excepting MDT3. Finally, those samples which show the largest κ_T , HDE1 and HDE3, were those exposed to the largest doses of radiation. It would be interesting in any forthcoming dielectrics program, especially one addressed to studying trapped-charge effects, to make a more careful study of charge buildup as a function of dose to determine the approach to an equilibrium charge state and then to determine the rate of relaxation of this charge after irradiation was ended. Such information is crucial in simulating the response of dielectrics charged in an exoatmospheric environment.

The shape of the post-irradiation TSC spectra for the medium-density samples are similar to those observed in preirradiation measurements. In general, the TSC increases with temperature; characteristic peaks or shoulders are evident at about 360°K . Such behavior was observed in last year's studies when TSC measurements were made on this polymer under similar burn-in conditions over a ramp range of 300 to 400°K (q.v. Figure 30, Ref 2). The behavior is also like that portion of the TSC spectra for T greater than 300°K shown in Figure 12. One sample, MDT3, shows a peak at 353°K , followed by a decline to zero, which is typical of the spectra for the majority of thermal annealings listed in Table 4. The similarity of shape and observed value of κ_T suggests that the relaxation mechanisms for these samples charged either by burn-in or radiation are similar and are related to those which govern normal conductivity in the polymer.

The TSC spectra of the ARCO HD polyethylene samples taken after irradiation show two patterns. In one, the thermally stimulated current increases with temperature until 340°K, above which temperature the current rise is much slower. In the other pattern, two peaks are evident at 360 to 370°K and 378 to 387°K, above which temperature the TSC goes to zero. Evidence of similar peaks have been seen in other spectra of this sample type (q.v., Table 3). The HDE3 sample whose temperature range was carried to 425°K also shows a peak at 410°K, comparable to one seen in HD polyethylene samples charged by friction, or positive corona charge.

The thermally stimulated current spectra for the low-density polyethylene samples measured 60 days after irradiation are the only ones in which the net emitted charge was negative. In order to completely depolarize each sample, the temperature ramp was carried to above 400°K. This was beyond the melting of the polymer, which was complete at 397°K according to its DSC spectrum. The high-temperature oscillations seen in the spectrum of LDE1 in Figure 19 are undoubtedly due to the deterioration of this capacitor as its melting point was approached. The spectra all show peaks between 375 and 400°K. In addition, there are smaller peaks at 340 to 360°K, a temperature interval where the pre-irradiation thermal anneals also showed prominent peaks. At the end of the temperature ramp, the persistent charge distributions were completely relaxed, so no isothermal annealings were carried out.

4.4 DISCUSSION OF RADIATION RELAXATION MEASUREMENTS

Our observations on the response of the polymer samples subjected to irradiation can be summarized as follows.

1. The general pulse shape observed during irradiation is one that rises linearly with the Linac pulse and decays with a $1/e$ time $\sim R_L C$. One sample, HDE3, behaved somewhat differently, emitting a relatively large amount of charge ($\kappa_R \sim 0.44$). Its pulse shape changed markedly during the course of the irradiation, showing not only sign changes but also a bipolar character. The net amount of charge released by this capacitor during its post-irradiation thermal annealing without any additional burn-in was also large ($\kappa_T = 1.39$).

2. For all samples, the net amount of charge released was much larger for burned-in samples than for those that were annealed. The average ratio of κ_R (burned in)/ κ_R (annealed) was 10.5:1 for the high-density capacitors, 8.5:1 for the medium-density samples, and 4:1 for the low-density samples.
3. For all of the samples, the ratio of the initial response to the asymptotic response $R_0/R_\infty > 1$. Even for the annealed samples $R_0/R_\infty \sim 3:1$.
4. The high-density samples as a group released the largest amount of charge when exposed to a series of radiation pulses expressed as the net charge released per unit area. The medium-density sample had the next greatest response. Because of partial depolarization prior to irradiation, it is not possible to accurately bound the radiation response of the low-density samples. However, they are morphologically similar to the medium-density samples, and one expects that their behavior should be similar.
5. The values of the κ_R observed were to the range of values of κ_T observed for these same samples measured during the prior series of thermally stimulated current measurements discussed in Chapter 3.
6. For comparison with cable response data discussed in Chapter 5, the observed emitted charge for the low- and medium-density samples induced by radiation consequent to burn-in is $\leq 62 \text{ pC/cm}^2$, while the two high-density samples released several hundred pC/cm^2 . Comparison with Tables 12 and 13 shows that the amount of charge per unit area released as a consequence of photon irradiation of the TFE cables and the TFE capacitors was comparable to that released by the low- and medium-density polyethylene samples. Expressed in terms of R_0 and R_∞ , and noting that a 1-cm length of most small coaxial cables has an outer dielectric surface area of $\sim 1 \text{ cm}^2$, the observed range of first-shot capacitor responses is comparable to that seen for the three cables whose radiation response is summarized in Table 11 (see Chapter 5 for tables).

7. The asymptotic responses of these capacitors R_{∞} are $\sim 10^{-15}$ C/rad, also typical of the output of these cables after a radiation annealing.
8. In equilibrium, the capacitor samples show polarization effects, i.e., the radiation field produced space charging whose effect was to counter the field-driven currents by generating an opposing conduction current.
9. Significant charge is released in the samples for doses of 1 krad(PE) per pulse as a result of the radiation-induced relaxation of persistent internal space and polarization charge. The state of uniform radiation response, i.e., radiation annealing, was reached after doses that were typically of the order of 50 krad(Si).

It is evident from our data that the presence of persistent internal polarization and space charge created as a consequence of burn-in in the polymer dielectric enhances the radiation response of these capacitors. Clearly, the net charge released by the samples that have been burned in is much larger than that released from annealed samples. It has been argued (Refs 41, 42) that similar effects can also be produced in layered metal-dielectric structures solely by the radiation-driven charge if one properly includes such effects as dose enhancement at high-Z/low-Z interfaces, deposition of charge because of the attenuation of the radiation beam, the return conduction currents that are driven by the fields created by deposited space charge, and the presence of gaps between interfaces. In fact, all of the phenomena observed in the inconsistent response of cables and of our capacitors can be simulated under the proper combination of radiation spectrum, dose, sample geometry including gaps, and correct modeling of the net flow of charge in the dielectric. However, we feel that, for the conditions under which our irradiations were carried out, these effects are not the principal determinants of the response of our samples. First, our irradiations were carried out with high-energy electrons (~ 40 MeV) rather than x-ray photons. Such electrons have a range of ~ 17 cm. As our samples were typically 1-cm thick, very few primary electrons were stopped in the sample. Second, most of the secondary

electrons emitted have energies of 1 keV or less (Ref 43). The observed range of such electrons is of the order of 0.1 μm , and those emitted from the electrodes into the dielectric will deposit insignificant amounts of charge or dose in the dielectric. There is also a small high-energy component with energies of the order of 10^5 eV and with about one-tenth the intensity of this low-energy component. Such electrons will penetrate the bulk dielectric, where they will be stopped. They might deposit significant additional charge and dose, as their range is of the order of the dielectric thickness.

One can estimate whether the secondary electrons contribute significant dose enhancement. The average amount of energy deposited per incident primary electron is about 5 keV per electron, based on their stopping power at these energies. The data of Reference 43 suggests that each primary electron produces about 0.01 high-energy secondary electrons from a metal like aluminum. This value decreases markedly as the thickness of the metal decreases below 0.01 g/cm^2 . In fact, the thickness of the metalization is about 10^{-5} cm, or 2.7×10^{-5} g/cm^2 . For type T samples, which contain 1-mil aluminum tabs, the surface density is 6.8×10^{-3} g/cm^2 . This implies that the dose enhancement contributed by an energetic secondary electron is less than 0.01×50 keV or 0.5 keV per incident primary. This energy is small relative to the dose delivered by the primary beam, and hence there is little dose enhancement. Thus, the dose measured by an external dosimeter is close to that delivered to the dielectric, provided that the differences in stopping powers are taken into account. One finds

$$\begin{aligned} \text{Dose(PE)} &= \left(\frac{1}{\rho} \frac{dE}{dx} \right)_{\text{PE}} \bigg/ \left(\frac{1}{\rho} \frac{dE}{dx} \right)_{\text{Si}} \times \text{Dose(Si)} \\ &= 1.18 \text{ Dose(Si)} \end{aligned} \quad (19)$$

for 40-MeV electrons according to Berger and Selzer (Ref 44). In the data of Table 9 we have not made this conversion as we do not judge the accuracy of the dosimetry to be much better than 10-20 percent.

One must still address the question of whether the observed effects are due to a significant accumulation of space charge because of stopping of energetic secondary electronics in the dielectric.

From the data in Table 8 it can be seen that the net response of samples with metalized electrodes (type E) is typically greater than that of a sample of the same type of film with foil tabs (type T) which underwent the same preconditioning. It is possible that this difference is due to deposited space charge which creates fields that drive currents that oppose the radiation response of the samples. Clearly, the number of such secondary electrons generated will be much larger in the type T samples than in the type E samples because the metal foil is much thicker than the metalization. However, the interpretation of our results is made difficult in that we are looking at the net response of many-layered structures, of the order of ~ 100 attenuating metal and dielectric layers. The net response of these samples is due to several components. First, there is the relaxation of space and polarization charges in the dielectrics. Second, there is the contribution of the radiation-driven charge, primarily the stopping of secondary electrons in the dielectric. Third, there are the radiation-enhanced conductivity currents created because of the presence of inhomogeneous charge distributions in the dielectric. The evidence that we have presented indicates that for these samples, under high-energy electron irradiation, the predominant effect is due to the relaxation of persistent internal fields. Unlike x-ray irradiation, the total dose delivered through the sample is relatively uniform. Because of this, and because we have a multi-layered structure, the effect of the motion of secondary electrons and conductivity currents are also relatively uniform in each layer. Therefore, the net contribution of those contributions to the total current other than that due to the relaxation of persistent internal fields tends to cancel when summed over the entire sample. This is evidenced by the fact that the asymptotic response of each sample is smaller than the initial response and relatively uniform for sample to sample. Whether the equilibrium response is positive or negative depends entirely on the structure of the capacitor, including the possibility that there may be small gaps between particular layers which will have a predominant effect on determining a sample's asymptotic response. We have remarked that after complete relaxation was achieved, radiation-induced polarization could be seen to diminish the net response of these samples. However, this was a much smaller effect than that due to relaxation of persistent

fields. In fact, even where significant dose enhancement effects occur, i.e., the x-ray irradiation of thick metal-dielectric systems (Ref 41), the effect of persistent polarization introduced by manufacturing or handling processes in polyethylene can still be seen to significantly alter the first pulse response of such structures.

The behavior of sample HDE3 was anomalous. It showed a large net charge release as well as a signal whose shape changed from pulse to pulse. It is our judgment that its behavior was due to the presence of gaps between the layers of these samples, introduced because of the manner in which it was wound, or a consequence of expansion and contraction during previous thermal cycling. If such gaps were present, burn-in might introduce specific significantly larger amounts of space charge into the polymer because of breakdown in them in a manner described in Chapter 3. In addition, the presence of the gaps would alter the radiation response of the capacitor because of secondary electron range enhancement and the return currents which flow if trapped air is present. Such effects have been postulated to produce pulse shapes comparable to those observed in HDE3 in cables (Ref 37).

It is significant that the high-density samples as a group released the largest amounts of persistent charge consequent to burn-in when exposed to ionizing radiation. We have noted in Chapter 3 that the conductivity of linear high-crystallinity polyethylenes is lower than that for low-density, low-crystallinity forms of this polymer. The stability of Corona-charged polyethylene electrets is enhanced as the crystallinity of the polyethylene is increased. Such evidence has been taken as indication that the traps that determine charge motion in these materials tend to be deeper than in the non-crystalline varieties of polyethylene. It is also possible that the concentration of such traps is dependent on the fractional crystallinity. This conclusion is implicit on the results of Sawa et al. (Ref 27). If this were true, then one might find that high-density, high-crystallinity samples are able to store more persistent charge. While the data of Table 8 suggests this fact, more measurements need to be undertaken to determine whether our results really reflect a morphological property of the polymer or are sample dependent. In particular, it would be interesting to perform a series of

experiments in which the charge storage properties of a given type of polyethylene are studied by varying its crystallinity by various thermal treatments.

Ideally, the response of these capacitors, which consist of alternating layers of metal and dielectric, can be predicted by one of the recently available codes such as that of Chadsey and coworkers (Ref 37) or Pignaret and Stroback (Ref 41) which have been developed to predict the behavior of metal-dielectric structures such as cables. Such codes can, in principle, take into account the presence of space-charge fields in the dielectric. In fact, to predict the radiation response of dielectrics, with persistent internal fields, one must specify the initial conditions, i.e., the spatial distribution of trapped charge and molecular dipoles and polymer dielectrics at the start of irradiation. The specification of the spatial distribution of molecular dipoles is relatively simple. Thermal annealing data imply that they are uniformly distributed throughout the dielectric. One can use the measured values of κ_T released consequent to burn-in, for example, to provide an upper bound on the dipole concentration, or in the absence of specific burn-in data, a value like $\kappa_0 - \kappa_\infty$. More problematic is developing a realistic physics model which describes how the radiation-generated electrons relax the dipole distributions. Radiation seems to be a much more efficient manner in producing a given degree of relaxation as measured by κ_R or κ_T than by heat. For example, if we take 50 krad as a typical dose required to produce the asymptotic state, i.e., complete relaxation of the persistent internal field created by burn-in, then this corresponds to an energy of about 0.1 cal/g. On the other hand, the energy introduced by thermal annealing, ΔQ , is given by $\Delta Q = C_p \Delta T$ where C_p , the specific heat, is ~ 1 cal/g $^\circ$ K for polyethylene. For a temperature rise of $\sim 100^\circ$ K, this corresponds to 100 cal/g.

A second problem in applying the codes is that we cannot specify with certainty where the trapped space charge resides. Model calculations should be carried out for various distributions of space charge ranging from one where all of the charge is trapped near the dielectric surface to one in which it is uniformly distributed throughout its volume. The former will be useful in simulating possible surface charging effects such as friction or extrusion. The latter can simulate volume charging by processes such as burn-in or

high-energy electron or gamma irradiation. As we have discussed in Chapter 3, part of this charge resides at the interfaces between crystalline and amorphous domains whose dimensions are of the order of several hundred angstroms, which is small compared to the thickness of the dielectric and thus can reasonably be modeled by a uniform charge distribution.

5. TETRAFLUOROETHYLENE DIELECTRIC CABLE AND CAPACITOR STUDIES

5.1 INTRODUCTION

The original impetus for studying persistent charge/polarization effects in metal-polymer dielectric systems was to understand the phenomena responsible for the anomalously large response of capacitors containing polymer film dielectrics when exposed to radiation pulses. However, it has more recently become evident that the radiation response of other metal-polymer dielectric systems, such as coaxial cables, may also be problematic. The possible appearance of a large first-pulse signal and the inconsistent response of a cable to a series of radiation pulses have made the prediction of system survivability/vulnerability difficult. Therefore, during the course of this program, it was mutually agreed between IRT and the COR that some of the effort that was to have been spent on examining charge storage and electrode effects [cf., item F2(d) of the Statement of Work] would be redirected to provide support to the, at that time, forthcoming DNA Cable Program. In this chapter the study made of the thermal and radiation response of series of semirigid Teflon dielectric cables is described. These cables have been used in instrumenting simulator and UGT SGEMP experiments, and are also used in, or are similar to, satellite cables. The second section of this chapter includes a review of the radiation response measurements made by Eric Weenas, while at IRT, on samples of these cables with the Simulation Physics, Inc. (SPI) Pulse 6000 x-ray facility early last year. For comparison, and as a first step in gathering input for the IRT/DNA Cable Program, we have also reviewed data on the response of these cables under different conditions of irradiation. The third section of this chapter discusses the thermally stimulated current measurements made on samples of the same types of cables as those exposed at SPI. These measurements were carried out to see if a correlation similar to that found for the capacitors exists between radiation response and thermal response of the cables. This section

also includes a discussion of the TSC spectra obtained for a series of Teflon-TFE capacitors. These measurements were made to provide improved data on the charge release consequent to burn-in as a function of temperature for this polymer, which is the most commonly employed dielectric in high-quality coaxial cables. The original TFE capacitor measurements (Ref 1) were taken at the beginning of this program when techniques for obtaining the TSC spectra were still under development.

5.2 RADIATION MEASUREMENTS

Two cable types were examined in the radiation test at SPI. These were a 0.1-inch o.d., all-aluminum conductor cable that was constructed according to the specifications of Dr. Carl Baum of the Air Force Weapons Laboratory, which we designate the 0.1-inch AFWL cable, manufactured by Uniform Tubes, Inc. The other cable was a standard 0.085-inch o.d., copper-jacketed (Cujack) cable manufactured by Cablewave Systems, Inc. In addition, a third cable type, a standard 0.141-inch o.d. Cujack cable (also from Cablewave) was thermally annealed. All three kinds of cables have been used to instrument sensors fielded in both simulator and UGT tests, and the Cujack cables are used in satellites as well. Their structures are summarized in Table 9. No pre-conditioning such as thermal annealing of these cables was carried out before irradiation. They were bent into circles for exposure.

The photon spectrum to which the samples were exposed is given in Figure 20. We estimate its peak to lie at about 52 keV, while the mean photon energy is about 61.8 keV. The full width at half maximum (FWHM) of the radiation pulse was about 70 nsec. The exposure fluences were all 0.4 mcal/cm^2 , except for the first pulse to which the 0.1 AFWL cable was exposed, which was 10 mcal/cm^2 .

The initial and asymptotic response of each cable is given in terms of its peak response expressed as $\text{ma}/(\text{cal/cm}^2) \cdot \text{cm}$ in Table 10. In order to compare these data to measurements made on the same cables at other facilities, it is necessary to convert the x-ray fluence (Φ) or flux ($\dot{\Phi}$) into an equivalent dose (dose rate) because most cable responses have typically been expressed in terms of the charge (current) per unit dose (rate) per unit

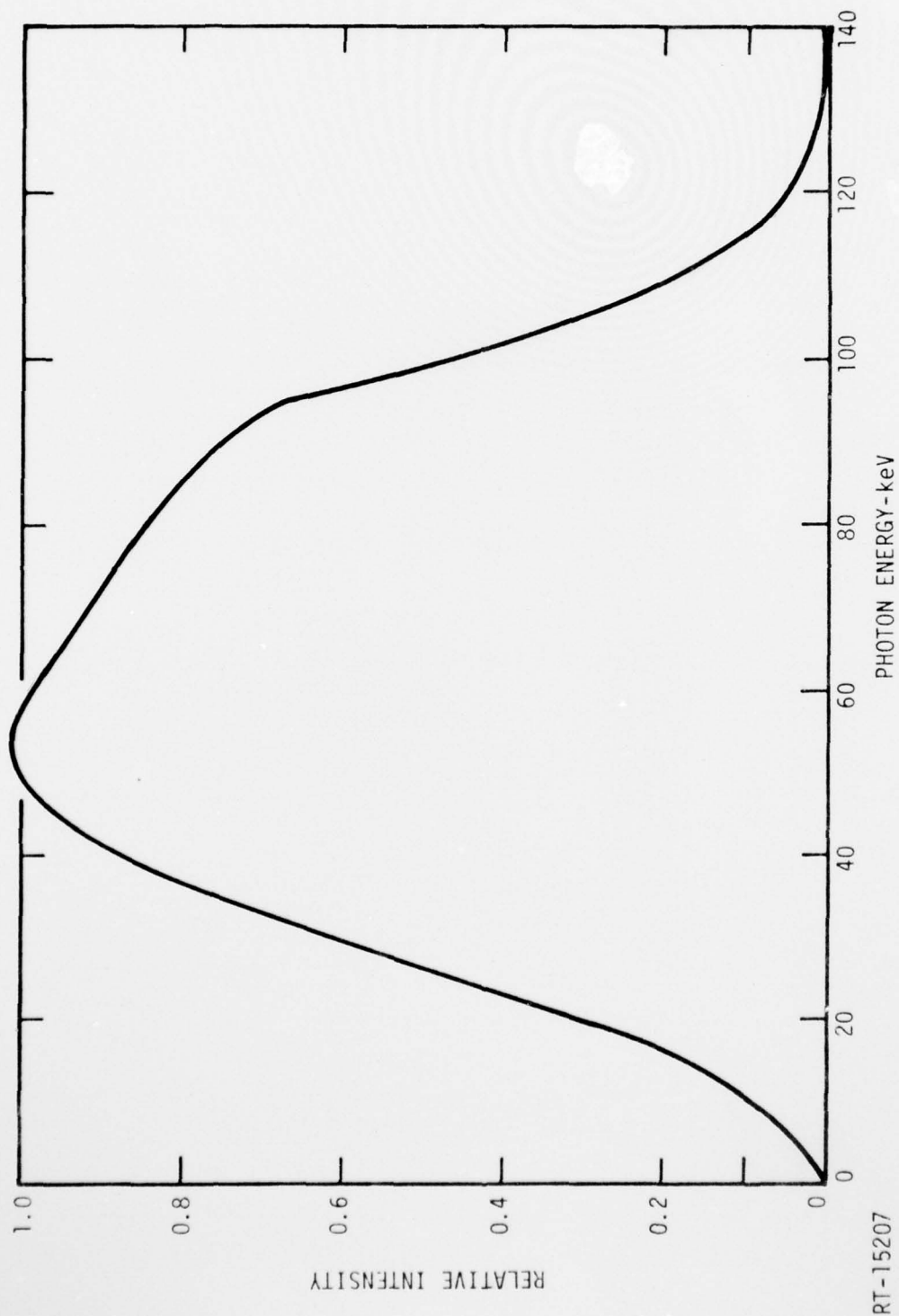


Figure 20. SPI Pulse 6000 x-ray spectrum determined from deposition profile

TABLE 9. SUMMARY OF TEST CABLE STRUCTURES

Type	Impe- dance (ohms)	Outer Conductor			Center Conductor		Dielec- tric	Manufacturer	Capacitance of Burn-In Samples (pF)	Outer Dielectric Surface Area (cm ²)
		o.d. (in.)	i.d. (in.)	Thickness (inches)	Material	o.d. (in.)	Material			
0.1 AFWL	50	0.100	0.080	0.010	Al	0.0244	Al	Uniform Tube	81.1	51.8
0.085 Cujack	50	0.085	0.066	0.0095	Cu	0.020	SPCW ^a	Cablewave Systems	90.1	47.4
0.141 Cujack	50	0.141	0.119	0.0115	Cu	0.036	SPCW ^a	Cablewave Systems	90.3	85.8

^aSPCW = Silver-plated copper-covered steel.

TABLE 10. SUMMARY OF CABLE RESPONSES - IRT/SPI

Type	ϕ (mcal/cm ²)	D [krad(Si)]	\dot{D}_{\max} [10 ⁹ rad(Si)/ sec]	Exposed Length (cm)	Cavity Pressure (torr)	Shot	Peak Signal (mV)	Response	
								mA/(cal/cm ²) • cm	10 ⁻¹⁵ amps/ [rad(Si)/sec] • cm
0.1 AFWL	10	3.37 ^a	48.1 ^b	28	10 ⁻⁴	1	600	-43	-8.9
	0.4	0.134	1.92	56	10 ⁻⁴	≥2	-2	-1.8	-0.37
0.085 Cujack	0.4	0.134	1.92	28	10 ⁻⁴	1	-100	-179	-37.1
	0.4	0.134	1.92	28	10 ⁻⁴	2-5	2	3.6	0.75
	0.4	0.134	1.92	28	760	6	6	10.7	2.23

a. For 337 krad(Si) = 1 cal/cm².b. For 4.81 x 10¹² rads(Si)/sec = Dose/FWHM.

length, where the dose is that delivered to an external dosimeter. An accurate estimate of the dose delivered to the cable dielectric would account for (a) attenuation of the x-ray pulse passing through the cable wall, (b) hardening of the spectrum, (c) dose enhancement effects because of the photoelectrons emitted at the conductor-dielectric interface, and (d) the presence of gaps between the conductors and dielectric. The significance of all of these effects on cable response have recently been identified (Ref 37). Most dosimetry to date has been expressed in terms of the dose delivered to a silicon dosimeter or TLD located at the position of the cable in the radiation field. This is equivalent to relating response to incident fluence. A conversion from fluence to external dose can be derived with the mean mass absorption coefficient in Si for the spectrum of Figure 19. For a thin absorber, the equivalent dose D is related to the fluence Φ by

$$D[\text{rad}(\text{Si})] = \Phi \left(\frac{\mu_a}{\rho} \right)_{\text{Si}}, \quad (20)$$

where μ_a/ρ is the average mass absorption coefficient. We estimate that this quantity is equal to $0.80 \text{ cm}^2/\text{g}$, based on tabulated values of the mass absorption coefficient as a function of energy for Si given by Evans (Ref 45). This is equivalent to a dose-fluence conversion of $337 \text{ krad}(\text{Si}) = 1 \text{ cal/cm}^2$. For a pulse whose FWHM is $T_{1/2} \simeq 70 \text{ nsec}$, typical for the SPI pulse 6000 pulse, the peak dose rate \dot{D}_{max} is approximately

$$\dot{D}_{\text{max}}[\text{rad}(\text{Si})/\text{sec}] = \frac{\Phi}{T_{1/2}} \left(\frac{\mu_a}{\rho} \right) = 4.8 \times 10^{12} \Phi(\text{cal/cm}^2). \quad (21)$$

Equations 20 and 21 have been used to convert the SPI data.

For comparison, we have summarized the measured radiation responses of samples of the same types of cables as determined by other investigators in Table 12. The response of each cable was that across a 50-ohm termination. The signal polarity was measured from center conductor to ground. The other IRT results were obtained at the TRW Vulcan facility, whose effective photon energy for dosimetry is about 725 keV. Those data of Notthoff, denoted MDAC

AD-A044 535

IRT CORP SAN DIEGO CALIF
RADIATION EFFECTS IN INSULATOR MATERIALS.(U)
FEB 77 J WILKENFELD

F/6 9/1

UNCLASSIFIED

INTEL-RT-8148-011

HDL-CR-77-089-1

DAA639-76-C-0089
NL

2 OF 2

AD
A044535



END
DATE
FILMED

10-77

DDC

TABLE 11. RELATIVE CABLE RADIATION RESPONSE

Type	By Whom/ Facility	Spectrum	Average Dose per Pulse [rad(Si)]	Response		Exposure Pressure (torr)
				R_0 amp/[rad(Si)]/sec]-cm	R_∞ amp/[rad(Si)]/sec]-cm	
0.1 AFWL	IRT/SPI	X-ray ^a	3370/134	-8.9×10^{-15}	-0.37×10^{-15}	10^{-4}
	IRT/Vulcan	Gamma	~ 3000	-1.0×10^{-15} ^b		760
	Aerospace/DPF	X-ray	~ 25	$-0.5 \rightarrow +1 \times 10^{-16}$ ^c		<100
0.085 Cujack	IRT/SPI	X-ray	134	-3.7×10^{-14}	0.75×10^{-15}	10^{-4}
	Aerospace/DPF	X-ray	~ 25	$1 \rightarrow 2 \times 10^{-16}$ ^c	2.23×10^{-15}	760
	MDAC/TREF PR-1590	Gamma	~ 1500	$\begin{cases} 7.9 \times 10^{-15} \\ -5.8 \times 10^{-15} \end{cases}$ ^d		<100
0.141 Cujack	IRT/Vulcan	Gamma	~ 3000	-5.0×10^{-15}		760
	Aerospace/DPF	X-ray	~ 25	$-1 \rightarrow +1 \times 10^{-15}$ ^c		<100
	MDAC/TREF FX-100	Gamma	400	-2.6×10^{-15}	-1.0×10^{-15}	760

^aThe denotation x-ray means a photon spectrum with energies predominantly below 100 keV. The denotation gamma means a photon spectrum with energies predominantly above 100 keV.

^bWhere only an initial response is listed, the asymptotic response is essentially unchanged.

^cThe cable response was spectrum dependent (Ref 47).

^dBipolar, peak responses of each polarity are given.

(Ref 46), were taken at the AFWL TREF facility on gamma simulators, one the FX-1000 and the other the PR-1590. The spectrum from these machines is basically the bremsstrahlung radiation produced by approximately 6-MeV electrons incident on the converter. The Aerospace Corporation data was obtained by Hai and Beemer (Ref 47) on the DPF facility, which is an x-ray machine.

In these tables we have tried to list some of the relevant factors describing the conditions of irradiation. It has now become clear that merely giving the response of a cable expressed as the charge release per unit dose per unit length is not sufficient. Any compilation of cable data must include the following elements. First, a knowledge of the flux, spectrum, fluence, and cable structure to calculate the driven-charge response, including dose enhancement across interfaces. Second, accurate values of material parameters to compute quantities such as the radiation-induced conductivity. Third, one must know if gaps are present between the dielectric and conductors and whether or not there is air present in these gaps. Fourth, some bound must be put on the amount and distribution of stored charge introduced into the cable dielectric by manufacturing, handling, or radiation in order to determine the initial state of the dielectric. The significance of a stored charge in enhancing the response of metal-dielectric systems is quite evident in the polyethylene capacitor data that is presented in Chapter 4 of this report.

The data taken at the SPI facility and shown in Table 10 are interesting in that they present a miniature compendium of observed cable responses to photons. Both cables show the first pulse anomaly; i.e., the first pulse response as measured by its shape, polarity, and charge emitted per unit dose is quite different from that for the n^{th} pulse asymptotic response. As is often the case, the net charge released per unit dose (R_0) was much larger than that released in its equilibrium state (R_∞). These cables reached an asymptotic state after only one pulse. Because of the difference between the first pulse fluences to which the cables were exposed, one cannot make more than an order of magnitude estimate on the size of the dose needed to (a) produce a detectable first pulse response, and (b) to reach an asymptotic state. These data suggest that dose regimes of 100 to several krads are significant, which is also confirmed by the other cable data presented in Table 11.

The response of the 0.085-inch Cujack cable was significantly enhanced in comparison to its response in vacuum when air was introduced into the test chamber. Such changes have been attributed to the motion of ionized gas present in gaps between conductor and dielectric surfaces (Ref 48). It is likely that the negative space-charge field set up in the cable dielectric, which extends out across the gap as a result of the previous irradiation (i.e., the first six pulses), caused an enhanced drift of electrons, created as a consequence of air ionization, toward the outer conductor, which is equivalent to an increase in the positive current flow through the load resistor.

We have tried to illustrate in the limited collection of data presented in Table 11 how measured cable response can vary if taken under different experimental conditions. These data were taken on cables obtained from the same manufacturer, although probably from different manufacturing runs. It has been claimed that one can observe a variation in the response of cables of the same nominal type obtained from different manufacturers of up to a factor of four or more (Ref 48). This observation emphasizes our point that the history of a cable from the time it is manufactured until it is irradiated must be known to adequately define the conditions under which it is tested. It can be seen that the initial charge output per unit dose for a given cable type under different irradiation conditions can vary by factors of several hundred. The Aerospace data were taken at the lowest doses, which typically were of the order of 20 rad(Si). They show a much smaller response than the other measurements taken at doses per pulse, which were 10 to 100 times larger. No first pulse effects were seen by them. However, several practice shots were typically fired in the DPF before data was taken (Ref 49). Therefore, the data listed in Table 11 included no information on the first pulse response of these cables. At the other extreme, the IRT Vulcan data, typically taken at an exposure of several krad(Si) per pulse also show no inconsistent cable behavior. Both the IRT/SPI measurements and the MCDAC/TREF FX-100 data taken at doses of 100 to 500 rads per pulse do show such a first-pulse anomaly. Notthoff in Reference 46 summarizes the results of measurements on the behavior of 26 cables when exposed to flash x-ray irradiation and remarks that the first pulse tended to be three to five times larger than the asymptotic output if normalized to equal dose.

The limited evidence currently available suggests that one sees first-pulse anomalies in cables in which significant amounts of trapped charge are present when the dose per pulse is of the order of 100 rads or so, and that an asymptotic state is reached in which the response of a cable becomes uniform when a dose of several krads has been accumulated. These findings are supported by the experiments of Pignaret and Stroback (Ref 41) which were designed to eliminate the effects of gaps on the response of the layered metal-dielectric structure. For samples exposed to a large flash x-ray such as a Vulcan, the dose delivered by a single pulse is evidently large enough to induce an asymptotic charge distribution in the cable dielectric, i.e., all evidence of its initial condition is wiped out in the first pulse. These comments apply to samples in which persistent charge/polarization is present because of manufacturing processes or prior handling. The dose required to reach a constant response is undoubtedly dependent on the initial state of the dielectric, i.e., on the amount of persistent charge/polarization. Clearly, the results of our measurements on polyethylene capacitors (summarized in Table 9 have demonstrated that the deliberate introduction of additional persistent charge/polarization not only significantly enhances the response of these capacitors, but also takes significantly greater doses (typically tens of krads) to reach a state where the charge output per unit dose becomes uniform. A similar conclusion was reached last year during our studies on capacitors with polar dielectrics. There, one observed significant response which changed from shot to shot for doses of ~ 10 krad(Si) per pulse. The total dose required to depolarize some of these samples was as high as 500 krad(Si).

Any future cable program that involves cable irradiation must be carefully designed so that the relative contributions of the various effects such as driven charge, dose enhancement, gaps, stored charge, and trapped charge to the response of a cable can be determined as a function of dose, dose rate, and spectrum. Only if this information is known can one use test data to make predictions with confidence about environments that may be of system interest. It is now believed that presently available codes can predict that part of the response of cables due to driven charge taking into account particular geometries, including gaps. However, testing is required to validate the

predictive ability of these codes. What is not yet available is an adequate description of stored or trapped charge introduced as a consequence of particular sequences of manufacturing processes, testing, handling, or exposure in a radiation environment to provide the initial conditions for the exercise of the code. It is the aim of a forthcoming IRT/DNA cable program to provide at least part of this information.

5.3 THERMAL MEASUREMENTS ON CABLES AND CAPACITORS WITH TEFLON DIELECTRICS

Thermal annealing measurements were made on samples of the cable types shown in Table 9. The tests were carried out to compare the charge released from these cables to an external circuit by a thermally induced relaxation to that induced by radiation. The cable samples were all three feet long and were coiled in a circle about 10 inches in diameter (about one turn) for insertion into the annealing oven. One end of each cable was left open, while the other end was connected via SMA connectors and external cabling to an electrometer. Thermally stimulated current measurements were carried out over the range of 300 to 510°K at a rate of 1.9°K/minute. As the cables were not completely depolarized at the end of the TSC measurements, they were then held at approximately 475°K for periods of about 24 hours until the net current release became constant or went to zero.

Four thermal annealing measurements were performed. The first three were done to establish an equilibrium state for each cable; i.e., the first annealing determined its initial response, and then two successive annealings established an asymptotic response. Finally, the TSC spectrum was measured consequent to a burn-in at $T_B = 473^\circ\text{K}$, $V_B = 1 \text{ kV}$, $t_B = 1.1 \text{ h}$. The burn-in temperature and voltage were set at the manufacturers' recommended maximums for the cables.

In addition to the foregoing, several thermally stimulated current measurements were made on a pair of Component Research Type D11C, 100V, TFE dielectric capacitors of a kind similar to those studied two years ago. These capacitors, whose properties are given in Table 12 are packaged in hermetically sealed evacuated metal cans. They have leads connected to the dielectric and electrodes with soft solder, which is also used to seal the ends of the can.

TABLE 12. TEFLON TFE CAPACITOR RESPONSE

Sample	C(nF) D (@ 1 kHz)	T _B (°K)	V _B (V)	t _B	Ramp Temperature (°K)	Isothermal Temperature (°K)	TSC Peaks (°K)	κ_T (Ramp)	κ_T (Isothermal)	κ_T (Total)
CRD11C PTFE #2 $\kappa=2.05$ t=9.9 μm A=1229 cm^2	217.7 0	None			299-524	517.5	?	-8×10^{-5}	-8.2×10^{-2}	-8.2×10^{-2}
	215.9 0	446	100	15h 7m	301-525	519	309, ν (380-420) (m)	3.4×10^{-3}	1.9×10^{-3}	5.3×10^{-3}
	215.8 0	447	100	15h 15m	298-530	523	309, 380(m), 410(m)	2.1×10^{-3}	6.3×10^{-4}	2.7×10^{-3}
CRD11C PTFE #3 $\kappa=2.05$ t=9.9 μm A=1230 cm^2	216.8 0	None			229-524	517.5	ν (392-409) (n)	-2.15×10^{-5}	-9.7×10^{-4}	-3.1×10^{-3}
	216.8 0	446	100	15h 7m	301-525	519	329, 385(m) ?, 410(m)	3.4×10^{-3}	2.0×10^{-3}	5.4×10^{-3}
	216.1 0	447	100	15h 15m	298-530	523	317, 380(m) ?, 410(m), 490(m)	4.5×10^{-3}	2.8×10^{-3}	7.5×10^{-3}

a. The symbol "n" denotes a current minimum ($i < 0$). The symbol "m" denotes a current minimum where $i > 0$. The symbol " ν " means a broad peak or minimum. The symbol "?" denotes data which may be spurious.

An initial set of data was taken with the samples as obtained. It was necessary to keep the annealing temperatures to less than 458°K (185°C) to prevent the leads from opening because of melting of the solder. It was found that the TSC spectra obtained under identical burn-in conditions were not reproducible. It was evident that a significant amount of persistent charge/polarization remains in these samples at 450°K which relaxes very slowly, so that a consequent isothermal annealing is required. During this annealing, fairly large persistent currents of several picoamperes were observed which decayed to zero very slowly over several days. The irreproducibility of the TSC spectra was probably because of the presence of significant persistent charge remaining from each previous run. Moreover, repeated thermal cycling of the samples caused a deterioration of the contacts to the electrodes as evidenced by a rise in the sample dissipation factor.

Therefore, a new set of measurements were made in which the capacitors were removed from their cans and fitted with mechanical contacts to the electrodes. When configured in this manner, the samples could be repeatedly cycled to temperatures of up to 530°K without any apparent deterioration. A series of burn-ins were conducted under typical quality assurance conditions with $t_B = 15$ h, $V_B = 100$ V, $E_B = 100$ kV/cm, and $T_B = 448^\circ\text{K}$. As the capacitors were not completely relaxed at the end of a TSC ramp, they were held at about 520°K and isothermally annealed. The current was observed to decay rapidly to zero or to a constant but small value of a fraction of a picoamp.

The capacitor data is discussed first, to provide a reference for our evaluation of the thermal annealing measurements on the cables. The results of the TSC measurements on the TFE dielectric capacitors are summarized in Table 12. Figure 21 shows the TSC spectra for one of the capacitors. Lines have been drawn through the individual data points to more clearly show their trend. The spectra for the other sample were similar. All of the TSC spectra possess a generally similar shape. As the sample temperature is raised from its initial value at $\sim 300^\circ\text{K}$, a relatively large amount of current was released, which reached a peak at about 309 to 330°K. At higher temperatures the TSC declines, reaching a minimum at $\sim 410^\circ\text{K}$. This temperature is close to the glass transition temperature (400°K) for this polymer (Ref 50). While it is difficult

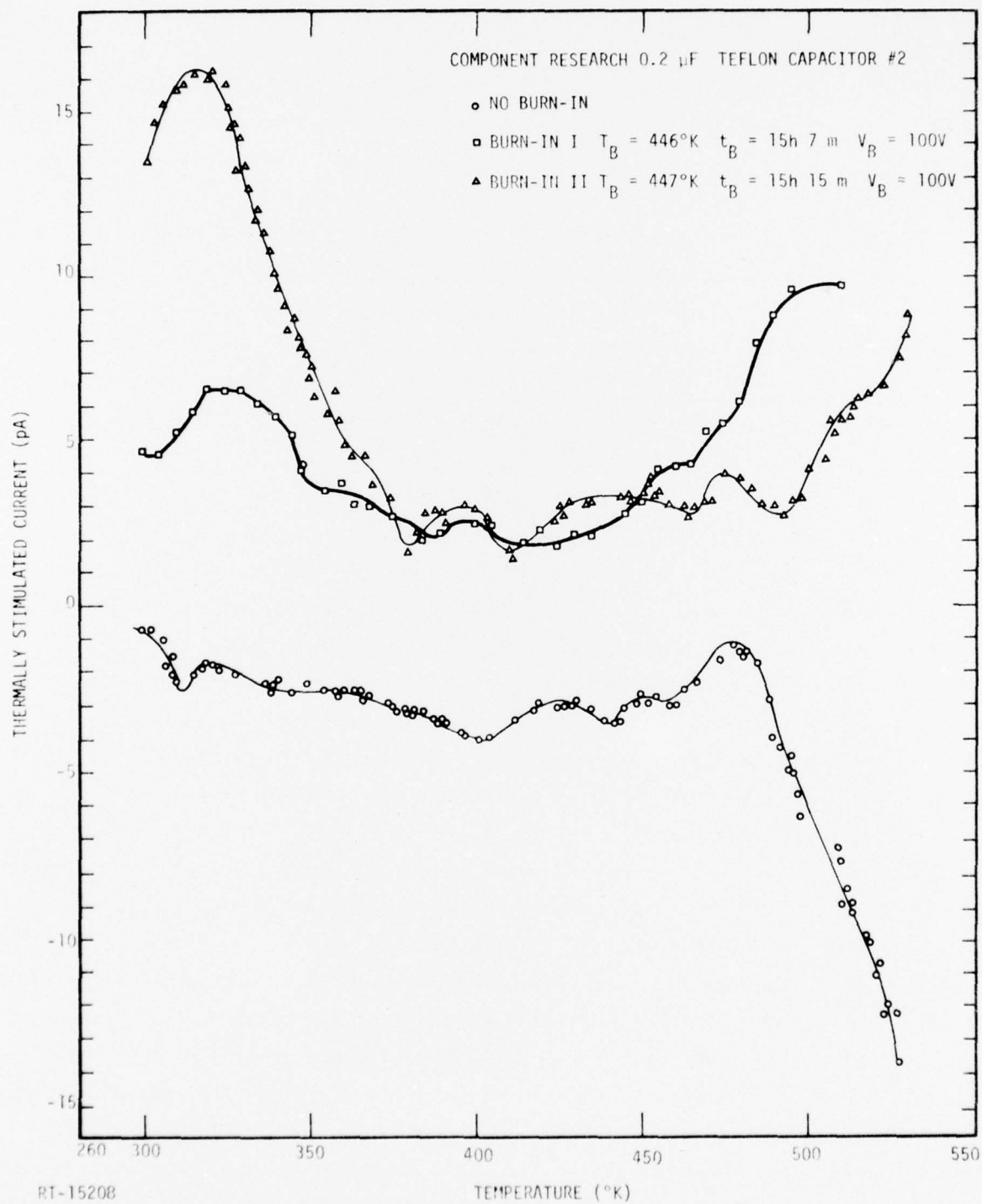


Figure 21. TSC spectra for a Teflon-TFE dielectric capacitor

to determine unambiguously because of the fluctuations in individual data points, there is evidence that small minima may also be present in the TSC spectra for these polymers at $\sim 380^\circ\text{K}$ and $\sim 490^\circ\text{K}$. At higher temperatures, all of the spectra for the samples after burn-in showed a rise in the current emitted. The initial TSC spectra of the two samples without burn-in went sharply negative, so the net κ_T for the ramp was negative. It is our judgment that the negative currents observed at the highest temperatures in these initial runs were a consequence of the incomplete annealing of these samples during prior runs where maximum temperature was limited by the melting point of the solder joints by which leads were attached to the electrodes. During the subsequent isothermal annealings for the burned-in samples, TSC currents went to zero in about one hour.

In Table 12, we have listed the net amount of charge released during the entire thermal annealing, as well as the separate contributions from the temperature ramp and the isothermal annealing in terms of the nondimensional parameters $\kappa_T(\text{Total})$, $\kappa_T(\text{Ramp})$, $\kappa_T(\text{Isothermal})$, respectively. These numbers have been computed with Equation 8. To convert them to an actual charge release, one need only substitute the sample and burn-in parameters given in Table 12. For the initial annealings, where no burn-in was applied, a κ_T was computed for a hypothetical $V_B = 100$ volts for comparison to the burn-in data. For reference, a κ_T of 1×10^{-3} corresponds to a released charge of 10.6 nC, or about 8.6 pC/cm². It can be seen that the net charge released under burn-in was positive, and that the observed bound on $\kappa_T < 7.5 \times 10^{-3}$.

The net charge released, expressed as κ_T , is much less than κ , the relative dielectric constant. Such a finding is reasonable. Polytetrafluoroethylene is a nonpolar polymer, as is polyethylene. Therefore, the nonelectronic component of the polarizability $\approx \kappa - n^2 = 2.05 - (1.35)^2 = 0.23$ is expected to be small. As the discussion presented in Chapter 3 points out, this difference is an upper bound on the amount of charge released in a thermal anneal consequent to burn-in by heterocharging. The net amount of charge released will be sample dependent, i.e., dependent on the concentration of dipoles or dissociable impurities introduced as a consequence of manufacturing procedures. The values of κ_T presented in Table 12 are, in fact, about equal to the value

of κ_R found for the radiation response of similar capacitors depolarized by 30-MeV Linac electrons (Ref 1). They are somewhat smaller than the values of κ_T found during an initial thermal depolarization of similar samples.

In Table 13 the data for the TSC measurements on the semirigid coaxial cables are presented. For comparison, the net charge release from the 0.100-inch AFWL and 0.085-inch Cujack cables during their SPI pulse 6000 irradiation are also shown. All charge release has been expressed in terms of the relevant κ 's. For the radiation data, and for the evaluation of the charge released during the thermal annealing of the cables without any burn-in, values of κ_R and κ_T were computed, using $V_B \equiv 1$ kV, which was the value used during the burn-in of these samples. Note that the cables were not burned in before irradiation. The TSC spectra for these cables are presented in Figures 22 through 24. Again, lines have been drawn through the individual datum to make their trends more readily visible. It is to be noted that the oscillations shown in the data of Figures 22 and 23 are probably not real. Measurement of current changes of ~ 100 fA is difficult with systems employing coaxial cables and connectors because of the noise introduced by the use of such components. It can be seen from Figure 24 that the currents emitted by the 0.085-inch Cujack cable are a factor of 10 larger and do not show these oscillations.

Several general observations can be made about the response of these cables when the persistent stored charge/polarization is relaxed by heat or radiation pulses. For the two cables irradiated, the net charge released as a consequence of this radiation is comparable to, or less than, that released during the initial temperature ramp for cables of these same types. Such behavior is similar to that observed for the series of capacitors examined last year (Ref 2) and for the polyethylene samples discussed in Chapter 4. These data further support our finding that thermal annealing may be used to bound the radiation response of cables due to the presence of stored charge. Second, for the 0.100-inch AFWL cable and the 0.141-inch cable, the amount of charge released to the external circuit does not appear to be significantly changed if each cable is subject to prior burn-in. On the other hand, the response of the 0.085-inch cable after burn-in is extremely large. The net

TABLE 13. CABLE RESPONSE

Cable	Burn-In Conditions	Anneal Temperature (°K)	Isothermal Temperature (°K)	TSC Peaks (°K)	κ_T (Ramp)	κ_T (Isothermal)	κ_T (Total)	κ_R
0.1 inch AFWL	As received	297-503	475	392(n), 470(n)	-2.4×10^{-2}	-8.0×10^{-2}	-1.0×10^{-1}	-3.1×10^{-2a}
	Anneal 2	295-507	473	430(n), 480	-5.7×10^{-2}	0	-5.7×10^{-2}	
	Anneal 3	295-504	473	460(n), 498?	-5.4×10^{-2}	-1.1×10^{-2}	-6.4×10^{-2}	
	[$T_B = 473^\circ K$, $V_B = 1$ kV $t_B = 1.1$ h]	306-514	477	475(n), 508	-6.0×10^{-2}	-1.1×10^{-2}	-7.1×10^{-2}	
0.085 inch Cujack	As received	297-503	475	478(n)	-1.17×10^{-1}	3.34×10^{-1}	2.3×10^{-1}	-1.1×10^{-2a}
	Anneal 2	295-507	473	400, 480(n)	-3.0×10^{-2}	1.30×10^{-1}	9.9×10^{-2}	
	Anneal 3	295-504	473	408, 475(n)	-7.6×10^{-2}	2.1×10^{-2}	-5.5×10^{-2b}	
	[$T_B = 473^\circ K$, $V_B = 1$ kV $t_B = 1.1$ h]	306-514	477	410(n)?, 470(n)	-4.0	1.0×10^{-1}	-3.9	
0.141 inch Cujack	As received	297-503	475	442(n)	-5.0×10^{-2}	4.6×10^{-2}	-0.4×10^{-2}	
	Anneal 2	295-507	473	424, 470	-6.5×10^{-2}	1.4×10^{-1}	7.3×10^{-2}	
	Anneal 3	295-504	473	425	-1.7×10^{-2}	9.6×10^{-2}	8.5×10^{-2}	
	[$T_B = 473^\circ K$, $V_B = 1$ kV $t_B = 1.1$ h]	306-514	477	440	-6.2×10^{-2}	1.4×10^{-2}	-4.9×10^{-2}	
1.0 uF PTFE	$T_B = 373^\circ K$	300-453	423		1.1×10^{-2}	2.2×10^{-2}	3.3×10^{-2}	6.7×10^{-5b}
	$V_B = 45$ V							
	$t_B = 16$ h							
Comp. Res. 05TL 3466								

^aIrradiated with SPI Pulse 6000 - x-ray spectrum ($<E>=61$ keV), ~ 134 rad(Si)/pulse.

^bIrradiated with IRT Linac (30-MeV electrons), ~ 2 krad(Si)/pulse.

^cThe symbol (n) denotes a minimum ($i < 0$). The symbol "a" denotes a broad peak. The symbol "b" denotes a possible peak.

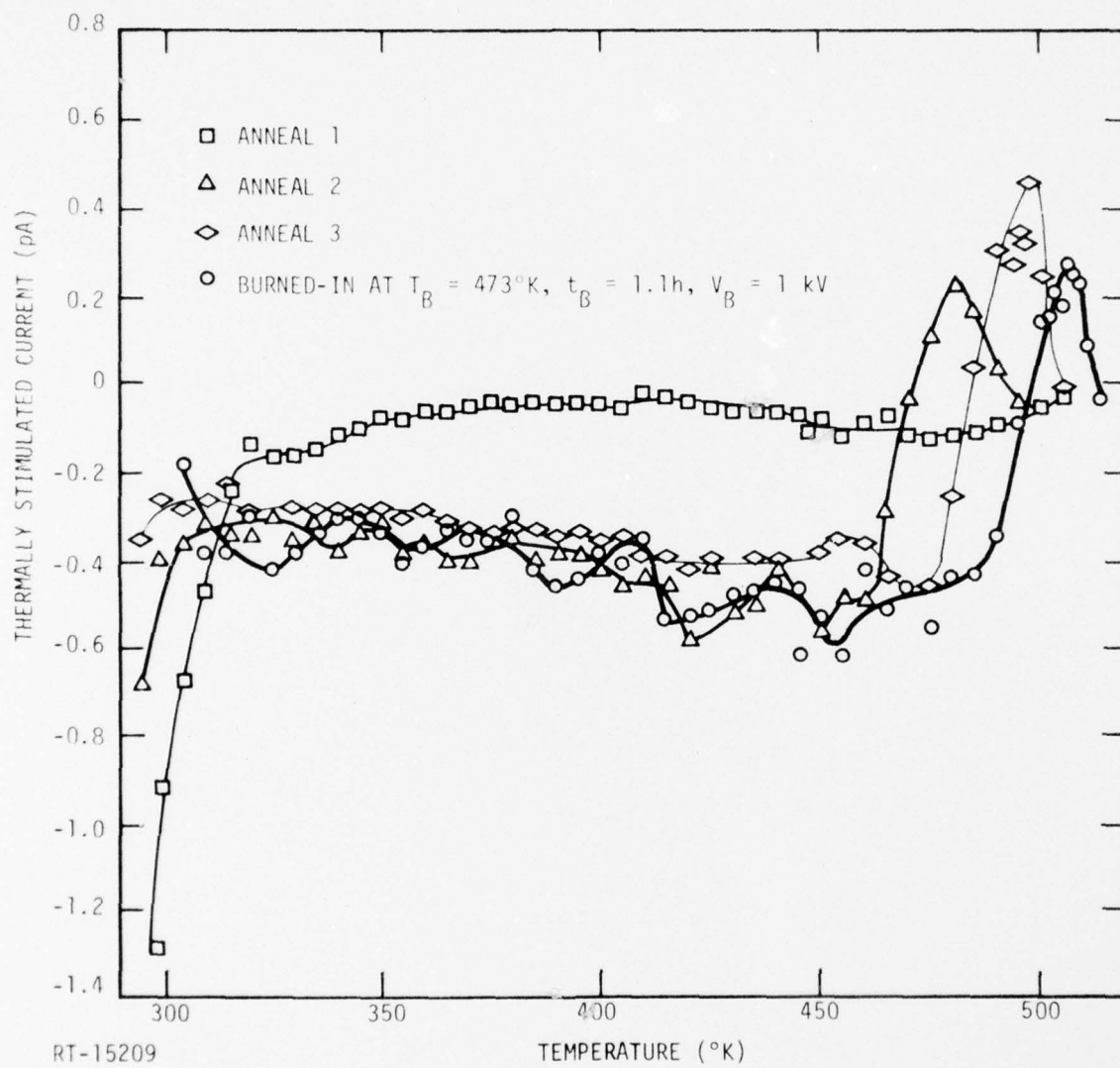


Figure 22. TSC spectra for 0.100-inch AFWL cable

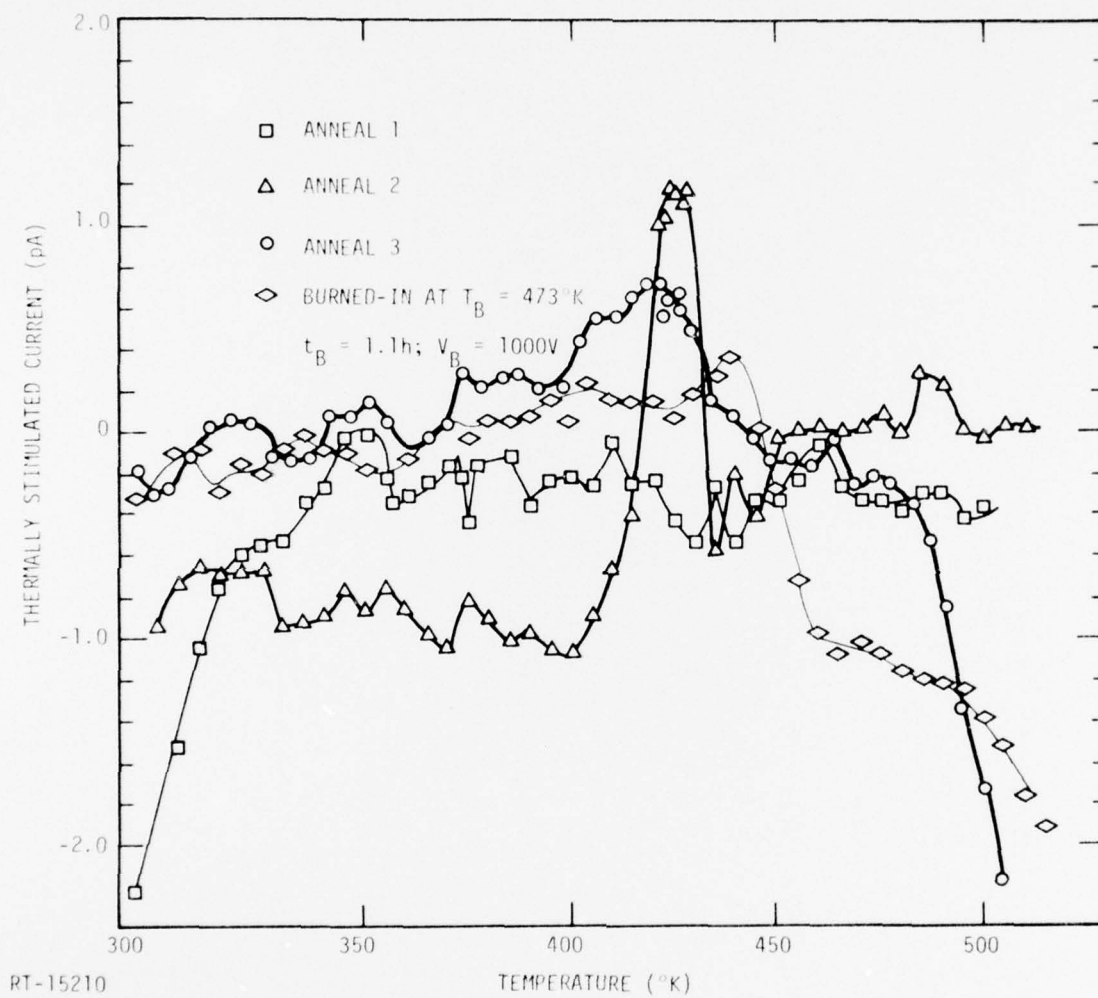


Figure 23. TSC spectra for 0.141-inch Cu-jack

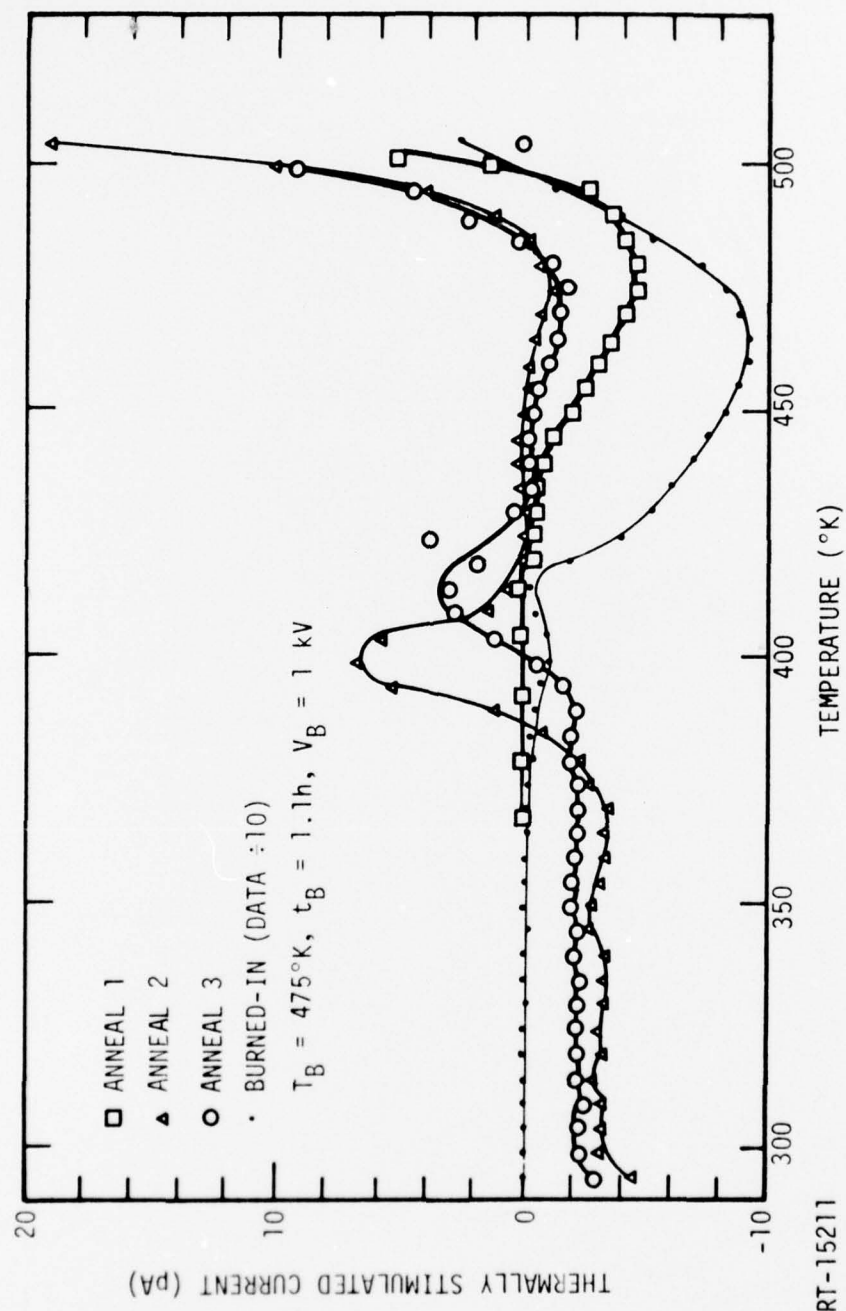


Figure 24. TSC spectra for 0.085-inch Cujack cable

charge released is a factor of 30 or so larger than that released from the annealed sample. Expressed as a κ_T , this charge release is ≈ -3.9 , which is nearly twice the magnitude of the normal dielectric constant (2.05) for polytetrafluoroethylene. Such large values of κ_T after heterocharging, i.e., burn-in under normal conditions, have only been seen for the thermal response of polar polymers where $\kappa \sim n^2 \sim \kappa$; i.e., the principal contribution to the total polarizability is nonelectronic due to the presence of aligned molecular dipoles or intrinsic impurity charges that are trapped at interfaces.

Another surprising aspect of the cable burn-in data is that the net charge released by these cables consequent to burn-in was negative; i.e., the net charge flow was from the center conductor of each cable biased at the higher potential during burn-in to the outer conductor, which was grounded. For relaxation after heterocharging, the net charge release should be positive (cf. Chapter 3) according to our sign convention as observed for the PTFE capacitors. The appearance of negative currents suggests that at least part of the charge released is a consequence of the motion of space charge in the polymer in the direction of the forming field.

With the exception of the burn-in data for the 0.085-inch Cujack cable, the net amount of charge released expressed as a κ_T was some 30 times or so larger than that released by the capacitors as a consequence of thermal anneal. However, such a comparison in this case is misleading. In Table 14 we have tabulated the net charge release per unit area for all of the samples examined that contain Teflon-TFE dielectrics. We have included in the table data for the three cables--the two Component Research 0.22- μ F capacitors, as well as a 1.0- μ F Component Research PTFE capacitor studied two years ago. It can be seen that the net charge released per unit area for these samples shows a much narrower range of variation (again with the exception of the 0.085-inch Cujack cable), typically being of the order of 100 pC/cm² or less.

These data suggest that the charge storage processes for the cable under burn-in is related to surface properties, i.e., represents charge stored near the dielectric surfaces. If the polarization charge were due solely to a uniform volume polarization due to the alignment of molecular dipoles or the accumulation of intrinsic impurity space charge at internal interfaces of

TABLE 14. CHARGE RELEASED FROM TEFLON DIELECTRICS

Sample	Run	Net Charge Released per Unit Area (pC/cm^2)			
		Ramp	Isothermal	Total	Radiation
0.1 AFWL	Initial	-18	-61	-79	-23
	Anneal 2	-44	~ 0	-44	
	Anneal 3	-41	-8	-49	
	Burn-in	-46	-8	-54	
0.085 Cujack	Initial	-109	320	211	-11
	Anneal 2	-28	120	92	
	Anneal 3	-71	20	-51	
	Burn-in	-3679	91	-3589	
0.141 Cujack	Initial	-26	24	-2	
	Anneal 2	-34	71	38	
	Anneal 3	-5	49	44	
	Burn-in	-32	7	-25	
1.0 μF PTFE	Burn-in	70	140	210	42
0.22 μF PTFE #2	Initial	-0.7	-706	-707	
	Burn-in 1	29	16	45	
	Burn-in 2	18	5	23	
0.22 μF PTFE #3	Initial	-18	-8	-27	
	Burn-in 1	29	17	46	
	Burn-in 2	39	24	63	

domains small compared to the thickness of the cable dielectric through the inhomogeneous polymer (Maxwell-Wagner polarization), the κ_T 's for the cable would be more nearly equal. This assumes that both the capacitor and the cable dielectrics have relatively equal concentrations of polarizable impurities. Such an assumption is not unreasonable as both were made from duPont Teflon-TFE. An observed constancy of κ_T was observed last year in a study of the thermal depolarization of capacitors from different manufacturers containing film of the same generic type but of different thicknesses. It is likely that the response of these latter capacitors is due to a volume effect. First, heterocharging of samples with good metalized electrodes is not thought to induce significant homocharging at the forming fields employed (Ref 51). Second, the net charge released per unit area from the capacitors if near the surface would probably be much larger because of the fact that the film is thinner than the cable dielectric. If the dielectric were charged with $\sim 1 \text{ nC/cm}^2$ to a surface depth of $\sim 10 \text{ }\mu\text{m}$ as a consequence of extrusion or friction (Refs 51,52), the resultant charge release per unit area, q , would be of the order of

$$q \approx (\rho_0 r_0) r_0 / 2\ell \quad (22)$$

for a dielectric of thickness ℓ charged uniformly to a depth r_0 with space-charge density ρ_0 (Ref 53). For the 0.085-inch cable, $\ell \approx 0.023 \text{ inch} = 584 \text{ }\mu\text{m}$. Then

$$q \approx 10^{-9} \frac{\text{C}}{\text{cm}^2} \frac{10}{584} \times \frac{1}{2} \approx 9 \text{ pC/cm}^2 \quad .$$

In fact, the observed charge released per unit area for the annealed samples is somewhat larger, suggesting that at least part of their response is due to a relaxation of a volume polarization.

The response of the 0.085-inch Cujack cable consequent to burn-in was large and negative (-3.6 nC/cm^2). This suggests the manner in which such a response might be created. The amount of charge released by the Teflon capacitors and the other cables was typically $\sim 100 \text{ pC/cm}^2$ or less. The amount of charge that can be injected into the polymer by corona discharge or electron

injection is much larger and is ultimately limited by air breakdown, but is of the order of 10 nC/cm^2 for dielectrics of thickness comparable to that in the 0.085-inch Cujack cable (Ref 40). The most likely explanation for the anomalously large response of this cable is as follows. During the course of the series of thermal annealing cycles, it was repeatedly heated to temperatures in excess of 500°K . This temperature is above the recommended operating limit for the cable, which is 433°K . It is quite likely that the repeated thermal cycling caused at least a partial separation of the inner and outer conductors and the dielectric because of their unequal rates of thermal expansion with the formation of gaps. If this is so, the application of high voltage across the cable could result in local breakdown across these gaps. Such breakdown can cause an injection of ions into the polymer (Ref 55), and is similar to homocharging by corona discharge. As the center conductor of the cable was at positive high potential during burn-in, it is likely that the injected ions would be positive. If, because of the gaps, the contact between the center electrode and the dielectric was at least partially blocking, the positive ions would tend to diffuse away from the blocking electrode into the bulk of the polymer, i.e., toward the outer conductor, resulting in a net negative replacement current flowing through the electrometer. The net charge per unit area released in this case would be comparable to the injected charge (Ref 25)

$$q = - \int_0^{r_0} \left[1 - \frac{x}{d} \right] \rho [x, T_0] dx \quad (23)$$

if the center injecting electrode is entirely blocking. As r_0/d for the cable is ≈ 0.01 , for a completely blocking electrode the observed charge would be equal to the injected charge. As the injecting electrode is probably only partially blocking, the net charge released is less.

It has been argued (Ref 48) that an important contribution to the anomalous response of cables is the presence of gaps between conductors and dielectrics. The presence of such gaps has only been confirmed after observing anomalous radiation responses by microphotography of cable sections (Ref 56) or by filling the gaps with a dielectric liquid and noting a diminished radiation response

(Ref 47). Our experience with the 0.085-inch Cujack cable suggests that it may be possible to pretest a cable for gaps by the application of high voltage followed by a TSC measurement. If significant homocharging occurs across these gaps because of breakdown, then it should be reflected in an anomalously large amount of current emitted during the thermal anneal.

While the general appearance of the TSC spectra for these cables and the TFE capacitors are dissimilar, they have some common features. The most significant is the rise in the TSC currents at temperatures above 475°K. This corresponds to a marked rise in the conductivity of this polymer (Ref 57). In addition, two of the samples (the 0.085-inch Cujack and the 0.141-inch Cujack) show peaks near or above the glass transition temperature (400°K) which gradually disappear as the sample was repeatedly annealed. The observed temperature dependence of the TSC current and the fact that the net current released to an external circuit was negative even after burn-in suggests that the predominant component of charged release to an external circuit reflects the motion of space charge in the polymer. It is difficult to ascribe any definite origin for the currents observed. Except in the case of the 0.1-inch aluminum cable, it was not possible to obtain a repeatable response under the same experimental conditions, i.e., repeated annealing, as it was for the capacitors. This may be due to a progressive deterioration in the state of both the Cujack electrodes and the dielectric, as well as their interface, as a consequence of repeated cycling to elevated temperature. In any case, the emitted TSC currents were small during repeated annealings compared to the sort of response one might expect to see if trapped charge were present.

6. SUMMARY AND ASSESSMENT

6.1 INTRODUCTION

The goals of this program have been threefold: first, to demonstrate the manner in which molecular or morphological features of polymer dielectrics determine their ability to store persistent space charge/polarization; second, to determine how the radiation response of metal-dielectric components is altered by the presence of such trapped charge and to provide bounds on their response; and third, to prescribe means for minimizing the effect of stored charge on the response of such systems if charged, or at least to make their response predictable.

Dielectric charging has been identified as potentially problematic in at least three systems. First, high-reliability Mil-Spec capacitors have shown an output of charge in irradiation that is much larger than the predicted photoconductivity response. Second, the signal generated by coaxial cables, when irradiated, is often unpredictable in the amount of charge released and even in its sign. This has been called the first-pulse anomaly. Third, dielectrics in spacecraft are exposed to the space radiation environment. They can accumulate significant amounts of trapped charge. This may lead to component failure due to a catastrophic event such as dielectric breakdown, or the presence of such charge may significantly alter their radiation response. Components in which such persistent charging is thought to be problematic include cables, thermal blankets, dielectrics associated with solar cells, spacers, and second surface mirrors. Clearly, to make vulnerability and survivability predictions, one must be able to bound the response of charge dielectrics. More desirable would be the minimization of deleterious effects from the contribution of stored charge to the radiation response of a system.

This chapter includes the significant conclusions obtained for this year's study on the relationship between the morphology of a model polymer polyethylene

and its ability to store space charge in its bulk. This chapter also includes a summary of the findings of our study on the thermal and radiation response of three semirigid coaxial cables containing Teflon-TFE (polytetrafluoroethylene) dielectrics. This work was carried out to provide a first-cut look at some of the factors responsible for the anomalous response of cables with polymer dielectrics. A summary of the relationship between the structure of polymers and their ability to store charge is then presented. As is discussed, one must examine the total problem, i.e., not only the polymer, but its environment (the manner in which it is charged, prior history, electrodes, and the type of radiation). Finally, we present suggestions for relevant problems to be addressed in determining the effect of stored charge, i.e., persistent internal charge introduced by manufacturing or handling, and trapped charge, i.e., a charge introduced by external radiation such as the exoatmospheric electron environment, on the radiation response of cables.

6.2 PRINCIPAL FINDINGS

Persistent internal fields were created in a series of polyethylene dielectric capacitors at temperatures chosen to encompass the important phase transitions in this polymer at forming fields of 100 kV/cm. The charge released as a function of temperature over the range 100°K to 400°K was measured (TSC). The polyethylenes were of three types, one low-density ($d = 0.922 \text{ g/cm}^3$, $w_c = 0.46$), the second a medium-density ($d = 0.935 \text{ g/cm}^3$, $w_c = 0.55$), and the third a high-density ($d = 0.950 \text{ g/cm}^3$, $w_c = 0.70$). These samples were chosen to span the range of crystallinities and degrees of chain branching for commercially available polyethylenes. The results of these measurements can be summarized as follows:

1. The general shape of the TSC spectra for all three kinds of polyethylenes are similar.
2. The low-temperature portion of the spectra of these polymers (<275°K) can be attributed to charge released from the electrodes as a consequence of the relaxation of molecular dipoles associated with carbonyl (C=O) groups introduced into polymer

chains as a consequence of chain oxidation. The molecular relaxation of these dipoles is associated with the coordinated motion of segments of the polymer chains at the γ and β transitions in the polymer, which occur at $\sim 148^\circ\text{K}$ and $\sim 240^\circ\text{K}$, respectively.

3. The charge emitted at higher temperatures is due to the thermally induced relaxation of space-charge fields. The trapped charge is for samples with metalized electrodes, primarily intrinsic, and is due to the dissociation of impurities introduced into the polymer during its manufacture.
4. Based on the results of our thermally stimulated current measurements, as well as those carried out by other investigators, and related data such as conductivity and mobility measurements for this polymer, one can make tentative identification of possible trapping sites related to morphological features of the polymer. These include: (a) the interstices between crystalline and amorphous domains in their inhomogeneous material; (b) regions of large free volume between molecular cores in the amorphous domains; and (c) defects in the crystalline domains associated with chain folds or chain misalignment because of the presence of side branches. These trapping sites not only are responsible for the long-term trapping of stored charge, but also determine the ordinary mobility of charge carriers in these materials. The same factors that make a nonpolar polymer like polyethylene an extremely good insulator also determine that it will efficiently store persistent charge.
5. Within the scatter of the data, there was no observed dependence of the thermally stimulated charge release under short circuit consequent to burn-in on crystallinity. For the most part, the amount of charge released was equivalent to a $\kappa_T < 0.06$ (cf. Equation 8 for a definition of this parameter). For a few samples $\kappa_T < 0.6$. There was no correlation observed between the appearance of such a large response and crystallinity. For comparison, the

relative dielectric constant κ of polyethylene ranges from 2.28 for low-density polyethylene to 2.34 for high-density polyethylene. For reference, a $\kappa_T = 0.06$ corresponds to a charge release per unit area of 0.53 nC/cm^2 , while $\kappa_T = 0.6$ is equal to a charge release of 5.3 nC/cm^2 . The charge stored on the electrodes of a polyethylene capacitor with an applied field of 100 kV/cm for $\kappa = 2.3$ would be equal to 203 nC/cm^2 . However, unlike the charge stored consequent to burn-in, when the capacitor is shorted, the normal bias charge will be dissipated.

6. It is believed that under ideal burn-in conditions, i.e., at low-forming fields, comparable to those used for these experiments, and with samples containing gapless electrodes, the creation of persistent internal fields is by heterocharging, i.e., the polarization of molecular dipoles and of intrinsic space charge which is trapped primarily at interfaces between crystalline and amorphous domains (Maxwell-Wagner polarization) and near the electrodes. Because polyethylene is a nonpolar polymer, the concentration of such polarization charge will be small and sample dependent, i.e., dependent on the impurity concentration present. One expects in this case that $\kappa_T \approx \kappa_0 - \kappa_\infty$, the slowly responding, nonelectronic contribution to the material polarizability. The value of this difference is 0.01 to 0.03, comparable to the values of κ_T observed for the majority of samples.
7. Where the observed charge release as a consequence of thermal depolarization was large ($\kappa_T > 1$), the altered shape of the TSC spectrum suggests that additional charge was injected into the bulk of the dielectric across the electrodes. As the bulk of the extra charge released occurs at temperatures near the melting point of the polymer, this suggests that the trapping sites for the injected homocharge are located in crystalline regions of the polymer. As the conditions under which the extra charge was introduced into the dielectric were not reproducible, it is not possible

to assign an exact mechanism to the manner of injection. However, a possible mechanism is injection across gaps between electrodes and dielectrics as a consequence of breakdown of air in these gaps.

8. Studies have been made which correlate the crystallinity of polyethylene with properties such as the mobility of conduction and the ability of the polymer to retain persistent trapped charge after injection. The conclusion of these studies is that the more crystalline the polymer, the more able it is to retain stored charge, i.e., the longer is the relaxation time for dissipating the excess space charge. This is reflected in the observed decrease in conductivity with increase in polyethylene crystallinity.

The radiation response of the same polyethylenes subsequent to the creation of persistent stored charge/polarization were studied. Relaxation of the internal polarization field was achieved with pulses of 40-MeV electrons, which deposited a dose of ~ 800 rads(Si) = 944 rad(PE) per pulse

The results derived from the capacitor irradiations can be summarized as follows:

1. The initial charge release per unit dose, R_0 , was always greater than the asymptotic response, R_∞ . In this sense, the behavior of those capacitors in which internal fields were created by burn-in mimics the inconsistent response often observed in cables; namely, that if a cable is exposed to a series of pulses, the observed signal changes from shot to shot, usually diminishing in amplitude and often changing sign until an asymptotic repeatable response is reached.
2. The net amount of charge released by a capacitor that was burned in was always greater than that released by a similar sample that had been thermally annealed. The average relative response expressed as the ratio $\kappa_R(\text{burned in})/\kappa_R(\text{annealed})$ was about 10.5 to 1 for the high-density samples, 8.5 to 1 for the medium-density

samples, and 4 to 1 for the low-density samples (see Equation 18 for a definition of κ_R). These findings clearly demonstrate that, under the particular conditions of irradiation, the radiation-induced relaxation of polarization charge in a dielectric can significantly enhance its response. As was discussed in Chapter 4, this effect is more important in determining the response of these layered metal-dielectric structures than the presence of gaps or dose enhancement effects. This is largely due to the fact that there is little dose enhancement in these samples and that the radiation-driven currents in each layer are relatively equal for irradiation by high-energy electrons whose range is much greater than the sample thickness. The net charge released per unit area by these samples was $<100 \text{ pC/cm}^2$ except for two of the high-density polyethylene samples where emission was larger. The observed values of κ_R were $<3.5 \times 10^{-2}$ for the burned-in samples, with the two above-mentioned exceptions. These were less than, but comparable to, the values of κ_T obtained for similar samples under identical burn-in conditions. These findings suggest that thermal annealing may be used as a screening technique to identify those metal-dielectric systems such as capacitors or cables which show an anomalous radiation response because of the presence of persistent space charge/polarization.

3. The initial responses, R_0 , observed ranged from $38 \times 10^{-15} \text{ C/rad-cm}^2$ to $\sim 1 \times 10^{-15} \text{ C/rad-cm}^2$, while the asymptotic responses, R_∞ , were all $\sim 5 \times 10^{-16} \text{ C/rad-cm}^2$, independent of their initial state. If one notes that a coaxial cable with a dielectric o.d. of ~ 0.1 inch has a surface area of about 1 cm^2 per centimeter of length, the observed capacitor responses are comparable to those observed for the semirigid coaxial cables discussed in Chapter 5 (cf. Table 11), which were exposed to a variety of photon spectra and fluences but which were not subject to any special preconditioning.

4. It typically required doses to the capacitors of the order of 50 krad(Si) to reach the state of asymptotic response. However, the point at which this state was reached was often difficult to assess in practice because of radiation-induced polarization in the dielectric; i.e., the radiation-field-produced space charging whose effect was to counter the field-driven currents by generating an opposing conduction current. Since trapped space charge in these dielectrics relaxes only slowly over periods of several months, it would be interesting to try to diminish the radiation response of metal dielectric structures by prior implantation of space charge. However, the radiation response of a metal dielectric system is sensitive to a variety of factors, including the type or radiation, its spectrum, and the direction of the radiation-driven charge in the dielectric. It is conceivable that under different irradiation conditions, the response of the metal-dielectric system might be enhanced much in the manner that the response of our capacitor is enhanced after polarization charge is stored in the dielectrics as a consequence of burn-in.

As a first-cut effort to identify those mechanisms responsible for the inconsistent behavior of cables when irradiated, a survey was made of the relative response of three solid-jacketed, semirigid cables containing Teflon-TFE dielectrics exposed to a variety of photon sources. Thermally stimulated current measurements were made on samples of the same cables to see if there was any correlation between the amount of charge released as a consequence of the radiation-induced relaxation of stored charge in the cables and that released by heat. The relevant radiation data presented in Table 11 indicates that the charge released per unit dose per unit length by samples of the same cable type can vary by orders of magnitude. Moreover, the pulse shape can be markedly different under different exposure conditions. The appearance of a first-pulse anomaly is evidently dose dependent. The relative response of these cables measured with the Aerospace DPF, an x-ray source which outputs about 25 rads(Si) per pulse, were significantly smaller than those taken at the other facilities, and showed a relatively constant signal from shot to shot.

The specific response for the three cables measured at the TRW Vulcan facility at doses of ~ 3 krad(Si) per pulse also showed a similar constancy. For doses per pulse in between these two extremes, i.e., between 100 rad(Si) and 1 krad(Si), an inconsistent cable response was observed. These limited data are in agreement with other observations (Reference 41 and this work) that the presence of stored charge introduced by manufacturing or handling may be significant in affecting the net behavior of cables for a total dose of one krad. At higher accumulated doses, radiation-driven space-charge effects will predominate; i.e., the asymptotic space-charge state of the cable will be determined by the radiation-deposited charge rather than any initial stored-charge distribution. Such a conclusion is tentative, to be taken with the caveat that under conditions where relatively large internal polarization fields are created deliberately by burn-in or inadvertently because a dielectric is charged by an external source, the total dose at which trapped charge is relaxed will be higher. This is suggested by our data for annealed versus burned-in polyethylene capacitors.

These data suggest that it is not adequate to give a single number for use in vulnerability/survivability predictions which defines the dose or dose-rate dependence of the signal output by a cable. It is clear that one must also specify the test conditions, i.e., spectrum, dose, dose rate, ambient atmosphere, prior history, presence of gaps, in order to properly predict the anticipated magnitude of the radiation-induced signal.

A series of thermally stimulated current measurements were made on samples of the three cable types where radiation response was evaluated. For comparison, the TSC spectra were obtained for two capacitors with Teflon-TFE dielectrics. The charge released to an external circuit from these capacitors consequent to burn-in is equivalent to a $\kappa_T < 7.5 \times 10^{-3}$ or less than 70 pC/cm^2 . This net charge release is comparable to that induced by radiation after burn-in for similar samples (Ref 1). This relatively small response is to be expected for nonpolar polymers in which persistent polarization fields are created by homocharging. The measured response is expected to be of the order of $\kappa_0 - \kappa_\infty$ in the absence of any charge injection.

The net charge released by the three cables was comparably small, ~ 100 pC/cm² of outer dielectric surface, independent of whether the samples had been annealed or burned in prior to measurement of the TSC spectra. The first annealing responses were all ≤ 200 pC/cm² and provide a bound to the charge released to an external circuit under irradiation if there is any correlation between κ_T and κ_R , as has been found to hold for the polyethylene capacitors. In fact, the net amount of charge per unit dose released to an external circuit by the two cables exposed at the SPI Pulse 6000 facility was even smaller than their thermal response. It was found for one cable, the 0.085-inch Cujack, that the net amount of charge released as a consequence of thermal annealing after burn-in was quite large, ~ 3.6 nC/cm². The magnitude of the released charge, as well as its observed polarity, suggests that a large amount of homocharging of this sample took place during burn-in, probably because of the presence of gaps between the conductor and dielectric. If this finding can be verified, one may be able to use the TSC method to test for gaps in cables to screen those that will show anomalous radiation responses because of their presence.

6.3 RELATIONSHIP BETWEEN POLYMER MORPHOLOGY, CHARGE STORAGE, AND RADIATION RESPONSE

It is clear that the ability to store persistent space charge/polarization is related to the morphology of polymers. For example, the polar polymers typically employed in capacitor dielectrics contain molecular dipoles that can be oriented under bias at elevated temperatures (burn-in). The impressed orientation will be frozen in at normal operating temperatures. One must raise the temperature of the polymer to one comparable to that for the glass transition (T_g), at which point large-scale molecular motion of the polymer chains occur to relax the dipole field. Similarly, the ability to store trapped space charge can be related to specific trapping sites in the polymer, as we have described for polyethylene. Because many polymers have complex structures and are inhomogeneous materials consisting of two phases, one crystalline, the other amorphous, the variety of possible trapping sites for free charge is much greater than for largely homogeneous inorganic materials. As we have discussed in Chapter 3, the presence of these traps plays a

predominant role in determining the low macroscopic mobilities for conduction in these materials. Thus, the properties of these materials which make them extremely good insulators also guarantee that they possess an abundance of sites for storing persistent charge. In fact, trapped space-charge densities of the order of 10 nC/cm^2 can be retained in nonpolar polymer foils for periods of several years. This behavior is now being exploited to produce transducers for devices such as microphones.

The strength of the persistent internal field created depends not only on the polymer morphology but also on the manner of injection. Under burn-in, i.e., heterocharging, where there is no external charge injection, the strength of the persistent field at temperatures well below T_g will be proportional to the nonelectronic component of the polarizability, i.e., proportional to $\kappa_0 - \kappa_\infty$, the difference between the static and high-frequency polarizabilities. In a polymer, this component arises from the alignment of molecular dipoles and space charge trapped at interfaces between domains in these inhomogeneous materials. These induce a net surface charge per unit area $q = (\kappa_0 - \kappa_\infty)\epsilon_0 E$. For typical forming condition in an experiment $E_B \sim 10^5 \text{ kV/cm}$. Thus, for a polar polymer where $\kappa_0 - \kappa_\infty \sim 1$, $q \sim 10 \text{ nC/cm}^2$. For a nonpolar polymer, such as polyethylene or Teflon, $(\kappa_0 - \kappa_\infty) \sim 0.05$, such that $q \sim 500 \text{ pC/cm}^2$. The net induced-charge density in this case is significant, as it represents the amount of charge per unit electrode area that flows through an external circuit or relaxation of the polarization fields.

On the other hand, the nonpolar polymers such as polyethylene and Teflon tend to be better at storing persistent space charge than the polar polymers. Nonpolar polymers tend to have lower volume conductivities than polar types, in part because the former tend to have lower concentration of dissociable impurities such as water, which can neutralize injected space charge. The amount of charge that can be trapped in these materials is determined by the probability of breakdown, either in air if present next to the surface of the sample, or because of large fields built up in the dielectric. It is possible to put surface charge densities of tens of nC/cm^2 into polymer films.

It is harder to specify the radiation response of these charged dielectrics. The radiation signal is equal to the replacement current flowing

through the circuit external to the metal-dielectric system. It is equal to the sum of the contributions to the net solenoidal current flowing in the dielectric. Contributions to this include, the radiation-driven current, consisting of primary electrons in electron irradiation, and secondary electrons generated by the interaction of the primary beam with the structure. There is also a photoconductivity current that flows in the dielectric because of the presence of an applied bias or because of fields trapped in the dielectric. Another contribution arises from the motion of space charge. There is also a contribution from the displacement current density which, if persistent polarization is present as represented by a polarization field $P(x,t)$, adds an extra term equal to $\partial P/\partial t$. The evaluation of most of these terms for particular conditions of irradiation is complicated and has only recently been carried out (Refs 37,41,42). Moreover, as is discussed in the next section, the relevant physics needed to describe the contribution to the net solenoidal current due to the motion of trapped space charge or to the relaxation of persistent polarization have not yet been incorporated into these models.

For the conditions under which our capacitor samples were irradiated, we believe that the predominant contribution to the net replacement current flowing in the external circuit was due to the relaxation of persistent internal fields by the radiation. Because we examined the behavior of layered samples exposed to electrons whose mean range was many times the sample thickness, it is likely that the driven-charge contribution was much smaller than that due to the motion of space charge or dipolar relaxation. In that case, one expects to find a correlation between the amount of charge released to an external circuit after burn-in by a thermal annealing or by a radiation annealing and the nonelectronic contribution to the material polarizability. The data presented in Figure 25 which summarizes our findings for this program indicate that this was more or less true.

6.4 RECOMMENDATIONS

It is our assessment that the factors responsible for the unexpectedly large signals produced by capacitors when irradiated are understood. The reputed inconsistent response of cables can be ascribed to an incomplete

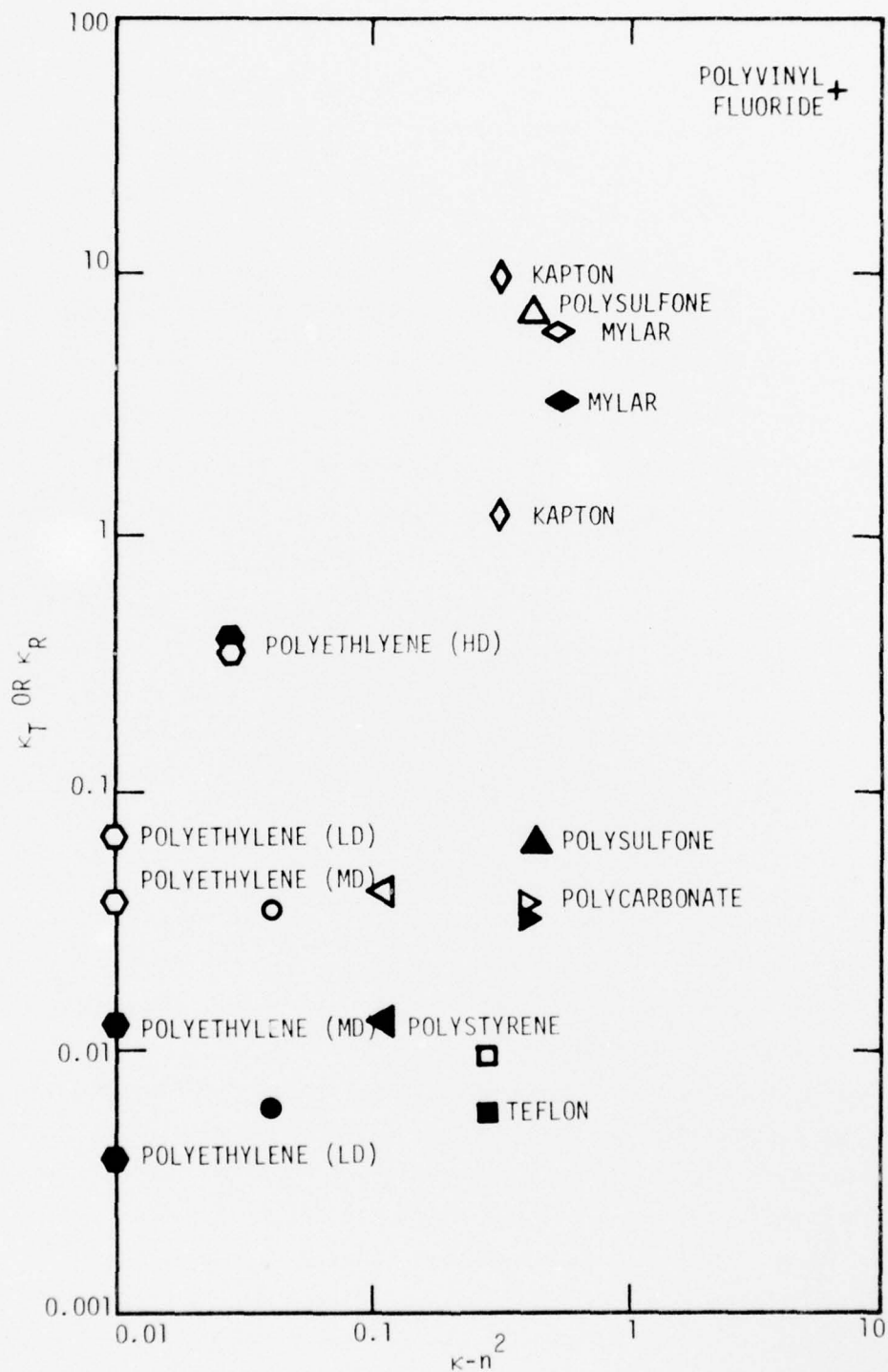


Figure 25. Normalized radiation and thermal depolarization response versus nonelectronic polarizability for samples charged by burn-in. The open symbols are the thermal response. The solid symbols are the radiation response.

understanding of the mechanisms that determine the radiation-induced signal. It is now believed that all of these factors have been identified. The clearest evidence of this can be found in the paper of Chadsey et al. (Ref 37). The phenomena that determine the net signal for a cable include:

1. The kinetic or radiation-driven charge including a correct accounting of dose and current enhancement at the interfaces between conductor and dielectrics.
2. The presence of gaps between conductors and dielectrics.
3. The return currents that will flow in the dielectric as a consequence of the space-charge fields that are created because of stopping of driven charge in the dielectric.
4. The radiation-induced relaxation of stored charge introduced by manufacturing processes such as polymerization or extrusion, of frictional charging due to handling, or of trapped charge introduced by prior irradiation, i.e., exposure to the natural or artificial exoatmospheric electron environment, or radiation testing.

It is felt that existing codes are capable of accounting for the contributions of the first three factors; i.e., the physics they embody are adequate to describe these processes. In regard to accounting for the behavior of stored or trapped charge in the cable dielectric when irradiated, the adequacy of the modeling is less clear. Two additions are required. First, one needs to determine the magnitude, distribution, and nature of the charge stored in a dielectric for a given method of injection. Second, one must incorporate into existing codes that can transport space charge in internal fields a mechanism that describes the manner in which radiation makes this trapped or stored charge mobile. In terms of the motion of intrinsic charge carriers, this can be done by the addition to the normal conductivity of a term due to transient conductivity, which typically predominates. The transient conductivity for most of the common insulators in an unpolarized state has been measured. The contribution of the motion of space charge in the insulator will add a term equal to

the product of the trap-modulated mobility and space-charge density to the photoconductivity term. In addition, a formalism must be derived to take into account the radiation-induced depolarization of the persistent internal polarization whose time rate of change represents an additional contribution to the displacement current (Ref 25).

Any program that attempts to develop the capability to predict the radiation response of cables must identify those regions of spectrum, dose, and dose rate, where each of these mechanisms is significant. This is necessary because the contributions of some of them are nonlinear with dose and dose rate. One can envisage an iterative program that would combine theoretical modeling and experimental verification. First, the existing models and codes would be exercised for reasonable space and polarization charge distributions. These would be estimated from the available literature on those processes postulated to store persistent stored or trapped charge. Particularly important cases to study would be the determination of the equilibrium state of spacecraft dielectrics under exposure to the exoatmospheric electron environment in order to determine whether such radiation charging may lead to dielectric breakdown. Next, an experimental program driven by the predictions of the models would be undertaken to test the predictive ability of the codes, to determine the processes responsible for the introduction of stored charge, and to ascertain the type, quantity, and spatial distribution of such persistent charge. In all cases such assessments should be made with an eye to their significance in a system environment, i.e., whether it enhances the radiation response of a cable to a sufficient degree to cause system upset or burnout. Finally, the results of the experimental program would be used to improve the codes.

REFERENCES

1. T. M. Flanagan, A. H. Kalma, R. E. Leadon, J. A. Naber, D. P. Snowden, and J. M. Wilkenfeld, "Transient Radiation Effects," Harry Diamond Laboratories Final Report HDL-CR-75-197-1, (IRT Report INTEL-RT 8008-007), March 1975.
2. R. E. Leadon, D. P. Snowden, and J. M. Wilkenfeld, "Radiation Effects in Semiconductor and Insulator Materials," Harry Diamond Laboratories Final Report HDL-CR-76-152-1, (IRT Report INTEL-RT 8008-007), April 1976.
3. A. Rosen, *IEEE Trans. Nucl. Sci.* NS-23, 1762 (1976).
4. J. Wilkenfeld and V. Junkkarinen, *Thermal and Radiation Depolarization of Persistent Charge Stored in Polymer Dielectrics*, Presentation at 1976 IEEE Conference on Nuclear and Space Radiation Effects, San Diego, California, July 1976.
5. An excellent concise introduction to the morphology of a polymer such as polyethylene can be found in R. J. Samuels, *Structured Polymer Properties*, (Wiley-Interscience, New York, 1974), Chapter 1.
6. An exhaustive discussion of the morphology of polymers is given in B. Wunderlich, *Macromolecular Physics*, (Academic Press, New York, 1974), Pt. I.
7. L. Boustead and A. Charlesby, *Proc. Roy. Soc.* A316, 291 (1970).
8. C. A. Sperati, "Physical Constants of Polyethylene," in J. Brandrup and E. H. Immergut (Eds.), *Polymer Handbook*, (Wiley-Interscience, New York, 1974), pp. V13-V22.
9. Wunderlich, op. cit. p. 388.
10. Ibid, Section 4.1.3.
11. R. L. Blaine, *Polymer Crystallinity. Application Brief TA12*, Instrument Products Department, E. I. duPont deNemours & Company.
12. L. E. Alexander, *X-Ray Diffraction Methods in Polymer Science*, (Wiley-Interscience, New York, 1967, Chapter 3).

13. Samuels, op. cit., Chapter 2.
14. S. Krimm and A. Tobolsky, *J. Poly. Sci.* 7, 57 (1951).
15. Alexander, op. cit. pp. 137-138.
16. Wunderlich, op. cit. pp. 388-401.
17. R. A. Creswell, B. I. Gribbon, M. A. Kabayama, and M. M. Perlman, *Telesis* 2/1/71, pp. 21-26.
18. R. F. Boyer, *Rubber Chem. Tech.* 36, 1303-1421 (1963).
19. J. van Turnhout, *Thermally Stimulated Discharge of Polymer Electrets*, (Elsevier, Amsterdam, 1975), pp. 93-96.
20. P. Fischer and P. Röhl, *J. Poly. Sci.: Polymer Phys. Edn.* 14, 531, 543 (1976).
21. J. van Turnhout, op. cit.
22. See Figure 4.4 of T. M. Flanagan, et al., "Transient Radiation Effects," Harry Diamond Laboratories Final Report on Contract DAAG39-73-C-0197, (IRT Report INTEL-RT 8008-007), February 21, 1975.
23. van Turnhout, *ibid*, pp. 199-200.
24. *ibid*, Chapter 1.
25. B. Gross, *J. Appl. Phys.* 43, 2449 (1972).
26. E. Sacher, *J. Macromolec. Sci. Phys.* B6, 151 (1972).
27. G. Sawa, M. Kawade, D. C. Lee, and M. Ieda, *J. Appl. Phys.* 13, 1547 (1974).
28. H. J. Wintle in *The Radiation of Chemistry of Macromolecules*, R. Nole (Ed.) (Academic Press, New York, 1972), Vol. 1, pp. 100-126.
29. D. K. Davies, *J. Phys.* D5, 162 (1972). 162 (1972).
30. H. F. Wintle, *J. Appl. Phys.* 41, 4004 (1970).
31. M. M. Perlman and J. Sonnenstine, *J. Appl. Phys.* 47, 5016 (1976).
32. R. A. Creswell, M. M. Perlman, and M. A. Kabayama, *Dielectric Properties of Polymers*, F. Karas (Ed.) (Plenum Press, New York, 1972).
33. M. M. Perlman and S. Unger, *J. Phys.* D5, 2115 (1972).

34. *ibid. Appl. Phys. Lett.* 24, 579 (1974).
35. van Turnhout, *op. cit.* p. 168.
36. *ibid* p. 16.
37. W. L. Chadsey, B. L. Beers, V. W. Pine, and C. W. Wilson, *IEEE Trans. Nucl. Sci.* NS-23, 1933 (1976).
38. B. Gross, *J. Electrostatics* 1, 125 (1975).
39. B. Gross, G. M. Sessler, and J. E. West, *J. Appl. Phys.* 47, 968 (1976).
40. J. van Turnhout, *J. Electrostatics* 1, 147 (1975).
41. J. Pigneret and H. Stroback, *IEEE Trans. Nucl. Sci.* NS-23, 1933 (1976).
42. A. R. Frederickson, *IEEE Trans. Nucl. Sci.* NS-22, 2556 (1975).
43. J. A. Naber and R. A. Berger, *IEEE Trans. Nucl. Sci.* NS-16, 260 (1969).
44. M. J. Berger and S. M. Selzer in *Natl. Acad. Sci. - Natl. Res. Council Publ.* 1133, 2nd Printing, 1967.
45. R. D. Evans, "Gamma-Ray and X-Ray Interactions," in *Radiation Dosimetry*, F. H. Attix and W. C. Roesch (Eds.) (Academic Press, New York, 1966, Vol. I, Chapter 3).
46. J. K. Notthoff, *Coaxial Cable Responses from FX-100 and PR-1590 Flash X-Ray Machines*, McDonnell Douglas Aircraft Corporation, Paper 1621, July 1971 (unpublished).
47. F. Hai and P. A. Beemer, *Cable Sensor Test and Development Program*, Aerospace Corporation Report TOR-0076 (6501)-1, 15 January 1976.
48. R. L. Fitzwilson, M. J. Bernstein, and T. E. Alston, "Radiation-Induced Currents in Shielded Multi-Conductor and Semi-Rigid Cables," *IEEE Trans. on Nucl. Sci.* NS-21, 276 (1974).
49. Frank Hai, private communication. We thank Dr. Hai for sending us copies of the reports describing his work in advance of publication.
50. W. A. Lee and R. A. Rutherford, "The Glass Transition in Polymers," in J. Brandrup and E. H. Immergut (Eds.), *The Polymer Handbook*, (Wiley, New York, 1975) Second Edition, p. III-150.
51. J. van Turnhout, *op. cit.*, Sections 1:2, 10:2.4, 10:2.5.
52. D. M. Taylor, T. J. Lewis, and T. P. T. Williams, *J. Phys.* D7, 1776 (1974).

53. J. van Turnhout, op. cit., Section 7:1.3.
54. ibid, p. 109.
55. ibid., Section 1:3.
56. D. Clement, private communication.
57. R. P. Reed, R. E. Schramm, and A. F. Clark, *Cryogenics* 13, 76 (1973).

DEPARTMENT OF DEFENSE

Commander in Chief
U S European Command, JCS
ATTN: ECJ6-P

Director
Defense Advanced RSCH Proj Agency
Architect Building
ATTN: NMR

Director
Defense Civil Preparedness Agency
Assistant Director for Research
ATTN: TS AED

Defense Communication Engineer Center
ATTN: Code R103P
ATTN: Robert Rostron
ATTN: Code 1035

Director
Defense Communications Agency
(ADR CNWDE: ATTN: CODE 240 for)
ATTN: Code 920
ATTN: Code 430
ATTN: Code B205
ATTN: Code 800
ATTN: NMR

Defense Documentation Center
12 cy ATTN: TC

Director
Defense Intelligence Agency
ATTN: DS-4A2
ATTN: DB-4C

Director
Defense Nuclear Agency
ATTN: TISI Archives
3 cy ATTN: TITL Tech Library
ATTN: DDST
ATTN: STVL
2 cy ATTN: RAEV
ATTN: RATN

Director of Defense Rsch & Engineering
Department of Defense
ATTN: S&SS (OS)

Commander
Field Command
Defense Nuclear Agency
ATTN: FCIMC
ATTN: FCPR

Director
Interservice Nuclear Weapons School
ATTN: Document Control

Director
Joint Strat TGT Planning Staff JCS
ATTN: JLTW-2

Chief
Livermore Division Fld Command DNA
Lawrence Livermore Laboratory
ATTN: FCPRL

National Communications System
Office of the Manager
ATTN: NCS-TS

Director
National Security Agency
ATTN: TDL
ATTN: Orland O. Van Gunten R-425

OJCS/J-3
The Pentagon
(Operations)
ATTN: J-3 RDTA BR WWMCCS Plans Div

OJCS/J-5
The Pentagon
(Plans & Policy)
ATTN: J-5 Plans & Policy Nuc Div

DEPARTMENT OF ARMY

Project Manager
Army Tactical Data Systems
U. S. Army Electronics Command
ATTN: Dwaine B. Huewe
ATTN: DRCPN-TDS-SD

Director
BMD Advanced Tech Ctr
Huntsville Office
ATTN: RDMH-O F. M. Hoke

Commander
BMD System Command
ATTN: BDMSC-TEN
ATTN: SSC-TEN

Dep Chief of Staff for Rsch Dev & ACQ
Department of the Army
ATTN: DAMA-CSM-N

Commander
Frankford Arsenal
ATTN: SARFA-FCD

Commander
Harry Diamond Laboratories
(CNWDI-Inner Envelope: ATTN: DRXDO-RBH)
ATTN: DRXDO-NP
ATTN: DRXDO-EM
ATTN: J. Halpin
ATTN: DRXDO-RCC
ATTN: DRXDO-TT Tech Library
ATTN: DRXDO-RC
ATTN: DRXDO-RCC
ATTN: DRXDO-RBH
ATTN: DRXDO-RBH
ATTN: J. McGarrity
ATTN: DRXDO-EM
5 cy ATTN: Harold E. Boesch, Jr.
5 cy ATTN: John A. Rosado

Commander
Picatinny Arsenal
ATTN: SARPA-ND-C-E
ATTN: SARPA-TS-I-E
ATTN: SMUPA-ND-W
ATTN: SARPA-ND-N
ATTN: SARPA-FR-E
ATTN: SMUPA-ND-N-E

Commander
Redstone Scientific Information Ctr
U. S. Army Missile Command
3 cy ATTN: Chief, Documents

DEPARTMENT OF THE ARMY (Continued)

Secretary of the Army
ATTN: Odusa or Daniel Willard

Director
TRASANA
ATTN: ATAA-EAC

Director
U. S. Army Ballistic Research Labs
ATTN: DRXBR-X
ATTN: DRXBR-AM
ATTN: DRXBR-AM
ATTN: DRXRD-BVL

Chief
U. S. Army Communications Sys Agency
ATTN: SCCM-AD-SV Library

Commander
U. S. Army Electronics Command
ATTN: DRSEL-GG-TD
ATTN: DRSEL-NL-O-4
ATTN: DRSEL-CT-HDK
ATTN: DRSEL-TL-ME
ATTN: DRSEL-TL-EN
ATTN: DRSEL-TL-TR
ATTN: DRSEL-TL-MD
ATTN: DRSEL-TL-ND
ATTN: DRSEL-TL-EN
ATTN: DRSEL-PL-ENV Hans A. Bomke

Commander in Chief
U. S. Army Europe and Seventh Army
ATTN: ODCSE-E AEAGE-PI

Commandant
U. S. Army Field Artillery School
ATTN: ATSPA-CTD-ME

Commander
U. S. Army Foreign Science & Tech Ctr
(Address CNWDI: ATTN: Document Control for:)
ATTN: DRXMR-HH

Commander
U. S. Army Mat & Mechanics Rsch Ctr
(Address CNWDI: ATTN: Document Control for:)
ATTN: DRXMR-HH

Commander
U. S. Army Materiel Dev & Readiness CMD
ATTN: DRCDE-D

Commander
U. S. Army Missile Command
ATTN: DRSMI-RRR
ATTN: DRCPM-LCEX
ATTN: DRSMI-RDG
ATTN: DRSMI-RGP
ATTN: DRCPM-PE-EA
ATTN: DRCPM-PE-EG

Commander
U. S. Army Mobility Equip R&D Ctr
(CNWDI to Army Mat Dev & Readiness Command)
ATTN: STSFB-MW

Chief
U. S. Army Nuc and Chemical Surety Gp
ATTN: MOSG-ND

Commander
U. S. Army Nuclear Agency
ATTN: ATCN-W

Commander
U. S. Army Test and Evaluation Comd
ATTN: DRSTE-NB
ATTN: DRSTE-EL

DEPARTMENT OF THE NAVY

Chief of Naval Operations
ATTN: CODE 604C3
ATTN: Robert A. Blaise

Chief of Naval Research
ATTN: Henry Mullaney Code 427
ATTN: Code 464
ATTN: Code 427
ATTN: Code 421

Commander
Naval Air Systems Command
Headquarters
ATTN: AIR-5202

Commander
Naval Electronic Systems Command
Headquarters
ATTN: PME 117-21
ATTN: ELEX 05323
ATTN: Code 504510
ATTN: Code 5032
ATTN: PME 117-T

Commanding Officer
Naval Intelligence Support Ctr
ATTN: NISC-611
ATTN: P. Alexander

Commander
Naval Ocean Systems Center
ATTN: Code 3100

Director
Naval Research Laboratory
ATTN: Code 4004
ATTN: Code 5210
ATTN: Code 2627
ATTN: Code 5440
ATTN: Code 7701
ATTN: Code 6631
ATTN: Code 5216
ATTN: Code 7770
ATTN: Code 601

Commander
Naval Sea Systems Command
2 cy ATTN: SEA-9931

Commander
Naval Ship Engineering Center
ATTN: Code 6174D2

Officer-in-Charge
Naval Surface Weapons Center
ATTN: Code 431
ATTN: Code WA52
ATTN: Code WA501 Navy Nuc Prgms Off
ATTN: Code WA50

Commander
Naval Surface Weapons Center
Dahlgren Laboratory
ATTN: William H. Holt

Commander
Naval Telecommunications Command
Headquarters
ATTN: N-7 LCDR Hall

Commander
Naval Weapons Center
ATTN: Code 533 Tech Lib

Commanding Officer
Naval Weapons Evaluation Facility
ATTN: Lawrence R. Oliver

Commanding Officer
Naval Weapons Support Center
ATTN: Code 70242
ATTN: Code 7024

Commanding Officer
Nuclear Weapons Trng Center Pacific
ATTN: Code 50

Director
Strategic Systems Project Office
Navy Department
ATTN: SP-2701
ATTN: NSP-2431
ATTN: NSP-2342
ATTN: NSP-230

DEPARTMENT OF THE AIR FORCE

Commander
ADC/DE
ATTN: DEEDS Joseph C. Brannan

AF Geophysics Laboratory, AFSC
ATTN: J. Emery Cormier
ATTN: Charles Pike
ATTN: LQR Edward A. Burke

AF Institute of Technology, AU
ATTN: Library AFIT Bldg. 640 Area B
ATTN: ENP Charles J. Bridgman

AF Material Laboratory, AFSC
ATTN: Library
ATTN: LTE

AF Weapons Laboratory, AFSC

ATTN: SAB
ATTN: NTS
ATTN: NT
ATTN: ELA
ATTN: ELS
ATTN: ELC
2 cy ATTN: DYC
ATTN: ELP
ATTN: SUL
ATTN: DEX
2 cy ATTN: NTS

AFTAC

ATTN: TFS
ATTN: TAE

Air Force Avionics Laboratory, AFSC
ATTN: DHE H. J. Hennecke
ATTN: DH LTC McKenzie
ATTN: AAT Mason Friar

Commander
ASD

ATTN: ENACC Rober L. Fish
ATTN: ASD-YH-EX LTC Robert Leverette
ATTN: ASD/ENESS Peter T. Marth

Headquarters
Electronic Systems Division/XR
ATTN: XRRT

Headquarters
Electronic Systems Division/YS
ATTN: YSEV

Commander
Foreign Technology Division, AFSC
ATTN: FTDP

HQ USAF/RD
ATTN: RDQSM

Commander
Rome Air Development Center, AFSC
ATTN: RBRP Clyde Lane

Commander
Rome Air Development Center, AFSC
ATTN: Peter D. Gianino
ATTN: FTS R. Dolan
ATTN: Edward A. Burke
ATTN: FT R. Buchanan

SAMSO/YEE
(Technology)
ATTN:

SAMSO/IN
(Intelligence)
ATTN: IND

SAMSO/MN
(Minuteman)
ATTN: MNNG
ATTN: MNNH

SAMSO/RS
(Reentry Systems)
ATTN: RSSE
ATTN: RSMG

SAMSO/SK
(Space Comm Systems)
ATTN: SKF Peter H. Stadler

SAMSO/SZ
(Space Defense Systems)
ATTN: SZJ CAPT John H. Salch

SAMSO/XR
(Development Plans)
ATTN: XRS

DEPARTMENT OF THE AIR FORCE (Continued)

Commander-in-Chief
Strategic Air Command

ATTN: NRI Stinfo Library
ATTN: XPFS MAJ Brian G. Stephan
ATTN: XPFS

ENERGY RESEARCH AND DEVELOPMENT ADMINISTRATION

University of California
Lawrence Livermore Laboratory

ATTN: Louis F. Wouters L-48 (Class L-18)
ATTN: Donald J. Meeker L-545 (Class L-153)
ATTN: Lawrence Cleland L-156
ATTN: William J. Hogan L-531
ATTN: Joseph E. Keller, Jr. L-125
ATTN: Donald W. Vollmer L-154
ATTN: Frederick R. Kovar L-31 (Class L-94)
ATTN: Hans Kruger L-96 (Class L-94)
ATTN: Walter W. Hofer L-24
ATTN: Ronald L. Ott (L-531)
ATTN: Tech Info Dept L-3

Los Alamos Scientific Laboratory

ATTN: Doc Con for John S. Malik
ATTN: Doc Con for Marvin M. Hoffman
ATTN: Doc Con for P. W. Keaton
ATTN: Doc Con for Richard L. Wakefield
ATTN: Doc Control for Reports Library
ATTN: Doc Con for J. Arthur Freed
ATTN: Doc Con for Bruce W. Noel
ATTN: Doc Con for Donald R. Westervelt

Sandia Laboratories

Livermore Laboratory

ATTN: Doc Con for Theodore A. Dellin

Sandia Laboratories

ATTN: Doc Con for Elmer F. Hartman
ATTN: Doc Con for Jack V. Walker 5220
ATTN: Doc Con for 5240 Gerald Yonas
ATTN: Doc Con for 3141 Sandia Rpt Con
ATTN: Doc Con for Org 9353 R. L. Parker
ATTN: Doc Con for Org 1933 F. N. Coppage
ATTN: Div 5231 James H. Renken
ATTN: Doc Con for R. Gregory Org 2140
ATTN: Doc Con for Org 2315 James E. Gover
ATTN: Doc Con for Org 2110 J. A. Hood

U. S. Energy Research & Development Administration
Albuquerque Operations Office

ATTN: Document Control for WSSB

OTHER GOVERNMENT AGENCIES

Central Intelligence Agency

Attn: RD/S1 Rm 5G48 HQ Bldg.
ATTN: Alice A. Padgett

Department of Commerce

National Bureau of Standards

(All Corres: Attn: Sec Officer for)
ATTN: Appl Rad Div Robert C. Placious
ATTN: Judson C. French

Department of Transportation

Federal Aviation Administration

Headquarters SEC Div, ASE-300

ATTN: Fredrick S. Sakate ARD-350

NASA

ATTN: Code Res Guid Con & Info Sys

NASA

Lewis Research Center

ATTN: N. J. Stevens
ATTN: Carolyn Purvis (No Class)
ATTN: Library (No R/D)

DEPARTMENT OF DEFENSE CONTRACTORS

Aerojet Electro-Systems Co.

Div. of Aerojet-General Corporation

ATTN: Thomas D. Hanscome

Aerospace Corporation

ATTN: Julian Reinheimer
ATTN: Irving M. Garfunkel
ATTN: C. B. Pearlston
ATTN: Frank Hai
ATTN: V. Josephson
ATTN: William W. Willis
ATTN: L. W. Aukerman
ATTN: Normal D. Stockwell
ATTN: Library

AVCO Research & Systems Group

ATTN: Research Lib A830 Rm 7201

Battelle Memorial Institute

ATTN: Robert H. Blazek

BDM Corporation

ATTN: T. H. Neighbors

BDM Corporation

ATTN: D. R. Alexander

Bendix Corporation

Communication Division

ATTN: Document Control

Bendix Corporation

Research Laboratories Division

ATTN: Mgr Prgm Dev Donald J. Niehaus

Bendix Corporation

Navigation and Control Group

ATTN: George Gartner

Boeing Company

ATTN: Itsu Amura 2R-00
ATTN: Kenneth D. Friddell MS 2R-00
ATTN: Howard W. Wicklein MS 17-11
ATTN: Robert S. Caldwell 2R-00
ATTN: Preston Geren
ATTN: Carl Rosenberg 2R-00
ATTN: David L. Dye MS 87-75
ATTN: Aerospace Library

Booz-Allen and Hamilton, Inc.

ATTN: Raymond J. Chrisner

Brown Engineering Company, Inc.

ATTN: John M. McSwain MS 18

University of California at San Diego

IPAPS, B-019

ATTN: Sherman de Forest

California Institute of Technology
Jet Propulsion Laboratory

ATTN: J. Bryden
ATTN: A. G. Stanley

Charles Stark Draper Laboratory, Inc.

ATTN: Paul R. Kelly
ATTN: Richard G. Haltmaier
ATTN: Kenneth Fertig

Computer Sciences Corporation

ATTN: Barbara F. Adams

Computer Sciences Corporation

ATTN: Richard H. Dickhaut
ATTN: Alvin T. Schiff

Control Data Corporation

ATTN: Jack Meehan

Cutler-Hammer, Inc.

AIL Division

ATTN: Central Tech Files Anne Anthony

DePlomb, Dr. Eugene P.

ATTN: Eugene P. DePlomb

Dikewood Industries, Inc.

ATTN: L. Wayne Davis
ATTN: K. Lee
ATTN: Tech Lib

E-Systems, Inc.

Greenville Division

ATTN: Library 8-50100

Effects Technology, Inc.

ATTN: Edward John Steele

EG&G, Inc.

Albuquerque Division

ATTN: Hilda H. Hoffman
ATTN: Tech Library

Exp & Math Physics Consultants

ATTN: Thomas M. Jordan

Fairchild Camera and Instrument Corp.

ATTN: Sec. Dept. for 2-233 David K. Myers

Fairchild Industries, Inc.

Sherman Fairchild Technology Center

ATTN: Mgr Config Data & Standards

University of Florida

ATTN: D. P. Kennedy

Ford Aerospace & Communications Corp.

(Formerly Aeronutronic Ford Corporation)

ATTN: J. T. Mattingley MS X22
ATTN: Donald R. McMorro MS G30
ATTN: Library
ATTN: Samuel R. Crawford MS 531

Ford Aerospace & Communications Operations
(Formerly Aeronutronic Ford Corporation)

ATTN: Tech Info Section
ATTN: Ken C. Attinger

Franklin Institute

ATTN: Ramie H. Thompson

General Dynamics Corp.

Electronics Div. Orlando Operations

ATTN: D. W. Coleman

General Electric Company

Space Division

Valley Forge Space Center

ATTN: Daniel Edelman
ATTN: John L. Andrews
ATTN: Joseph C. Peden VFSC, Rm 4230M
ATTN: Larry I. Chasen

General Electric Company

Re-Entry & Environmental Systems Division

ATTN: Robert V. Benedict
ATTN: John W. Palchefskey, Jr.

General Electric Company

Ordnance Systems

ATTN: Joseph J. Reidl

General Electric Company

TEMPO-Center for Advanced Studies

ATTN: Royden R. Rutherford
ATTN: John D. Illgen
ATTN: DASIAC
ATTN: William McNamara
ATTN: M. Espig

General Electric Company

Aircraft Engine Business Group

ATTN: John A. Ellerhorst E2

General Electric Company

Aerospace Electronics Systems

ATTN: Charles M. Hewison Drop 624
ATTN: W. J. Patterson Drop 233

General Electric Company

ATTN: David W. Pepin Drop 160

General Electric Company-TEMPO

Attn: DASIAC

ATTN: William Alfonte

General Research Corporation

ATTN: John Ise, Jr.
ATTN: Robert D. Hill

Georgia Institute of Technology

Georgia Tech Research Institute

ATTN: R. Curry (UNCL only)

Goodyear Aerospace Corporation

Arizona Division

ATTN: B. Manning

Grumman Aerospace Corporation

ATTN: Jerry Rogers Dept 533

GTE Sylvania, Inc.

Electronics Systems Grp-Eastern Division

ATTN: Charles A. Thornhill, Librarian
ATTN: James A. Waldon
ATTN: Leonard L. Blaisdell

GTE Sylvania, Inc.

ATTN: A S M Dept S. E. Perlman
ATTN: David P. Flood
ATTN: H & V Group
ATTN: Paul B. Fredrickson
ATTN: H & V Group Mario A. Nurefora
ATTN: Comm Syst Div Emil P. Motchok
ATTN: Charles H. Ramsbottom
ATTN: Herbert A. Ullman

Harris Corporation

Harris Semiconductor Division

ATTN: Carl F. Davis MS 17-220
ATTN: T. L. Clark MS 4040
ATTN: Wayne E. Abare MS 16-111

Hazeltine Corporation

ATTN: Tech Info Ctr M. Waite

Honeywell Incorporated

Avionics Division

ATTN: Ronald R. Johnson A1622

Honeywell Incorporated

Avionics Division

ATTN: Richard B. Reinecke MS 725-5
ATTN: Stacey H. Graff MS 725-J
ATTN: Harrison H. Noble MS 725-5A

Honeywell Incorporated

Radiation Center

ATTN: Technical Library

Hughes Aircraft Company

ATTN: Dan Binder MS 6-D147
ATTN: Kenneth R. Walker MS D157
ATTN: Billy W. Campbell MS 6-E110
ATTN: John B. Singletary MS 6-D133
ATTN: Tech Library

Hughes Aircraft Company, El Segundo Site

ATTN: William W. Scott MS A1080
ATTN: Edward C. Smith MS A620

IBM Corporation

ATTN: Frank Frankovsky

IIT Research Institute

ATTN: Irving N. Mindel
ATTN: Jack E. Bridges

Institute for Defense Analyses

ATTN: IDA Librarian Ruth S. Smith

INTL Tel & Telegraph Corporation

ATTN: Alexander T. Richardson

ION Physics Corporation

ATTN: Robert D. Evans

IRT Corporation

ATTN: James A. Naber
ATTN: Ralph H. Stahl
ATTN: R. L. Mertz
ATTN: MDC
ATTN: Dennis Swift

JAYCOR

ATTN: Andrew Woods
ATTN: Eric P. Wenaas

JAYCOR

ATTN: Catherine Turesko
ATTN: Robert Sullivan

Johns Hopkins University

Applied Physics Laboratory

ATTN: Peter E. Partridge

Kaman Sciences Corporation

ATTN: Jerry I. Lubell
ATTN: Walter E. Ware
ATTN: W. Foster Rich
ATTN: Library
ATTN: John R. Hoffman
ATTN: Donald H. Bryce
ATTN: Albert P. Bridges

Litton Systems, Inc.

Guidance & Control Systems Division

ATTN: John P. Pretzler
ATTN: Val J. Ashby MS-67
ATTN: R. W. Maughmer

Lockheed Missiles & Space Co., Inc.

ATTN: L. Rossi Dept 81-64
ATTN: Edwin A. Smith Dept 85-85
ATTN: Philip J. Hart Dept 81-14
ATTN: Benjamin T. Kimura Dept 81-14
ATTN: Samuel I. Taimuty Dept 85-85
ATTN: George F. Heath Dept 81-14

Lockheed Missiles and Space Co., Inc.

ATTN: Tech Info Ctr D/Coll

M.I.T. Lincoln Laboratory

ATTN: Leona Loughlin Librarian A-082
ATTN: Jean L. Ryan

Martin Marietta Aerospace

Orlando Division

ATTN: William W. Mras MP-413
ATTN: Jack M. Ashford MP-537
ATTN: Mona C. Griffith Lib MP-30

Martin Marietta Corporation

Denver Division

ATTN: Ben T. Graham MS PO-454
ATTN: J. E. Goodwin MS 0452 (UNCL only)
ATTN: Research Lib 6617 Jay R. McKee

Maxwell Laboratories, Inc.

ATTN: Victor Fargo

McDonnell Douglas Corporation

ATTN: Technical Library

McDonnell Douglass Corporation

ATTN: Stanley Schneider
ATTN: Paul H. Duncan, Jr.

Mission Research Corporation

ATTN: Roger Stettner
ATTN: Daniel F. Higgins
ATTN: Conrad L. Longmire
ATTN: William C. Hart

Mission Research Corporation

ATTN: David E. Merewether
ATTN: Larry D. Scott

Mission Research Corporation-San Diego
ATTN: J. P. Raymond
ATTN: V. A. J. Van Lint

Mitre Corporation
ATTN: Theodore Jarvis

Motorola Incorporated
Semiconductor Group
ATTN: James R. Black

Motorola, Incorporated
Government Electronics Division
ATTN: Tech Info Ctr A. J. Kordalewski

National Academy of Sciences
National Materials Advisory Board
ATTN: R. S. Shane Nat Materials Advsy

University of New Mexico
Dept. of Campus Security and Police
ATTN: W. W. Grannemann (UNCL Only)

University of New Mexico
Electrical Engineering & Computer Science Dept
ATTN: Harold Southward

Northrop Corporation
Electronic Division
ATTN: George H. Towner
ATTN: Boyce T. Ahlport

Northrop Corporation
Northrop Research and Technology Ctr
ATTN: J. R. Srouer
ATTN: David N. Pocock
ATTN: Library
ATTN: Orlie L. Curtis, Jr.

Northrop Corporation
Electronic Division
ATTN: Vincent R. DeMartino
ATTN: John M. Reynolds
ATTN: Joseph D. Russo

Physics International Company
ATTN: Doc Con for John H. Huntington
ATTN: Doc Con for Philip W. Spence
ATTN: Doc Con for Ian D. Smith
ATTN: Doc Con for Charles H. Stallings

Pulsar Associates, Inc.
ATTN: Carleton H. Jones, Jr.

R&D Associates
ATTN: Richard R. Schaefer
ATTN: Leonard Schlessinger
ATTN: William J. Karzas
ATTN: S. Clay Rogers
ATTN: William R. Graham, Jr.

Rand Corporation
ATTN: Cullen Crain

Raytheon Company
ATTN: Gajanan H. Joshi Radar Sys Lab

Raytheon Company
ATTN: Harold L. Flescher

RCA Corporation
Government Systems Division
Astro Electronics
ATTN: George J. Brucker

RCA Corporation
David Sarnoff Research Center
ATTN: K. H. Zaininger

RCA Corporation
Government Systems Division
Missile & Surface Radar
ATTN: Andrew L. Warren

RCA Corporation
Camden Complex
ATTN: F. Van Keuren 12-5-2

Rensselaer Polytechnic Institute
ATTN: Ronald J. Gutmann (UNCL Only)

Research Triangle Institute
ATTN: Eng Div Mayrant Simons, Jr.

Rockwell International Corporation
ATTN: J. Spetz
ATTN: James E. Bell HA10
ATTN: K. F. Hull
ATTN: Donald J. Stevens FA70
ATTN: N. J. Rudie FA53
ATTN: L. H. Pinson FB41
ATTN: George C. Messenger FB61

Rockwell International Corporation
ATTN: John F. Roberts

Rockwell International Corporation
ATTN: T. B. Yates

Rockwell International Corporation
Collins Division
ATTN: Dennis Sutherland

Sanders Associates, Inc.
ATTN: James L. Burrows
ATTN: R. G. Despathy, Sr. P E 1-6270

Science Applications, Inc.
ATTN: J. Robert Beyster
ATTN: Larry Scott

Science Applications, Inc.
Huntsville Division
ATTN: Noel R. Byrn

Science Applications, Inc.
ATTN: J. Roger Hill

Science Applications, Inc.
ATTN: Charles Stevens

Science Applications, Inc.
ATTN: William L. Chadsey

Simulations Physics, Inc.
ATTN: Roger G. Little

Singer Company
Data Systems
ATTN: Tech Info Center

Singer Company
Security Manager
ATTN: Irwin Goldman Eng Management

Sperry Flight Systems Division
Sperry Rand Corporation
ATTN: D. Andrew Schow

Sperry Rand Corporation
Sperry Division
ATTN: Paul Maraffino
ATTN: Charles L. Craig EV

Sperry Univac
ATTN: James A. Inda MS 41T25

Stanford Research Institute
ATTN: Philip J. Dolan
ATTN: Arthur Lee Whitson
ATTN: Setsuo Dairiki

Stanford Research Institute
ATTN: MacPherson Morgan

Sundstrand Corporation
ATTN: Curtis B. White

Systems, Science and Software, Inc.
ATTN: David A. Meskan

Systems, Science and Software, Inc.
ATTN: Andrew R. Wilson
ATTN: Ira Katz

Syston-Donner Corporation
ATTN: Harold D. Morris

Texas Instruments, Inc.
ATTN: Donald J. Manus MS 72

Texas Tech University
ATTN: Travis L. Simpson

TRW Defense & Space Systems Group
ATTN: O. E. Adams R1-1144
ATTN: Robert M. Webb R1-2410
ATTN: Tech Info Center/S-1930
ATTN: R. K. Plebuch R1-2078
ATTN: Aaron H. Narevsky R1-2144
ATTN: H. H. Holloway R1-2036

TRW Defense & Space Systems Group
ATTN: Earl W. Allen 520/141
ATTN: F. B. Fay
ATTN: J. M. Gorman 520/114
ATTN: R. Kitter

TRW Systems Group
ATTN: Donald W. Pugsley

United Technologies Corporation
Norden Division
ATTN: Conrad Corda

Vought Corporation
ATTN: Technical Data Ctr
ATTN: Charles H. Coleman

Vought Corporation
Michigan Division
ATTN: James F. Sanson B-2
ATTN: Tech Library

Westinghouse Electric Corporation
Defense and Electronic Systems Center
ATTN: Henry P. Kalapaca MS 3525